THE ROLE OF CARBONACEOUS RESIDUES IN PLATINUM CATALYSED HYDROCARBON REFORMING REACTIONS

THESIS
SUBMITTED FOR THE DEGREE
OF
DOCTOR OF PHILOSOPHY
OF THE
UNIVERSITY OF GLASGOW.

BY

GRAHAM J. HAUGHEY, B.Sc.

JULY, 1987.

SUMMARY

The effect of the deposition of carbonaceous residues on the performance of two different Pt/γ-Al_2O_3 bifunctional reforming catalysts has been studied during continuous flow experiments performed at 500°C and 9.5 atm. using n-heptane as a model hydrocarbon feedstock. With both catalysts, the deposition of carbonaceous residues resulted in an overall decline in catalytic activity. This decline occurred most rapidly during the early stages of the reaction but progressively slowed with increasing time-on-stream until eventually a stable catalytic activity was attained. Significant variations in catalyst selectivity were observed to occur as a consequence of the deposition of carbonaceous residues. Increases in isomerisation selectivity of 11% and 16% occurred for the two catalysts. Corresponding decreases occurred in the aromatisation selectivities (4% and 10%) and hydrocracking selectivities (5% and 6%) of the catalysts, whilst the selectivities with respect of hydrogenolysis remained essentially constant. These selectivity changes are interpreted in terms of a coking process in which the metallic function of the bifunctional reforming catalysts is more selectively poisoned than the acidic function. It is therefore deduced that carbonaceous residues preferentially reside on the metallic function of bifunctional reforming catalysts. Differences in the nature of the individual product yield and selectivity changes observed for the two different catalysts with the deposition of carbonaceous residues, are interpreted in terms of the different metal loadings of the catalysts.

In addition, pulse-flow experiments have been performed with n-heptane at 500°C in the absence of hydrogen gas. These experiments have revealed that, under these conditions, the catalytic activity is enhanced by the presence of surface carbonaceous residues. The nature of the yield and selectivity

changes which occurred with the deposition of the carbonaceous residues during the pulse-flow experiments, indicate that this increase in activity is related to the ability of the surface carbonaceous deposit to actively donate hydrogen to reacting surface species.

Studies performed at 500°C, using [14-C] radiolabelled n-heptane, have shown that during reforming an exchange of carbon occurs between the surface carbonaceous deposits and gas phase hydrocarbon. Moreover, this exchange process does not depend on the presence or otherwise of hydrogen gas. The radio-chromatographic analysis of the product mixtures obtained during the [14-C] studies, has shown that a range of different chemical species, having carbon numbers from C1 upwards and exhibiting a variety of structures, were incorporated into the gas phase from the carbonaceous deposit during this exchange.

ACKNOWLEDGEMENTS

I would like to offer my sincere thanks to my supervisor, Dr. G. Webb for his help and guidance throughout this study.

I am also greatly indebted to Mr. T. Boyle, Mr. K. Shephard and Mr. R. Kennedy for their technical assistance, and to all my friends and colleagues in the surface chemistry department who helped to make the whole thing a very worthwhile experience.

I gratefully acknowledge the award of the CASE studentship by the SERC and the use of the research facilities at I.C.I., Wilton. I should also like to thank Dr. M.A. Day of I.C.I., Wilton for his many helpful suggestions and constructive criticism.

A great deal of the credit for the successful completion of this work must go to my Mum and Dad who not only laboured long and hard in typing the manuscript but, together with the rest of my family, gave me an immense amount of support and encouragement. To them I would like to say a very special thankyou.

Finally, I would like to thank Liz, without whom I could never have made it.

I dedicate this work

with love and gratitude

to Elizabeth.

CONTENTS

CHAPTER FIVE - TREATMENT OF RESULTS

CHAPTER SIX - RESULTS

CHAPTER SEVEN - DISCUSSION

Appendix

References.

CHAPTER ONE

INTRODUCTION

- oOo -

1.1 CATALYTIC REFORMING

1.1.1 Industrial Significance

Catalytic reforming is a hydrocarbon conversion process which is of fundamental importance in both the petroleum industry and the petrochemicals industry.

In the petroleum industry crude oil is converted into, predominantly, hydrocarbon mixtures suitable for use as fuels. The petrochemicals industry on the other hand is concerned with the production of the chemical building blocks upon which the manufacture of a diverse range of oil based commodities such as paints, foams, dyes etc., depends. The production of fuel, particularly for transportation, remains as the principal use of crude oil with the former industry accounting for some 90% of all crude oil extracted worldwide. Although the petrochemicals industry is subordinate to the petroleum industry in terms of oil tonnage, it too operates on a major scale with approximately 90% of all industrially produced chemicals having oil as their raw material source (1).

In the initial fractional distillation of crude oil, each resultant hydrocarbon distillate "fraction" meets volatility or molecular weight specifications that make it potentially suitable for a particular purpose. Accordingly, the fractions which are extracted for conversion into fuels suitable for use in internal combustion engines (for example, automobile engines), and from which the chemical building blocks used in the petrochemicals industry are generated, are the light gasoline and heavy gasoline fractions which are collectively referred to as "naphtha". Naphtha is therefore the hydrocarbon fraction boiling between ca.40°C and 180°C consisting of C4 - C12 hydrocarbons. Although the detailed composition of any given naphtha is peculiar and is characteristic of the geographical location of its source, all are comprised almost exclusively of a mixture of

linear paraffins, branched paraffins, naphthenes (fully saturated 5 and 6 membered rings) and aromatics, with the paraffinic species, whether linear or branched, being vastly predominant. The % composition of a typical middle eastern naphtha, for example, is shown in table 1.1

TABLE 1.1 - % COMPOSITION OF MIDDLE EASTERN NAPHTHA (2)

	COMPONENTS			
	Straight Chain Alkanes	Branched Chain Alkanes	Cyclo-Alkanes	Aromatics
C5	13	7	1	-
C6	7	6	2	-
C7	7	6	4	2
C8	8	9	5	4
C9	5	10	3	1
TOTAL	40	38	15	7

One of the most stringent criteria which has to be satisfied in the petroleum industry in order for a hydrocarbon mixture to be suitable for use as a fuel in an internal combustion engine, is that it has sufficiently high anti-knock character, that is, that it combusts in a steady and regular manner. The degree of knock exhibited by any given hydrocarbon mixture can be defined quantitatively by assigning to it an 'octane rating'. This is

given by the % volume of iso-octane in the iso-octane/n-heptane mixture to which the hydrocarbon mixture under consideration is equivalent in terms of its combustion characteristics. Thus, an octane rating of between 85-95 is required, for example, for fuels suitable for the high compression ratio internal combustion engines of motorised vehicles. In general, the naphtha hydrocarbon fraction obtained from the initial crude oil distillation process requires enrichment in order for it to meet this high octane rating requirement. Such enrichment can be achieved catalytically, by augmenting the concentration of the aromatic and, to a lesser degree, iso-paraffinic compounds present within the naphtha fraction, without decreasing to any great extent the average molecular weight of the hydrocarbon species present. The overall conversion process is termed catalytic reforming.

In addition to their value in the petroleum industry, aromatics, in the form of benzene, toluene and mixed xylenes (BTX mixtures), also represent one of the two main groups of intermediates upon which the production of many associated petrochemical products is based. For example, materials such as 'Terylene', polyester films , nylon fibres and 'Perspex' are all derived originally from an aromatic building block. The role of catalytic reforming within the petrochemicals industry is, therefore, to generate a hydrocarbon mixture from which these aromatic intermediates can be separated. This is achieved via aromatisation of the large concentrations of linear and branched paraffinic and naphthenic species present within the crude oil naphtha fraction, this fraction being suitable as the carbon numbers of the compounds it embraces are consistent with the preparation of the desired benzene, toluene and xylene intermediates.

Industrial reforming is, in general, carried out under conditions of high temperature (480-520° C) and high total pressure (150-350 p.s.i.). The actual conditions employed in any given system are, however, determined by a number of factors including the product requirements of the particular process that is in operation.

1.1.2 Reforming Catalysts

Around the 1950's it was discovered that the molecular structural changes that are desirable from a reforming point of view, that is, the conversion of paraffinic and naphthenic species to branched paraffins and aromatics, could be achieved very conveniently by passing the naphtha, in the presence of excess quantities of hydrogen gas, over a catalyst that combined both metallic and acidic characteristics (3).

Catalysts that integrate two distinct catalytically active phases in this manner are termed 'bifunctional'. In a bifunctional reforming catalyst the metal component (typically platinum) is generally present to the extent of 1% by weight or less. In common with all supported metal catalysts the metal exists in the form of small crystallites randomly dispersed on a porous and refractory oxide support material. In reforming catalysts the support material consists, almost invariably, of the γ - allotropic form of alumina (Al_2O_3), the surface of which has been treated with a chlorine (or less frequently fluorine) containing compound to the extent of around 1% by weight.

In the unchlorided state, alumina is characterised by an incomplete layer of surface hydroxyl groups together with residual surface oxide and aluminium ionic defects (4)(5). Chlorine introduced to this surface readily exchanges with the hydroxyl groups present (6)(7), one effect of which is to greatly enhance the intrinsically relatively low capacity of the alumina to act as a catalyst for hydrocarbon rearrangements. The introduction of chlorine onto the support surface therefore, creates the essential bifunctionality that characterises a reforming catalyst.

Thus, in addition to having the ability to catalyse hydrogenation-dehydrogenation reactions which are characteristic of metallic/

catalysts, reforming catalysts are also effective in catalysing the isomerisation, ring closure and ring enlargement reactions of hydrocarbons which are generally associated with acid catalysis.

The acidity of the chlorine treated alumina surface, whilst being evident from its ability to promote acid-catalysed reactions, can be readily verified by the titration of the acid sites with basic molecules such as ammonia, quinoline, pyridine, etc. (8). It remains a matter of contention, however, whether the acidity is of a Brönsted (protonic) or Lewis (electron-accepting) nature. Many authors (9)(10) have attributed the faculty with which this surface promotes hydrocarbon rearrangements (thought to proceed via carbonium ion formation from olefin intermediate species (section 1.1.4)) to an increased mobility of the surface hydroxyl protons, this being induced by adjacent electron-withdrawing chloride ions. Alternatively, it has been demonstrated using infra-red techniques (11)(12), that the titration of acidic sites on unchlorided alumina with ammonia or pyridine does not involve the simultaneous formation of ammonium or pyridinium ions. Indeed, Peri (11) has shown that on alumina predried to 1070 K (very low surface hydroxyl content) 90% of the ammonia adsorbed retains its molecular integrity, presumably by co-ordination with incompletely co-ordinated surface aluminium sites which are acting as Lewis acids. The Lewis acidity associated with surface aluminium ions is also likely to be enhanced by the presence of adjacent surface chloride ions (13).

It is apparent therefore that hydroxyl groups present on the surface of unchlorided alumina exhibit little, if any, proton donating tendancy and make no significant contribution to surface acidity. In the presence of surface chloride ions however, both Brönsted and Lewis acidity may be important in promoting hydrocarbon conversion reactions with the relative contributions made by each to the total acidic activity probably

being dependent on the chlorine content of the alumina surface and the residual surface hydroxyl concentration that remains after the dehydration of the alumina.

Over the last two decades or so, the conventional Pt/γ-Al_2O_3-Cl monometallic catalysts used in commercial reforming processes have been largely superseded by bimetallic species which contain a second promoting metal in addition to the platinum. Although the patent literature contains many examples of bimetallic reforming catalysts that are claimed to offer superior performance to Pt/γ-Al_2O_3-Cl, the species that is most commonly employed on a commercial basis is Pt-Re/γ-Al_2O_3-Cl. Indeed, it was estimated (14) in 1976 that perhaps some 90% of all industrial reforming processes utilised this catalyst. Whilst it is generally accepted that the Pt-Re/γ-Al_2O_3-Cl catalyst does not offer an enhanced initial activity relative to the unpromoted Pt/γ-Al_2O_3-Cl catalyst (15), it has been widely reported (16)(17) that the bimetallic species is more selective for the formation of $C5^+$ "reformate" products. Moreover, the Pt-Re/γ-Al_2O_3-Cl catalyst exhibits a vastly superior resistance to deactivation (section 1.2.2) which enables it to operate at its initial high activity for a prolonged period.

It has been pointed out, however (17), that the selectivity improvements afforded to a reforming catalyst by combining the Pt with Re are only observed in the presence of a non negligible quantity of sulphur, and that the unsulphided Pt-Re catalyst in fact exhibits a much poorer selectivity in comparison to the monometallic Pt catalyst due to the inherently very high hydrogenolysis activity of the Re. Indeed, it is now standard industrial practice, both in the preparation of monometallic Pt and bimetallic Pt-Re catalysts, for a controlled quantity of sulphur to be deposited onto the metal function of the catalyst before use. The controlled sulphidation of the metal function, whether it contains Re or not, has been shown to be beneficial both in terms of enhanced catalyst activity maintenance (section 1.2.2)

and desirable selectivity modifications, the two phenomena being not entirely unrelated. A number of studies (17)(18) have demonstrated, for example, that the incorporation of sulphur onto a reforming catalyst tends to temper the very high initial dehydrogenation activity of the metal surface. Moreover, several authors (19)(20) have commented on the ability of sulphur to selectively suppress the hydrogenolysis activity of the Pt metal. Thus, in the case of the bimetallic Pt-Re catalyst species, sulphiding permits the stabilising effect of Re to be enjoyed without incurring a concomitant increase in hydrogenolysis activity.

1.1.3 Reforming Reactions

The major reactions taking place in the catalytic reforming of naphtha feedstocks over bifunctional reforming catalysts are: i) dehydrogenation of cyclohexanes to aromatics, ii) dehydrogenation of paraffins to olefins, iii) isomerisation of n-alkanes to branched alkanes, iv) dehydroisomerisation of alkylcyclopentanes to aromatics, v) dehydrocyclisation of alkanes to aromatics, and vi) hydrogenolysis and hydrocracking reactions to give low molecular weight products.

Under typical reforming conditions (section 1.1.1) the dehydrogenation of cyclohexane species to produce aromatics is the reaction which occurs most rapidly. Naphthene dehydroisomerisation, as well as the isomerisation and dehydrogenation reactions of paraffins, are also fairly rapid. The dehydrocyclisation and fission reactions proceed at a relatively slow rate.

The thermodynamics of the reactions listed above can be considered by referring to the equilibrium constants, K, and the heats of reaction for the conversions of representative C6 hydrocarbons at 500°C (table 1.2)(21).

TABLE 1.2 - EQUILIBRIUM CONSTANTS AND HEATS OF REACTION FOR C6 HYDROCARBON REACTIONS (773K)

REACTION	K (773K)	HEAT OF REACTION ($kJ.mol^{-1}$)
Cyclohexane → Benzene + $3H_2$	$6x10^{5}$	+221
n-Hexane → n-Hexene + H_2	$3.7x10^{-2}$	+130
n-Hexane → 2-Methyl Pentane	1.1	-5.9
n-Hexane → 3-Methyl Pentane	0.76	-4.6
Methylcyclopentane → Cyclohexane	0.086	-16.0
n-Hexane → Benzene + $4H_2$	$0.78x10^{5}$	+266
n-Hexane → C_1-C_5 Fragments	-	Highly Exothermic

It can be seen that the dehydrogenation of cyclohexanes and the dehydrocyclisation of n-alkanes to give the desired aromatic products, are both highly endothermic reactions and involve the evolution of hydrogen. This also applies to the dehydrogenation of paraffins to olefins which, although it occurs to only a small extent in reforming, is nonetheless a very important reaction as olefins appear to act as intermediates in some of the reforming conversions (section 1.1.4). In terms of equilibria it would seem desirable, therefore, to operate at the highest temperatures and lowest hydrogen pressures possible in order to maximise the yield of aromatic product and olefin intermediate. In practice, however, kinetic considerations (section 1.1.4) and a desire to maintain a high catalyst activity (section 1.2.1) impose constraints on the maximum possible temperatures and the minimum possible hydrogen pressures that can be employed.

1.1.4 Mechanisms and Kinetics

A mechanistic interpretation of reforming which involves the participation of both the metallic and acidic catalytic functions and

which accounts, in part, for experimentally observed product distributions, was postulated as long ago as 1953 by Mills and co-workers (22). The reaction scheme, which was formulated in response to experiments that compared the conversion of various hydrocarbon reactants over catalysts containing only a dehydrogenation function, only an acidic function, or both catalytic functions, is illustrated in figure 1.1 in which n-heptane is used as a representative hydrocarbon feedstock. According to this mechanism, paraffinic species are dehydrogenated on the metal to form olefins which then migrate to the acidic sites. At the acidic sites the olefins are converted into carbonium ions which undergo skeletal isomerisation or ring closure reactions. The transference of a proton to the support regenerates an unsaturated intermediate which is subsequently saturated by interaction, once again, with the metal sites. Alternatively, naphthenic species, formed via paraffin cyclisation or which are present within the naphtha feedstock, are readily converted into aromatics via dehydrogenation on the metal catalytic function or by a combination of acid catalysed ring enlargement followed by dehydrogenation (dehydroisomerisation). Early work by Weisz (23) has demonstrated very convincingly that the intermediates in these bifunctional reactions are true gas phase species that are transported between the metal and acidic sites by gaseous diffusion.

The validity of a mechanism, such as that shown in figure 1.1, in which the formation of unsaturated species is a pre-requisite in the isomerisation, dehydroisomerisation and cyclisation reactions, is confirmed, not only by the fact that small quantities of olefins are often detected in reforming product mixtures (24), but also by corroborative evidence obtained from a number of kinetic studies. Sinfelt and co-workers (25), for example, studied the kinetics of n-pentane isomerisation over a catalyst containing 0.3% by weight Pt supported on acidified alumina. For a fixed n-pentane to hydrogen reactant ratio the rate of isomerisation at 372°C was found to be independent of total pressure throughout the pressure

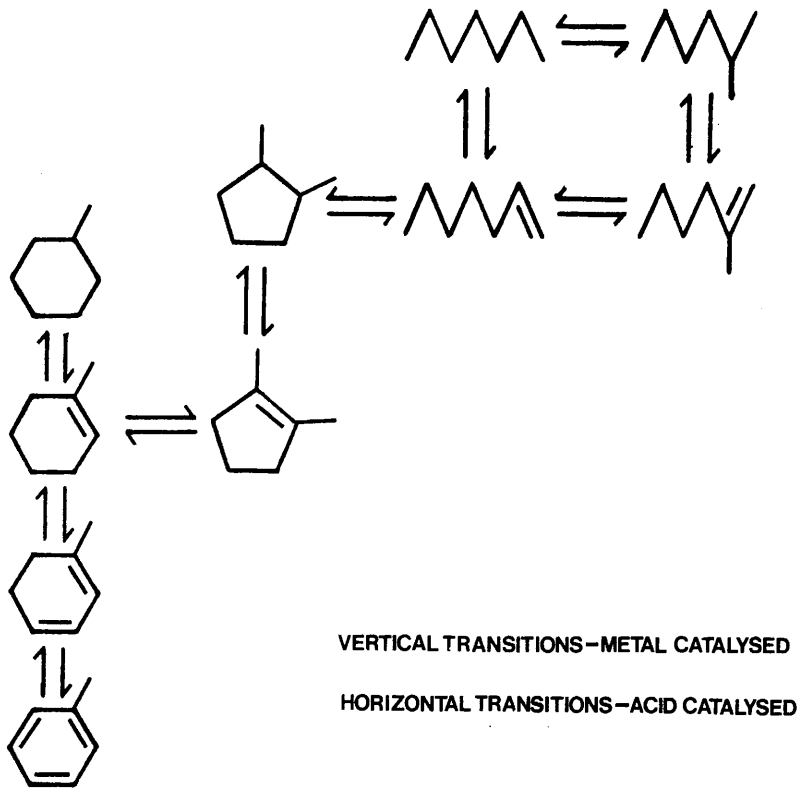

Figure 1.1 – Sequence of Reactions on a Dual Functional Reforming Catalyst. (22)

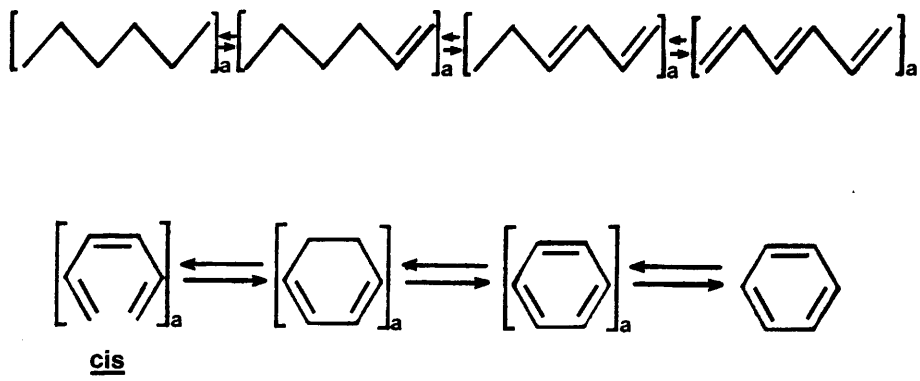

Figure 1.2 – Direct Metal Catalysed 1,6 – Ring Closure. (34)

range 7.7 to 27.7 atm., but for any given pressure the isomerisation rate increased as the n-pentane to hydrogen ratio increased. Quantitatively similar results were obtained by Christoffel and Paál (26) when studying the rate of isomerisation of n-hexane over a fresh Pt/acidified alumina catalyst and a range of total pressures. The observation that the rate of hydrocarbon isomerisation exhibits, respectively, a positive and negative partial pressure dependency with respect to the hydrocarbon and hydrogen reactants (which is indeed the case throughout the range of reactant partial pressures commonly employed in industry) can be readily interpreted in terms of the mechanism shown in figure 1.1. According to this mechanism the isomerisation of, for example, n-hexane is given by,

$$\text{n-hexane} \overset{\text{Pt}}{\rightleftharpoons} \text{n-hexene} + H_2$$

$$\text{n-hexene} \xrightarrow[\text{Site}]{\text{Acid}} \text{iso-hexene}$$

$$\text{iso-hexene} + H_2 \overset{\text{Pt}}{\rightleftharpoons} \text{iso-hexane}$$

If it is assumed that the isomerisation of the olefin on the acidic centres is the slow rate-determining step, then the rate of the reaction can be expressed as

$$\text{rate} = k_1 \, [nC_6{}^{=}]a \quad \ldots\ldots\ldots\ldots \quad (1)$$

where k_1 is the rate constant and $[nC_6{}^{=}]a$ represents the concentration of n-hexene on the acidic sites. If equilibrium is established between n-hexane, n-hexene and hydrogen in the initial dehydrogenation step, then the concentration of n-hexene in the gas phase ($nC_6{}^{=}$) is given by

$$(nC_6{}^{=}) = K_1(nC_6)/(H_2) \quad \ldots\ldots\ldots\ldots \quad (2)$$

where K_1 is an equilibrium constant and (nC_6) and (H_2) are, respectively, the concentrations of n-hexane and hydrogen

in the gas phase. Assuming further that adsorption equilibrium is established between n-hexene in the gas phase and on the acidic sites and that this is best described in terms of a Freundlich isotherm (25) then

$$[nC_6^{=}]a = K_2(nC_6^{=})^n \quad \ldots\ldots\ldots\ldots (3)$$

where K_2 is the adsorption coefficient and n has a value of between 0 and 1. Substituting equations (2) and (3) into equation (1) gives

$$\text{rate} = k_2[(nC_6)/(H_2)]^n$$

which is consistent with the empirically derived rate relationships described above (25)(26). Thus, the mechanism illustrated in figure 1.1 is in accordance with the observed kinetics for paraffin isomerisation.

Moreover, under typical reforming conditions, the rate of dehydroisomerisation of C5 naphthenic species and of paraffin dehydrocyclisation demonstrate a similar inverse hydrogen partial pressure dependency (27)(28). As with the rate of isomerisation, the negative hydrogen partial pressure dependencies of the cyclisation and dehydroisomerisation rates are easily rationalised in terms of a mechanism that involves, in each case, an initial rapid dehydrogenation step to produce an unsaturated intermediate species. Increasing the hydrogen partial pressure has the effect of limiting the concentration of unsaturated intermediate attainable at equilibrium, which results in a decrease in the overall rate of reaction.

In the kinetic treatment just outlined the assumption that the initial dehydrogenation step proceeds rapidly to equilibrium and is not normally, therefore, rate-limiting, appears to be justified, at least in the case of the isomerisation and dehydroisomerisation reactions. Thus, Sinfelt, Hurwitz and Rohrer (29), studying the reactions of n-heptane and methylcyclopentane on a Pt/acidified alumina catalyst, observed that under a fixed set of conditions

increasing the metal loading of the catalyst from 0.1% to 0.6% by weight had little or no effect on the rates of the isomerisation and dehydroisomerisation reactions. Apparently sufficient dehydrogenation activity existed even at the very lowest metal loading to establish the maximum attainable equilibrium concentration of unsaturated intermediate. The isomerisation and dehydroisomerisation rates were, therefore, controlled by a rate limiting step that took place on the acidic catalytic function. Further confirmation of this was obtained by these workers when it was observed (25) that, under identical conditions, the rate of n-pentane isomerisation on a Pt/acidified alumina catalyst was very similar to the rate of methylbutene formation from pent-1-ene, the latter reaction being catalysed by the same catalyst but in the absence of any Pt dehydrogenation function.

In contrast to their observation that the isomerisation and dehydroisomerisation reaction rates were independent of the Pt metal loading of a reforming catalyst, Sinfelt and co-workers (29) noted that the rate of n-heptane dehydrocyclisation, whilst not being directly proportional to the catalyst Pt content, increased by a factor of about two over the range 0.1% to 0.6% by weight Pt. Similar observations have been made by other workers (24). The incongruence that exists between this observation and the fact that the reactant partial pressure dependency data described previously is consistent with a bifunctionally catalysed dehydrocyclisation mechanism in which the metal-catalysed steps proceed rapidly to equilibrium even at the very lowest catalyst metal content, can be reconciled by recognising that, under the conditions used by these workers which were typical of those used in a commercial reforming process, a further metal-catalysed dehydrocyclisation route must exist in addition to the bifunctional mechansim already described. The ability of a Pt surface to catalyse the dehydrocyclisation of paraffins to aromatics in the absence of any acidic catalytic activity at reforming temperatures has indeed been demonstrated using monofunctional supported Pt(30) and Pt single crystal catalysts (31). Several such studies,

notably those of Dautzenberg and Platteeuw (32) and Davis and Venuto (33), have concurred in showing that the metal-catalysed cyclisation route is most likely to proceed via a direct 1,6 ring closure mechanism that does not involve the formation of a C5 cyclic intermediate. Thus, in a catalytic reforming system the total aromatisation activity of the bifunctional reforming catalyst is given by the sum of the rates of two contributory aromatisation mechanisms, one involving the participation of both the metal and acidic catalytic functions, the other being catalysed solely by the metal.

Clarification of the mechanism involved in the latter of the above reactions has been obtained by Paál and Tétényi (34) from [14-c] radiolabelling experiments. These workers produced benzene over Pt black catalysts at temperatures of between 390-480°C using a reactant mixture that consisted of either [14-c] labelled n-hexane and inactive 1-hexene, or radiolabelled n-hexane and inactive cyclohexane. All three reactant species when injected alone gave benzene. However, the authors reasoned that in the case of, for example, the latter reactant mixture, if the cyclohexane was a surface intermediate in the formation of benzene from n-hexane, then this cyclohexane would mix with the inactive cyclohexane and in so doing increase the specific activity of the cyclohexane obtained as product. Thus, the specific activities of the product species obtained from the labelled n-hexane mixtures indicated that 1-hexene is formed from n-hexane over Pt but that cyclohexane is not, and therefore the latter species cannot participate in the Pt catalysed cyclisation mechanism. Similar experiments involving mixtures of labelled 1-hexene with inactive cyclohexene, 1,3 - cyclohexadiene and 1,3,5 - hexatriene, implicated an n-hexane cyclisation pathway in which 1,3,5-hexatriene and 1,3 -cyclohexadiene, but not cyclohexane or cyclohexene, served as intermediates. Paál and Tétényi therefore postulated the "stepwise" aromatisation mechanism that is illustrated in figure 1.2. The mechanism proposes that

equilibrium is established between mono, di and tri-olefinic species on the surface. The formation of the cyclohexadiene and thence the aromatic is believed to involve the metal-catalysed cyclisation of the tri-olefin intermediate in its cis - geometric form.

As stated previously, in a catalytic reforming system reactions which lead to the formation of product species having a lower carbon number than the reactant hydrocarbons, i.e. hydrogenolysis and hydrocracking reactions, invariably accompany the desired isomerisation and dehydrocyclisation processes. Although both hydrogenolysis and hydrocracking involve the rupture of carbon-carbon bonds with concomitant hydrogenation, the resultant product distributions, and the mechanism by which they are produced, are distinct. Thus, on a bifunctional reforming catalyst, the hydrogenolysis of saturated reactant species occurs on the metal function of the catalyst, whereas hydrocracking can take place via interaction with the acidic function alone or may involve the co-operative action of the metal and acidic functions.

The catalytic hydrogenolysis of saturated hydrocarbons on various metal surfaces has been reviewed by Sinfelt (35). The earliest reported investigations of the kinetics and mechanism of the hydrogenolysis of simple hydrocarbons were those of Taylor et al (36). These workers, studying ethane hydrogenolysis on supported Ni catalysts, reported a fairly large inverse dependence of the rate on the hydrogen partial pressure. In fact, this observation has since been shown to be a general feature of hydrocarbon hydrogenolysis on many supported metal catalysts including those of cobalt and the group viii metals.

In the case of ethane hydrogenolysis on Pt catalysts, the following reaction scheme is consistent with much of the experimental data (21)

$$C_2H_6(g) \rightleftharpoons C_2H_5(ads)+H(ads)$$
$$C_2H_5(ads)+H(ads) \rightleftharpoons C_2Hx(ads)+aH_2(g)$$
$$C_2Hx(ads) \longrightarrow \text{ads. C1 fragments} \xrightarrow{H_2} CH_4(g)$$

where (ads) and (g) denote, respectively, adsorbed and gaseous species, and a is equal to (6-x)/2. Thus, the initial step in the sequence involves the rupture of a carbon-hydrogen bond to produce an adsorbed C_2H_5 species. Further dehydrogenation follows to generate a hydrogen deficient C_2Hx surface intermediate which subsequently undergoes carbon-carbon bond scission to form monocarbon fragments. These fragments are then hydrogenated to give methane by interaction with a molecule of hydrogen. If it is assumed that equilibrium is established in the first two steps of the sequence and further that the carbon-carbon bond scission is rate-determining, then the experimentally observed kinetics can be rationalised by considering that the effect of increasing the hydrogen partial pressure is to limit the equilibrium concentration of C_2Hx (ads) intermediate and hence decrease the rate of hydrogenolysis (21). The presence of substantial quantities of methane and ethane in a reforming product mixture can be attributed to hydrogenolysis reactions. These species are formed either as primary hydrogenolysis products or by the secondary hydrogenolysis of primary product fragments.

In contrast, the hydrocracking of linear and branched alkanes proceeds via olefinic and thence carbonium ion intermediates (37). Once formed, the carbonium ions undergo extensive degradation on the acidic catalytic centres via successive **β**-eliminations to generate, almost exclusively, C3 to C6 fragments. The product distributions obtained from hydrocracking reactions generally contain large amounts of branched products due to the re-arrangement of the intermediate carbonium ions to the favoured tertiary configuration.

1.2 COKING OF REFORMING CATALYSTS

In catalytically promoted hydrocarbon conversion processes, such as cracking and reforming, the desired molecular conversions are invariably accompanied by the formation of hydrogen deficient carbonaceous residues (coke) on the surface of the catalyst.

The accumulation of such deposits results in substantial catalyst deactivation through the blockage of active sites and necessitates that plant shutdown and regeneration procedures be periodically undertaken to restore the catalyst activity to an acceptable level.

Carbonaceous residues tend to form most rapidly in the initial stages of the catalytic reaction when a maximum number of free catalytic sites are available for poisoning (38)(39). However, as the coverage of the catalytic surface by these deposits becomes more extensive, producing a corresponding reduction in the number of accessible surface sites, the rate of the coking reaction itself progressively decreases until, in many instances, a limiting concentration of surface carbonaceous residues is approached. This is the normal situation with commercial reforming catalysts (40)(41) which, under industrial conditions, operate in the presence of surface coke deposits that, if permitted, can accumulate to give concentrations equivalent to perhaps 5-10% of the original catalyst weight (42).

1.2.1 Characterisation of Carbonaceous Residues

A wide range of both physical and chemical analytical techniques have been applied to the characterisation of the surface carbonaceous residues associated with bifunctional reforming catalysts and the results from many such investigations have recently been reviewed by Wolf and Alfani (43). Although the detailed nature of these deposits appears to be dependent on many of the reaction parameters, a complex heterogeneous surface material in which mono and polycyclic aromatic rings and aliphatic linkages co-exist and which is comprised of both graphitic and amorphous regions, is consistent with much of the characterisation data.

Eberly and co-workers (44), for example, used infra-red spectroscopy to examine the coke deposits formed at 445°C on a 13% Al_2O_3, 87% SiO_2 acidic cracking catalyst from a variety

of high molecular weight hydrocarbons e.g. hexadecane, 1-butylbenzene, 1-methylnaphthalene. The coked catalyst samples were dissolved in a KOH solution for 2 hours and the infra-red spectra of the solutions recorded. Absorption bands attributable to $-CH_2$, $-CH_3$ and aromatic groups were observed in the spectra of the coked catalysts associated with both the aromatic and non-aromatic reactant species, although the deposits formed from the latter tended to be more paraffinic in nature.

Similarly, several x-ray diffraction studies, notably those of Appleby et al (45) and Haldemann and Botty (46), have reported evidence for the presence of condensed aromatic structures of low hydrogen content in the coke deposits associated with hydrocarbon conversion catalysts. In the latter study, x-ray diffraction techniques were used to examine the structure of the coke retained by a SiO_2/Al_2O_3 catalyst after the cracking of a gas oil hydrocarbon fraction. These workers found that some 50-60% of the coke deposit was organised having a pseudographitic structure. The remaining material consisted of aromatic systems and polynuclear aromatics with aliphatic and alicyclic appendages.

Raman spectroscopy has been shown by Espinat et al (47) to provide a very sensitive method for the characterisation of coke deposits. By considering the ratio in intensities of the 1355 cm^{-1} and 1600 cm^{-1} spectral bands which are associated, respectively, with pregraphitic carbon (i.e. condensed polyaromatic rings) and graphitic coke, these workers were able to assess the significance of coke content, hydrogen/hydrocarbon reactant ratio, and nature of the metallic phase, on the structures of the coke deposits associated with a number of different reforming catalysts. Both pregraphitic and graphitic type deposits were found to be present on platinum/acidified alumina catalysts which contained coke contents ranging from between 0.29-27.3% by weight. For a given catalyst coke content, however, increasing the hydrogen/hydrocarbon reactant ratio under which the coking was incurred, decreased the extent of graphitisation in favour of the

pregraphitic phase. A similar effect was encountered when the platinum catalyst was promoted with either rhenium or iridium.

The analysis of coke combustion products has been extensively used as a means of determining the H/C stoichiometry of the coke deposits associated with a variety of catalytic systems and has demonstrated conclusively that many distinct coke structures exist. The results obtained from many such analyses have been summarised in the previously cited review by Wolf and Alfani (43). Davis, Zaera, and Somorjai (42), however, have combined the techniques of Auger electron spectroscopy (AES) and hydrogen thermal desorption to ascertain the chemical composition of the coke deposits remaining on a number of platinum single crystal catalysts after n-hexane conversions had been performed within the temperature range 300-405°C. Thus, AES provided a quantitative measure of carbon coverage by yielding a value for the surface carbon to surface platinum atomic ratio, whilst the hydrogen content of the surface deposit was obtained via temperature programmed hydrogen desorption. It was found that the H/C stoichiometry of the coke deposit was dependent upon the reaction temperatures, ranging from between H/C= 1.6 and H/C = 1.0 for reactions carried out at 300°C and 405°C respectively. The authors have pointed out that these chemical compositions are intermediate between those expected for polyacetylene (H/C = 1.0) and polyethylacetylene (H/C = 1.5) or related surface structures such as those illustrated in figure 1.2.

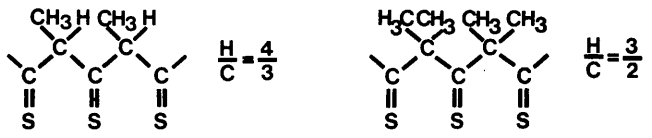

FIGURE 1.2 - PROPOSED STRUCTURES FOR CARBONACEOUS RESIDUES ON Pt (42)

Moreover, AES when used in conjunction with carbon monoxide adsorption-desorption studies, the latter providing a means of titrating the uncoked platinum sites, revealed that the carbonaceous deposits exhibited a more 3-dimensional character when formed at higher temperatures.

Temperature programmed oxidation techniques have been used in a number of studies to distinguish between the coke deposits associated with the metallic and acidic functions of reforming catalysts (48)(49)(50). Figoli et al (48), for example, have used differential thermal analysis to monitor the temperature programmed oxidation of the carbonaceous residues that were retained on a $Pt/\delta\text{-}Al_2O_3\text{-}Cl$ catalyst after interaction with a naphtha feedstock under a variety of industrial type conditions. Under all conditions, two different zones of coke combustion were detected during the temperature programmed oxidation, one from 123°C to 369°C and the other from 369°C to 555°C. Similar sequential oxidations have been reported by other workers (51)(52) for $Pt/\delta\text{-}Al_2O_3\text{-}Cl$ catalysts that had been coked by mono-reactant hydrocarbon feedstocks.

By comparing the temperature programmed oxidation characteristics of a coked $Pt/\delta\text{-}Al_2O_3\text{-}Cl$ catalyst to those of coked Pt/SiO_2 and acidified Al_2O_3 catalysts, Figoli et al (48) were able to assign the low temperature oxidation zone to coke associated with the metal catalytic function and the high temperature zone to coke associated with the alumina support. Moreover, from the chromatographic analysis of the combustion products obtained during each of the combustion zones, they deduced that the H/C ratio of the coke formed on the metal was higher than that of the support coke deposit which, state the authors, suggest that the coke residing on the metal is of a less highly polymerised nature than that which is retained by the support. Similar conclusions have been arrived at by Parera et al (49).

A number of surface science spectroscopic techniques, other

than AES, have been shown to be capable of providing useful complimentary information in the elucidation of the structure of surface hydrocarbon species. Somerjai and Zaera (53), for example, have demonstrated the successful application of LEED and HREELS in investigations on the structure of adsorbed hydrocarbon monolayers associated with Pt single crystal catalysts. Information regarding the bond lengths and bond multiplicities within the metal-adsorbate layer, and indeed the chemical identity of surface groups, can be derived by such techniques.

1.2.2 Origin and Formation of Carbonaceous Residues

The coking of the catalyst surface that occurs during the catalytic reforming of hydrocarbons, and indeed during many commercial hydrocarbon conversion processes, is generally considered to be initiated by the retention on the catalyst surface of strongly adsorbed coke precursor molecules (15)(44)(45)(54-56)(60). These coke precursor molecules subsequently undergo condensation and polymerisation reactions on the catalyst surface, with simultaneous loss of hydrogen, to generate extensive hydrogen deficient carbonaceous residues that, as described previously (section 1.2.1), can be detected and characterised by a wide range of analytical techniques.

In general, the precursor molecules that are directly responsible for catalyst coking are not themselves normal constituents of the hydrocarbon feedstock, but are rather formed through the interaction of certain species within the feedstock with the catalyst surface. That this is indeed the case in the reforming of typical industrial naphthas over bifunctional Pt/δ-Al_2O_3 catalysts is evident from the work of Bertolacini and Pellet (15). These workers have demonstrated that although an intimate mechanical mixture of Pt/δ-Al_2O_3 and Re/δ-Al_2O_3, when used in the reforming of an industrial naphtha, exhibited a superior activity maintenance relative to the Pt/δ-Al_2O_3 catalyst alone,

the promotional effect was removed when the Re/ϑ-Al_2O_3 catalyst was re-located upstream of the Pt/ϑ-Al_2O_3 catalyst. As the promotional effect of the Re/ϑ-Al_2O_3 catalyst, when in the mechanical mixture, occurred in the absence of any direct chemical interaction between it and the Pt/ϑ-Al_2O_3 catalyst, it is highly likely that the Re/ϑ-Al_2O_3 catalyst was active in the removal of coke precursor molecules that would eventually have fouled or blocked the Pt/ϑ-Al_2O_3 catalyst. Moreover, as the displacement of the Re/ϑ-Al_2O_3 catalyst upstream from the Pt/ϑ-Al_2O_3 coincided with the removal of the promotional effect, it is clear that the coke precursor molecules were not contained within the naphtha feedstock itself but were instead only formed after the naphtha had interacted with the Pt/ϑ-Al_2O_3 catalyst. Similar conclusions regarding the origin of coke precursor molecules have been obtained by John, Pachovsky and Wojciechowski (54). These workers studied the cracking of various crude oil extracts over a commercial cracking catalyst and concluded that coke formation was not the direct result of primary reactions but rather resulted from the secondary reactions of primary reaction products.

In the many studies which have sought to gain an insight into carbonaceous residue formation on catalyst surfaces and in particular the nature of the coke precursors, small unsaturated molecules have consistently been shown to exhibit a very high coke forming tendancy relative to their saturated counterparts, and the formation of such species within a catalytic system is therefore believed to be an essential pre-requisite for carbonaceous residue formation. Cooper and Trimm (40), for example, compared the coking characteristics of a Pt/ϑ-Al_2O_3-Cl reforming catalyst using a variety of different monohydrocarbon feedstocks and observed that, under a fixed set of experimental conditions typical of those used in an industrial reforming system, the rate of deposition of carbonaceous residues from n-hexene was approximately three times greater than that from n-hexane. In a similar study, Appleby and co-workers (45) examined the amount of coke deposited on a SiO_2/Al_2O_3 catalyst during the cracking of a number of

aliphatic and polycyclic model compounds. In concurrence with the results of the previous study, these authors reported that, for a given set of conditions, aromatic and olefinic feedstocks were far more virulent in terms of coke production than the corresponding saturated species. They further speculated that in the case of the olefins, coke was formed via aromatic nuclei which subsequently underwent further condensation and dehydrogenation reactions.

A number of more detailed reaction schemes, all of which have invoked the use of small unsaturated molecules as precursors, have however been postulated to account for carbonaceous residue formation on catalyst surfaces. Bertolacini and Pellet (15), for example, attributed the rapid coking of a Pt/δ-Al_2O_3-Cl catalyst which was used in the reforming of a cyclopentane rich feedstock, to a mechanism in which the cyclopentane molecules underwent an initial excessive dehydrogenation reaction on the metallic function of the catalyst to generate cyclopentadiene molecules. The cyclopentadiene molecules, acting as coke precursors, then dimerised to naphthalene which in turn subsequently polymerised to generate a more extensive aromatic deposit. Further mechanisms in which unsaturated coke precursor molecules were considered to have been formed via the dehydrogenation of reactant species by the catalyst surface, have been proposed by Tauster and Koros (55) and by Levinter et al (56). The former interpreted the retention of carbonaceous materials that occurred on the surface of a supported chromia catalyst during its interaction with n-propane, in terms of a mechanism involving the cyclisation and alkylation of C6 and C9 olefinic fragments generated by the combination of unsaturated C_3 coke precursors. Levinter et al (56), on the other hand, formulated the following reaction scheme to account for the formation of carbonaceous residues on the surface of a layered Pt/δ-Al_2O_3 catalyst during naphtha reforming:- naphtha feedstock → dienes → resins + asphaltenes → carboides.

Several authors (44)(54)(57) have commented on the possible role of

hydrogen acceptor molecules in the formation of unsaturated coke precursors. Thus, the unsaturated species required to initiate coke formation are formed not through the abstraction of hydrogen by the catalyst surface, but rather through the donation of hydrogen from the adsorbed reactant molecules to acceptor molecules which are themselves unsaturated. Mechanisms involving olefinic acceptor molecules, for example, have been postulated by John, Pachovsky and Wojeichowski (54) and by Eberly et al (44) to account for the formation of coke on commercial cracking catalysts during the cracking of saturated hydrocarbons. In the case of linear saturates, the latter workers envisaged a mechanism in which coke was formed via the condensation, cyclisation and progressive growth of highly unsaturated species generated by a series of successive hydrogen donations from individual feedstock molecules to a plurality of acceptor molecules.

Blue and Engle (57), Thomas (58) and Greensfelder and Voge (59) have attributed the high coke forming tendency of naphthenes, which has been demonstrated on numerous occasions (15)(40) (60), to the readiness of the naphthenic molecules to donate hydrogen to unsaturated acceptor molecules.

1.2.3 Factors Affecting Residue Formation

The rate and extent of deposition of carbonaceous residues on the surface of a reforming catalyst is governed by many factors, including not only the conditions under which the catalyst is operated but also the composition and structure of the catalyst itself.

It has been known for many years, for example, that conditions of high temperature and low pressure within a reforming system, whilst being beneficial from the point of view of reaction kinetics and equilibria, tend to favour the rapid accumulation of carbonaceous residues on the catalyst surface (61)(62). Consequently, the temperatures and pressures actually employed

in commercial reformers (section 1.1.1) represent a compromise between the desire to attain high product yields and the desire to maintain catalyst stability.

The influence of temperature and pressure on the severity of the coking process has been demonstrated in numerous studies (40)(42)(48)(63). Gillespie and co-workers (63), for example, studied the conversion of n-heptane on a variety of Pt single crystal catalysts and observed that for a given catalyst and a fixed set of conditions, the rate of retention of carbonaceous materials increased almost linearly with increasing reaction temperature. Figoli et al (48) on the other hand, using an accelerated deactivation technique (64), derived non-linear expressions to describe the relationship between the temperature and pressure variables and the amount of carbonaceous material deposited on the surface of a Pt/δ-Al_2O_3-Cl catalyst during naphtha reforming. Moreover, in the case of the pressure dependence, these authors identified a critical value below which the coking rate was particularly severe.

The molar ratio of hydrogen to hydrocarbon (H:Hc) in the feedstock gas mixture and the space velocity have also been shown to exert a considerable influence on the rate and extent of catalyst coking. With respect to the former parameter, several studies have demonstrated that, for a fixed pressure, an increase in the (H:Hc) reactant ratio results in a reduced coking rate and for this reason commercial reforming processes are invariably carried out in the presence of excess quantities of hydrogen gas. The impediment of coke formation in the presence of excess hydrogen has been attributed to the accelerated rehydrogenation and suppression of the unsaturated coke precursor molecules (42)(65).

The dependence of the catalyst coking rate on space velocity has been shown by Eberly et al (44) to be a complex matter. Studying the kinetics of coke deposition during the cracking of n-hexadecane and gas oil on silica-alumina catalysts, these

authors observed that although changes in the rate of coke deposition on the catalyst could be correlated with changes in the space velocity, the exact nature of this correlation was influenced by other factors such as the reaction time and the position within the catalyst bed. Figoli et al (48) have, however, reported that for a fixed coking period and constant conditions, the total amount of carbonaceous material retained on the surface of a Pt/ɣ-Al_2O_3-Cl catalyst during naphtha reforming increased with decreasing space velocity. As with the pressure, a critical space velocity existed below which the coking rate was particularly severe.

Several studies have demonstrated that the rate of carbonaceous residue formation on a reforming catalyst is strongly dependent on the chemical identity of the species present within the hydrocarbon feedstock. Beltramini et al (60), for example, compared the coke forming tendancies associated with a series of paraffinic, naphthenic and aromatic monohydrocarbon feedstocks during their interaction with a bifunctional Pt/ɣ-Al_2O_3-Cl reforming catalyst and observed that, for a fixed coking period, the naphthenic and aromatic feedstocks produced more coke than the paraffinic species. Moreover, in the case of the paraffinic and the aromatic feedstocks, there existed a general trend towards more rapid coke formation with increasing molecular weight, although with the latter species the position and structure of the side chains attached to the aromatic ring were also shown to be important. A similar correlation between molecular weight and coke forming tendancy has been noted in other studies (45)(66).

A number of studies (15)(40), including that of Beltramini et al (60), have identified the C5 naphthenic structure as being particularly potent with respect to coke formation. Indeed, Cooper and Trimm (40) have found that under typical reforming conditions the amount of coke deposited on a bifunctional Pt/ɣ-Al_2O_3 catalyst from a methylcyclopentane feedstock greatly exceeded that produced from a variety of other C6 hydrocarbons including cyclohexane and benzene. Similarly, Bertolacini and

Pellet (15) detected a very significant increase in the rate of coking of a Pt/δ-Al_2O_3 catalyst during naphtha reforming on doping the naphtha with cyclopentane.

The composition and structure of reforming catalysts, like the conditions under which they are operated, are constrained as much by the need to keep the catalyst surface free of carbonaceous residues as by the desire to achieve high activity. The deposition of excess quantities of chlorine on the surface of a reforming catalyst has, for example, been shown by Parera et al (65) and Bishara et al (67) to be coincident with an increase in the rate of coke deposition. This was attributed by both sets of workers to a reduction in the rate of rehydrogenation of the unsaturated coke precursor molecules caused by the action of the chlorine in preventing the spillover of feedstock hydrogen from the metal catalytic function to the support. Thus, although the incorporation of chlorine into a reforming catalyst is essential from the point of view of creating a catalyst with the desired acidic characteristics (section 1.1.2), the amount of chlorine on the catalyst must be kept below a certain limiting value (normally around 1%) if rapid catalyst coking is to be avoided.

It is also a well established fact that the contamination of the hydrocarbon feedstock fed to a reforming catalyst by sulphur containing compounds can result in an accelerated decline in catalyst activity (1)(62). The sulphur compounds are thought to adsorb irreversibly on the metal catalytic sites which thus prevents the adsorption and reaction of the reactant molecules (20)(68). As pointed out previously, however, (section 1.1.2) the addition of a controlled small quantity of sulphur to reforming catalysts is in fact known to be highly beneficial to the catalyst both in terms of an improved selectivity and an enhanced resistance to deactivation. The latter is related to the ability of the sulphur to selectively suppress the intrinsically very high initial dehydrogenation activity of the metal catalytic function (18). As a consequence of this ability, the rate of production of unsaturated coke precursor molecules, and hence coke, is reduced (69).

Hence, as with the chlorine, the amount of sulphur that is normally present in reforming catalysts represents an optimum balance between the processes of catalyst promotion and catalyst poisoning.

Several studies have indicated that the metal loading of a reforming catalyst and the size of the metal crystallites can play a very significant role in determining the degree to which the catalyst becomes covered with carbonaceous residues during use. Barbier and co-workers (51), for example, observed that the total amount of coke retained on the surface of a Pt/ð-Al_2O_3 catalyst during its interaction with a cyclohexane feedstock increased as the metal loading of the catalyst was increased. Other studies have indicated, however, that for a fixed metal loading the metal crystallites themselves become more resistant to coking as the metal dispersion increases. Lankhorst and co-workers (70), for example, studied the reactions of n-hexane over a series of monometallic Pt/SiO_2 catalysts having various average metal particle sizes, and considered that the greater activity and selectivity maintenance exhibited by the more highly dispersed catalysts was indicative of a reduced rate of carbonaceous residue laydown. This phenomenon was attributed by these authors to the greater proportion of edge and corner surface atoms present in the smaller crystallites. According to Somarjai and Blakely (71) such sites are less vulnerable towards coke deposition than those possessing a higher degree of co-ordinate saturation.

The superior activity maintenance exhibited by many bimetallic reforming catalysts relative to the monometallic Pt/ð-Al_2O_3-Cl species (section 1.1.2), has often been attributed to an ability of the secondary promoting metal to inhibit the formation of carbonaceous residues on the active Pt and acidic sites. Margitfalvi et al (72) and Bertolacini and Pellet (15), for example, have proposed that the Re present in Pt-Re/ð-Al_2O_3-Cl is capable of intercepting harmful C5 naphthenic coke precursors that are formed over the Pt during reforming, and converting them into less harmful paraffins through hydrogenolysis. In a similar vein, Carter et al (16) have concluded that the high hydrogenolysis activity of Ir was primarily responsible for the greatly reduced coking rate of Pt-Ir/ð-Al_2O_3-Cl relative to Pt/ð-Al_2O_3-Cl during reforming.

1.2.4 Effect of Carbonaceous Residues on Catalyst Performance

The retention of carbonaceous materials on the surface of hydrocarbon conversion catalysts is known to result in substantial catalyst activity loss. Indeed, in commercial catalytic processes, the rate at which such residues accumulate on the catalyst surface is one of the principal factors in determining the length of time that a catalyst charge remains in use.

The existence of an association between catalyst deactivation and coking is exemplified by the fact that spent catalyst charges can often be restored to their original high activity by regeneration procedures in which the carbonaceous materials are removed from the catalyst surface (61). More direct evidence for such a relationship exists, however, in the fact that the rate of activity decline within a catalytic system can often be directly correlated with the rate of carbonaceous residue formation on the catalyst surface. Toei et al (73), for example, have shown that during the dehydrogenation of n-butane on a chromia-alumina catalyst, the attainment of a stable catalytic activity after an initial period of activity decline was accompanied by the establishment of a limiting concentration of surface carbonaceous materials. Similarly, in the reforming of a hydrocarbon naphtha fraction over a bifunctional $Pt/\delta\text{-}Al_2O_3$ catalyst, Parera et al (41) observed that an initial rapid deposition of carbonaceous material on the catalyst surface coincided with a rapid decline in catalyst activity. Moreover, the gradual decrease in the rate of deactivation that occurred with increasing time-on-stream was paralleled by a corresponding reduction in the rate of carbonaceous residue deposition (48).

As well as being detrimental towards catalyst activity, however, carbonaceous residues have also, on numerous occasions, been shown to be responsible for changes in catalyst selectivity. The ability of the surface residues to selectively suppress certain surface reactions to a greater extent than others has, in general, been attributed to the preferential adsorption of the residues

on the sites responsible for particular catalytic reactions.

In the case of catalytic reforming, attempts to discern the effect of carbonaceous residue deposition on catalyst selectivity have been largely confined to studies involving the interaction of single hydrocarbon species with monofunctional Pt catalysts. Davis, Zaera and Somorjai (42), for example, investigated the role of strongly adsorbed carbonaceous deposits on Pt single crystal catalysts during the conversion of n-hexane. According to these authors, the deposition of the residues on the catalyst surface resulted in a significant enhancement in the selectivity of the catalyst for the aromatisation and hydrogenolysis reactions relative to isomerisation and C5-cyclisation. Moreover, within the isomerisation reaction, the selectivity for 2-methylpentane formation relative to 3-methylpentane formation was lower on the carbon covered surface when compared to the initially clean Pt. Similar results have been obtained by Karpinski and Koscielski (74) and by Lankhorst and co-workers (70) during n-hexane conversion over supported Pt/SiO_2 catalysts. In the latter study (70), Lankhorst and co-workers compared the effect that the deliberate deposition of surface carbonaceous residues had on the activity and selectivity of a series of Pt/SiO_2 catalysts having different metal particle sizes. These workers observed that for each catalyst the major effect of carbonaceous residue deposition was to increase the dehydrocyclisation selectivity with a simultaneous decrease occurring in the isomerisation selectivity.

The extent, however, to which the results obtained from studies involving monofunctional catalysts can be extrapolated to describe the selectivity changes taking place during reforming processes over bifunctional catalysts, remains unclear. Christoffel and Paál (26), for example, have shown that in the reaction of methylcyclopentane over a bifunctional $Pt/\delta\text{-}Al_2O_3$ catalyst, the formation of carbonaceous residues on the surface of the catalyst results in the partial deactivation of the Pt function in as much as it loses its isomerisation and hydrogenolysis activity whilst the dehydrogenation activity remains unchanged.

Figoli et al (48), on the other hand, have provided evidence for the selective loss of dehydrocyclisation activity with increasing carbonaceous residue formation during naphtha reforming over bifunctional Pt/ϑ-Al_2O_3. In accordance with these findings, Beltramini et al (60) observed that the formation of carbonaceous residues on Pt/ϑ-Al_2O_3-Cl during its interaction with n-hexane, produced a significant increase in the isomerisation selectivity of the catalyst whilst simultaneously decreasing the dehydrocyclisation activity.

Thus, despite the considerable amount of effort that has been spent in studying the interaction of carbonaceous residues with reforming catalysts, a satisfactory description of how the surface residues influence the selectivity of a bifunctional catalyst, under its normal operational conditions, has yet to emerge.

CHAPTER TWO

OBJECTIVES OF THE PRESENT WORK

- oOo -

The principal objective of this study is to gain a clearer understanding of the role played by permanently retained surface carbonaceous materials in the catalytic reforming of hydrocarbons over bifunctional Pt/γ-Al_2O_3-Cl reforming catalysts.

To achieve this objective, the following investigations will be undertaken using n-heptane as a model hydrocarbon feedstock:

i) Variations in the activity and selectivity of two different Pt/γ-Al_2O_3-Cl catalysts will be determined under industrial type conditions with a view to examining the relationship between these parameters and the accumulation of carbonaceous materials on the catalyst surface, and to ascertain whether the nature of this relationship is dependent on the physical and chemical characteristics of the catalyst.

ii) The coking characteristics of a reforming catalyst will be examined during reactions performed in the absence of reactant hydrogen to gain an insight into the effect exhibited by hydrogen on carbonaceous residue formation and to establish whether reactant hydrogen influences the way in which the performance of a reforming catalyst is modified by carbonaceous residue formation.

iii) The pre-labelling of the surface of a reforming catalyst with [14-C] labelled carbonaceous materials will be used in conjunction with radiochromatographic techniques as a means of investigating (a) the build-up of carbonaceous materials on the catalyst surface and (b) the possible exchange of hydrocarbon between these surface carbonaceous residues and gas phase hydrocarbon during the catalytic reforming process, with particular reference to the determination of the chemical identity of the hydrocarbonaceous species incorporated into the gas phase products during any such exchange.

CHAPTER THREE

CATALYSTS

- oOo -

3.1 CATALYST PREPARATION AND REDUCTION

Two supported platinum metal catalysts, RC1 and RC2, were used throughout the course of this study. Both catalysts were prepared using a procedure which involved the impregnation of a ϑ-alumina (Al_2O_3) support with chloroplatinic acid (H_2PtCl_6) followed by adjustment of the support chlorine level. The preparations of the two catalysts differed, however, in the relative quantities of reactant materials used in the impregnation and chlorination process, and in the post-chlorination treatment of the catalysts.

The following account describes the impregnation and chlorination procedure as applied to the preparation of catalyst RC1:-

50g. of ϑ-alumina (Condea Alc 169) was mixed with 10 cm^3 of 10% v/v acetic acid and 5 cm^3 of deionised water. This was ground with mortar and pestle to ensure complete mixing. 15g. batches of the mixture were pressed under a pressure of 570 atm. and the resultant granules were then ground and sieved to a diameter of 425-1000 micrometers. The granules were calcined for 84 hours in a 20 l/hr. air flow, the temperature being raised, during an initial period, from ambient temperature to 610°C at a rate of 150°C/hr.

About 5g. of chloroplatinic acid was weighed accurately and dissolved in 25 cm^3 of deionised water with 0.5 cm^3 of concentrated hydrochloric acid. The solution was filtered and made up to 50 cm^3 with deionised water. 2.2 cm^3 of this was added to 47.5 cm^3 of deionised water with 0.05 cm^3 of concentrated hydrochloric acid. 25g. of the calcined ϑ-alumina granules was added to the mixture which was then covered and left to stand overnight. After the excess liquid had been decanted off, the granules were transferred to a porcelain dish and dried in an oven. The temperature of the oven was ramped from ambient temperature to 110°C at 1°C/min and was held there for 3 hours. The dried granules were then

recalcined for 3 hours in a 20 l/hr. air flow with the temperature being raised from ambient temperature to 500°C at 100°C/hr.

The relative quantities of ϑ-alumina and chloroplatinic acid used in this impregnation, were consistent with the preparation of a supported Pt/ ϑ-Al_2O_3 catalyst containing 0.3% by weight platinum.

Neutron activation analysis of the catalyst granules after the impregnation process, revealed a residual chlorine content of ca. 0.42% by weight. To augment the chlorine content, 10g. samples of the impregnated material were loaded, separately, into a reactor tube and were then heated, at a rate of 180°C/hr., from ambient temperature to 500°C in an air flow of 2.0 l/hr. 1.0 molar hydrochloric acid was introduced into the air flow, via a syringe pump and vapouriser, at a constant rate of 3.0 cm^3/hr. to complete the impregnation and chlorine adjustment of catalyst RC1.

Catalyst RC2 was prepared in an identical manner except that the reactant quantities used were consistent with the preparation of a catalyst containing 1.0% by weight platinum. Moreover, after the impregnation and chlorination procedure, catalyst RC2 was submitted for reduction and sintering treatment. Small 6g. samples of RC2 were reduced for 24 hours, at 500°C, in a 2.4 l/hr hydrogen flow. The bulk of the reduced material was then sintered in small quantities. Hence, after the catalyst had been subjected to a 1 l/hr. nitrogen flow at 610°C for 4 hours, 3% oxygen was introduced into the nitrogen flow. The oxygen/nitrogen gas blend was flowed over the catalyst, at 1 l/hr. and 610°C, for a further 4 hours. The sintered material was then reduced, once again, under the conditions noted above.

After impregnation and chlorine adjustment, catalyst RC1 was simply reduced for 24 hours at 500°C in a 2.4 l/hr. hydrogen flow.

All catalyst charges were re-reduced in situ before experiments. This final reduction was carried out in a 0.8 l/hr. hydrogen flow with the temperature being raised, steadily, from ambient temperature to 500°C during the initial 24 hours of a 36 hour reduction period.

3.2 CHARACTERISATION OF FRESH CATALYSTS

A range of both physical and chemical analytical techniques were applied to the freshly prepared catalysts in order to characterise them in terms of their specific surface areas, metal dispersions, chlorine contents etc. (Note: much of the work described in the following sections of this chapter was carried out in the laboratories of I.C.I., Wilton during the course of the study).

3.2.1 Hydrogen Chemisorption

Hydrogen chemisorption experiments on the prepared catalysts were performed using a Micromeretics Digisorb 2500 instrument. The selective adsorption of the hydrogen adsorbate onto the platinum metal, at room temperature, provided a convenient method of determining, not only the total platinum surface area exposed or accessible to the adsorbate, but also the mean platinum crystallite diameter ($\bar{d}$) and the platinum dispersion (defined as Pt(s)/Pt(t), where Pt(s) and Pt(t) are the number of surface and bulk platinum atoms, respectively, per unit weight of catalyst).

Assuming an H(ads)/Pt(s) adsorption stoichiometry of 1:1, the quantity of hydrogen adsorbed by the platinum surface at monolayer surface coverage, V_m, as determined from the associated adsorption isotherm, provided a measure of the total number of surface platinum atoms, Pt(s), present per unit weight of catalyst. Taking a value of 6.02 $(\text{Å})^2$ for the cross-sectional area of a surface platinum atom, the specific platinum surface areas of catalysts RC1 and RC2 were calculated (table 3.1).

TABLE 3.1: Determination of Specific Platinum Surface Area

	RC1	RC2
Volume of H_2 (ml) Ads. at Monolayer Coverage (Vm). g^{-1} Catalyst (20°C)	0.204	0.615
Moles of H Atoms Ads. g^{-1} Catalyst	1.82×10^{-5}	5.49×10^{-5}
No.of H Atoms Ads. g^{-1} Catalyst	1.09×10^{19}	3.31×10^{19}
No.of Pt Surface Atoms (Pt(s)) $.g^{-1}$ Catalyst (assuming 1:1 stoichiometry)	1.09×10^{19}	3.31×10^{19}
x 6.02 ($\mathring{A}$)^2 Pt(s)$^{-1}$(($\mathring{A}$)^2 Pt(s)$^{-1}$)	0.66×10^{20}	1.99×10^{20}
Platinum Surface Area ($m^2.g^{-1}$ Catalyst)	0.66	1.99

The dispersions of RC1 and RC2 were easily obtained from these values (table 3.2).

TABLE 3.2: Determination of Platinum Dispersion

	RC1	RC2
No.of Pt Surface Atoms (Pt(s)) $.g^{-1}$ Catalyst	1.09×10^{19}	3.31×10^{19}
No.of Bulk Atoms $.g^{-1}$ Catalyst. (Assuming 0.31% and 1.08% by weight Pt for RC1 and RC2 respectively).	0.96×10^{19}	3.33×10^{19}
Metal Dispersion (%)	113.54	99.40

The mean platinum crystallite diameters ($\bar{d}$) of catalysts RC1 and RC2 were determined using the following relationship:-

$$\bar{d} = \frac{6 \times 10^4}{p.\ Sa} \qquad \ldots\ldots\ldots (1)$$

where $\bar{d}$ = mean diameter of supported metal crystallites (Å)

p = density of platinum ($g.cm^{-3}$)

Sa = surface area per gram of platinum ($m^2.g^{-1}$).

The derivation of this equation is based on a model of a supported metal catalyst in which all the metal particles are assumed to be spherical and of identical size. The platinum density ($p = 21.45\ g.cm^{-3}$) and the appropriate Sa value ($212.90 m^2.g^{-1}$ Pt, and $248.75 m^2.g^{-1}$ Pt for RC1 and RC2, respectively,) were substituted into equation (1) to obtain the $\bar{d}$ values that are shown in table 3.3.

TABLE 3.3: Mean Platinum Crystallite Diameters

	RC1	RC2
Mean Platinum Crystallite Diameter ($\bar{d}$)	13.14 Å	11.24 Å

3.2.2 Transmission Electron Microscopy

Transmission electron microscopy was used in an attempt to corroborate the mean platinum crystallite diameter ($\bar{d}$) values obtained from the hydrogen chemisorption analysis (section 3.2.1) and, moreover, to determine the platinum crystallite size distribution of catalysts RC1 and RC2. For catalyst RC1, the distribution of platinum crystallite sizes, as determined by this technique, is illustrated in figure 3.1. The graph indicates

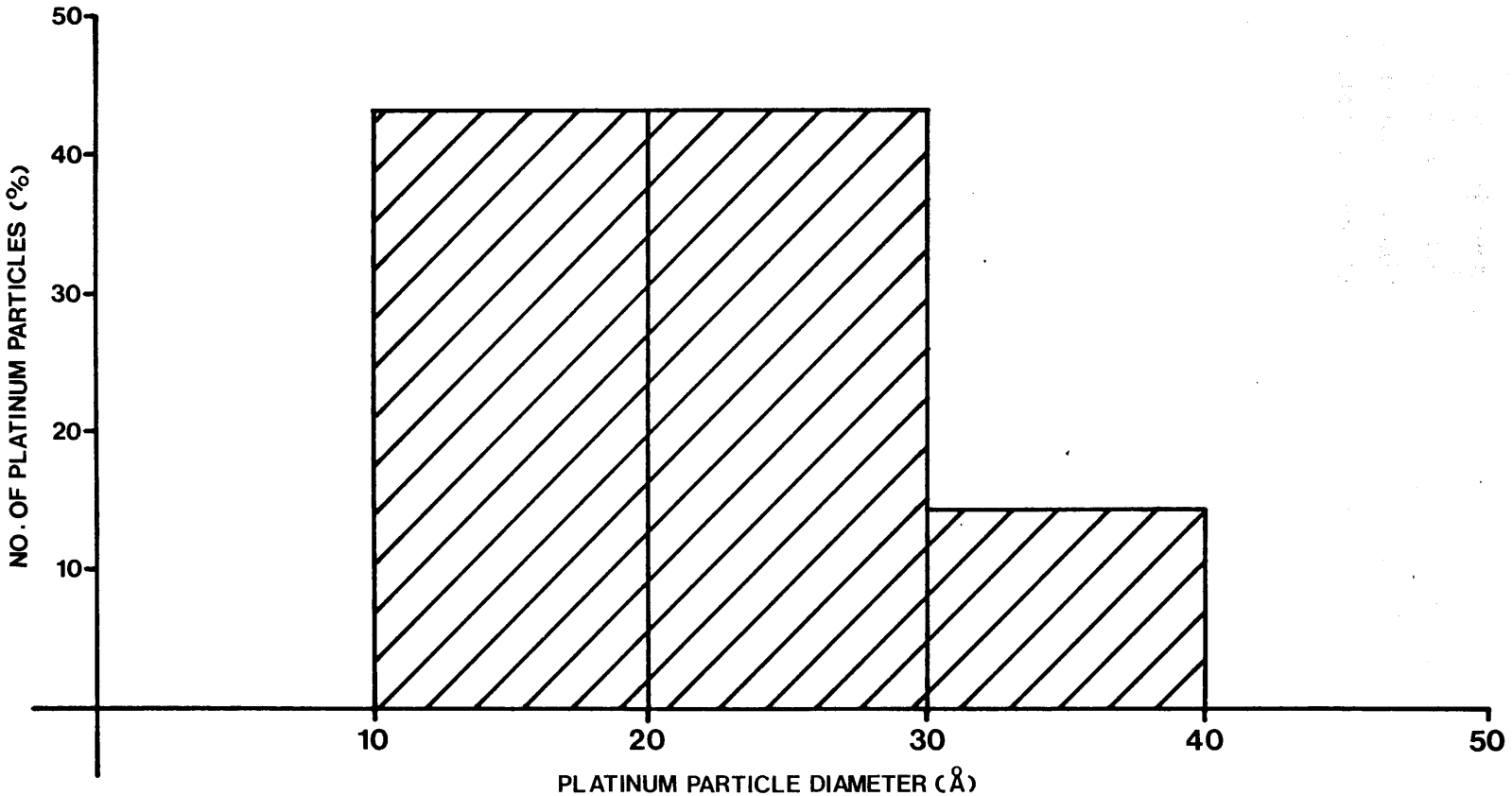

Figure 3·1 – Distribution of Platinum Crystallite Sizes for RC1(T.E.M)

a mean crystallite size of 22Å. Although the $\bar{d}$ value specified here for catalyst RC1 is in excess of the corresponding hydrogen chemisorption value, it should be noted that the transmission electron microscopy technique is not conducive to the detection of particles with a diameter of <10Å. Therefore, the $\bar{d}$ value of 22Å is probably slightly exaggerated. No platinum crystallites were detected during the analysis of catalyst RC2 which indicated that all had a diameter of <10Å.

3.2.3 Surface Area Measurement

The specific surface areas of catalysts RC1 and RC2 were measured using a Micromeritics Mic 2200 Rapid Surface Area Analyser which had been previously calibrated against surface area standards. The method of analysis used by this instrument involved the uptake of nitrogen gas by the surface of the samples at liquid nitrogen temperature and amounted to a modification of the conventional B.E.T method of surface area determination.

One form of the B.E.T equation which describes the adsorption of gas upon a solid surface is:-

$$\frac{P/Ps}{V[1-(P/Ps)]} = \frac{1}{Vm\ C} + \frac{[C-1]P}{[VmC]\ Ps} \qquad \ldots\ldots\ldots(2)$$

where

V = volume (at S.T.P.) of gas adsorbed at pressure P.

Ps = the saturation pressure (the vapour pressure of liquefied gas at adsorption temperature).

Vm = the volume of gas required to form a monolayer.

C = constant related to the energy of adsorption.

Thus, when experimental data are plotted in the form of (P/Ps)/V[1-(P/Ps)] on the ordinate against (P/Ps) on the abscissa, a straight line generally results for (P/Ps) values between 0.05 and 0.35 (solid line in figure 3.2). The intercept and slope of the straight line are 1/VmC and (C-1)/VmC respectively. The monolayer volume, Vm, can, therefore, be expressed as the reciprocal of the value obtained by summing the slope plus the intercept. The surface area of the adsorbing sample is then calculated from the monolayer covering gas volume Vm, the area covered by a single gas molecule, the Avogadro number, and the molar volume of the gas.

However, the reciprocal slope of a line drawn through, for example, (P/Ps) = 0.30 and the origin (dotted line in figure 3.2) does not differ greatly from that of the solid line drawn through the data points. An approximated line such as this, which requires gas adsorption to be carried out at only one single (P/Ps) relative pressure value, can therefore be used as a means of rapidly determining the specific surface area of a solid. Allowance has to be made, however, for the discrepancy in the intercept values of the two lines. Comparison of the surface areas generated by the two alternative methods, for a large number of corresponding samples, has revealed that the error in the rapid method, due to the neglect of the ordinate intercept, is approximately proportional to the actual surface area of the sample as determined by the full B.E.T determination. Therefore, a calibration graph, expressing the relationship between the surface area values generated by the full B.E.T method and the rapid method, can be constructed to enable corrections to be made to the specific surface area values obtained from the slightly less accurate, but less laborious, rapid method of surface area determination.

The specific surface areas of catalysts RC1 and RC2 were determined on the Mic 2200 instrument by the rapid method

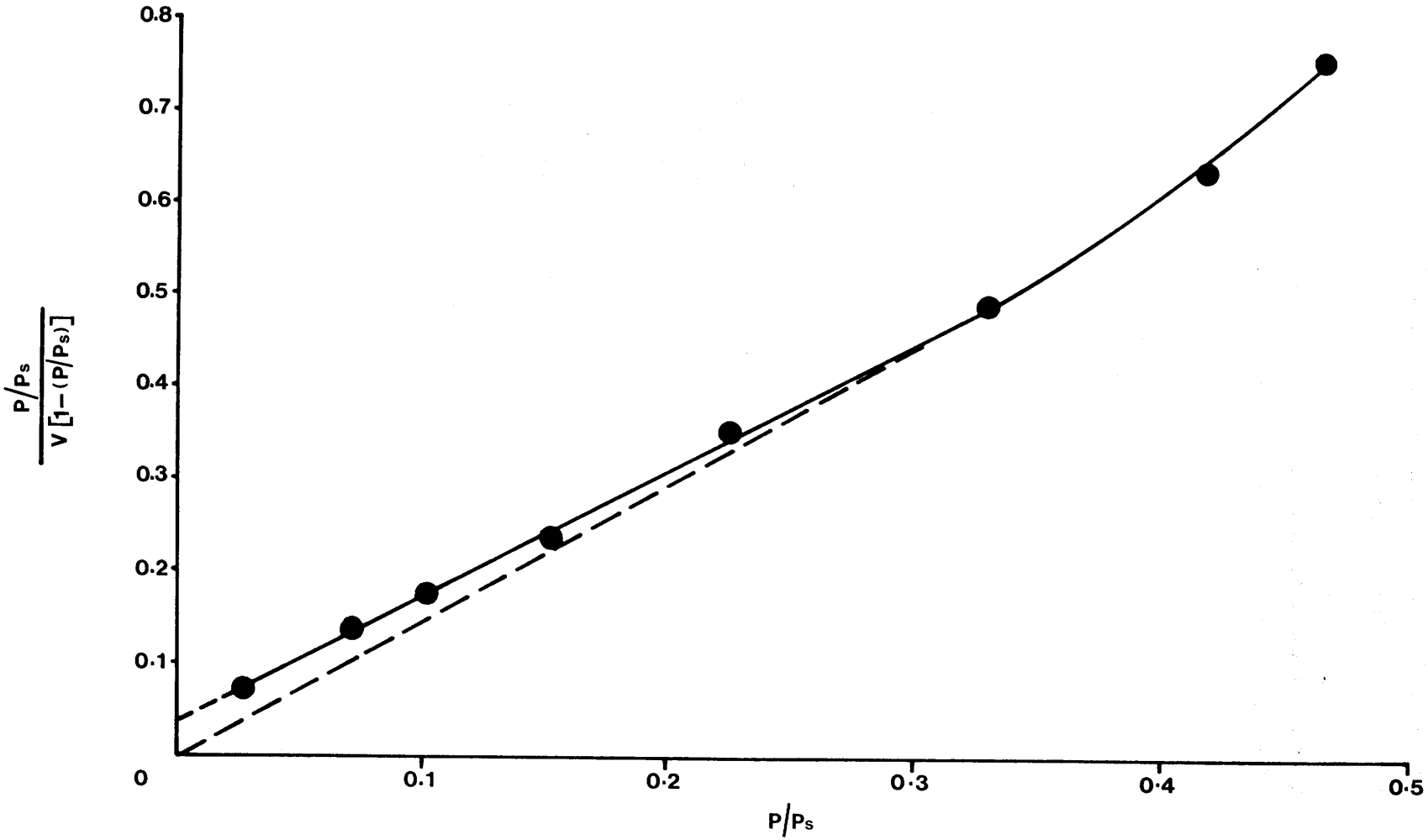

Figure 3·2 – Adsorption of Nitrogen on a Solid Surface at Liquid Nitrogen Temperature.

of analysis. The measurements were based on the volume of nitrogen adsorbed on each sample at liquid nitrogen temperature at the single relative pressure point of 0.3. Before adsorption the catalyst samples were outgassed for 100 minutes at 140°C.

After the appropriate corrections had been made, the specific surface areas of the catalysts were as shown in table 3.4.

TABLE 3.4: Specific Surface Areas of Catalyst RC1 and RC2

	RC1	RC2
Specific Surface Area $.g^{-1}$ Catalyst ($m^2.g^{-1}$)	203.70	98.94

3.2.4 Mercury Porosimetry

The pore structures of catalysts RC1 and RC2 were characterised by mercury porosimetry using a Micromeritics AutoPore 9200 instrument.

Mercury porosimetry analysis is based on the volume of mercury forced into the pores of a sample by an applied pressure, this being measured by the change in electrical capacitance of a cylindrical coaxial capacitor formed by an outer metallic shield around a penetrometer stem and an inner capillary of mercury. As the applied pressure is increased, the uptake of mercury by the porous sample is increased. The total pore volume of a porous sample can, therefore, be derived by increasing the applied pressure until the sample becomes saturated with mercury. The saturation intrusion volume of the mercury is taken as a measure of the total pore volume of the sample.

The calculation of pore diameters is based on the capillary law governing liquid penetration into small pores. This law, in the case

of non-wetting liquids, such as mercury, and assuming cylindrical pores, is expressed by the equation:-

$$D = - (1/p)\ 4\gamma \cos\theta \quad \ldots\ldots\ldots\ldots (3)$$

where D = pore diameter

p = applied pressure at which penetration occurs

γ = the surface tension of the penetrating liquid

θ = the contact angle.

The pore surface area is calculated from the pressure-volume work expended in forcing mercury into the pores. The work dW required to immerse an area, dA, of pore wall is expressed by the relationship:-

$$dW = \gamma \cos\theta \ dA = - PdV \quad \ldots\ldots\ldots\ldots (4)$$

The total pore area is then:-

$$A = - \frac{1}{\gamma \cos\theta} \int_{Vmin}^{Vmax} PdV \quad \ldots\ldots\ldots\ldots (5)$$

where Vmax and Vmin correspond, respectively, to the volume of mercury present in the capillary column when pores of maximum size are first penetrated and when pores of minimum size are filled.

Samples of catalysts RC1 and RC2 were outgassed overnight in an oven, which was maintained at 100°C, before being loaded into the AutoPore 9200 penetrometer sample chambers which were subsequently evacuated to a pressure of 4.5×10^{-2} mm Hg. The samples were maintained at this pressure for 10 minutes. The pressure applied to the penetrometer mercury columns was then increased, incrementally, from an initial pressure of ca 1.5 p.s.i.g to a final pressure of ca 60,000 p.s.i.g with

the cumulative intrusion volume of mercury taken up by each sample being recorded at each of the successive intermediate pressure values. The resultant plots of mercury intrusion volume versus applied pressure are shown in figures 3.3(a) and 3.3(b) for catalysts RC1 and RC2, respectively.

The total pore volume, total pore area and average pore diameter values of catalysts RC1 and RC2 were derived from the graphs using the procedures described and are given in table 3.5.

TABLE 3.5: Pore Structures of Catalysts RC1 and RC2

	RC2	RC1
Total Pore Volume ($cm^3.g^{-1}$)	0.67	0.62
Total Pore Area ($m^2.g^{-1}$)	110.29	203.60
Average Pore Diameter ($mx10^6$)	0.024	0.012

3.2.5 Neutron Activation Analysis

Fresh samples of catalysts RC1 and RC2 were submitted for neutron activation analysis in order to determine both the platinum metal loading and support chlorine level of the prepared catalysts after their respective post-chlorination treatments.

Neutron activation analysis is a trace elemental analytical technique in which an unknown sample is bombarded with thermal neutrons. The chemical elements present within the sample are identified and assayed after irradiation by measurement of characteristic γ-radiation emitted from radionuclides formed in the (n,γ) reaction.

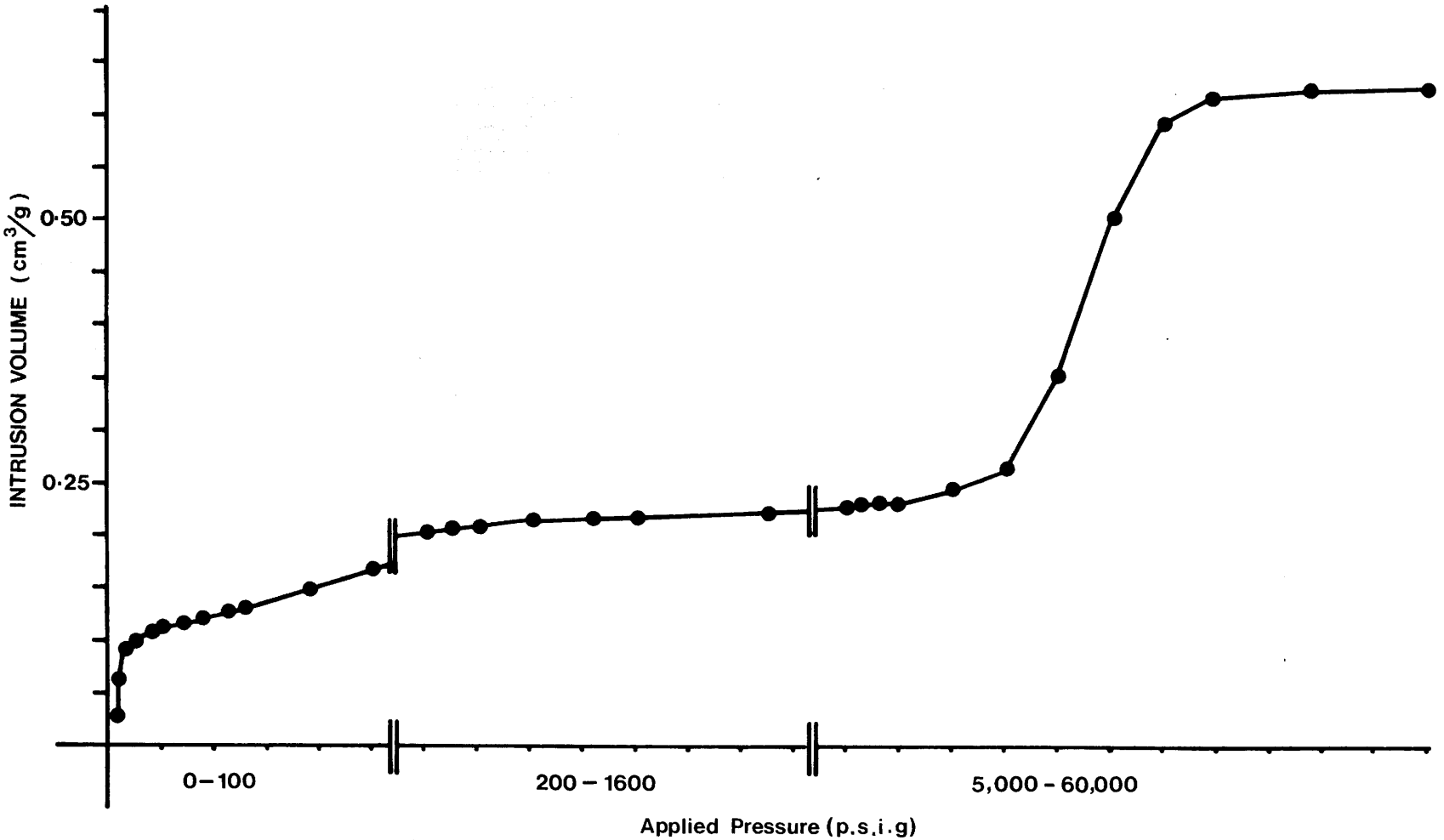

Figure 3·3 (a) – Mercury Intrusion Volume versus Applied Pressure for Catalyst RC1

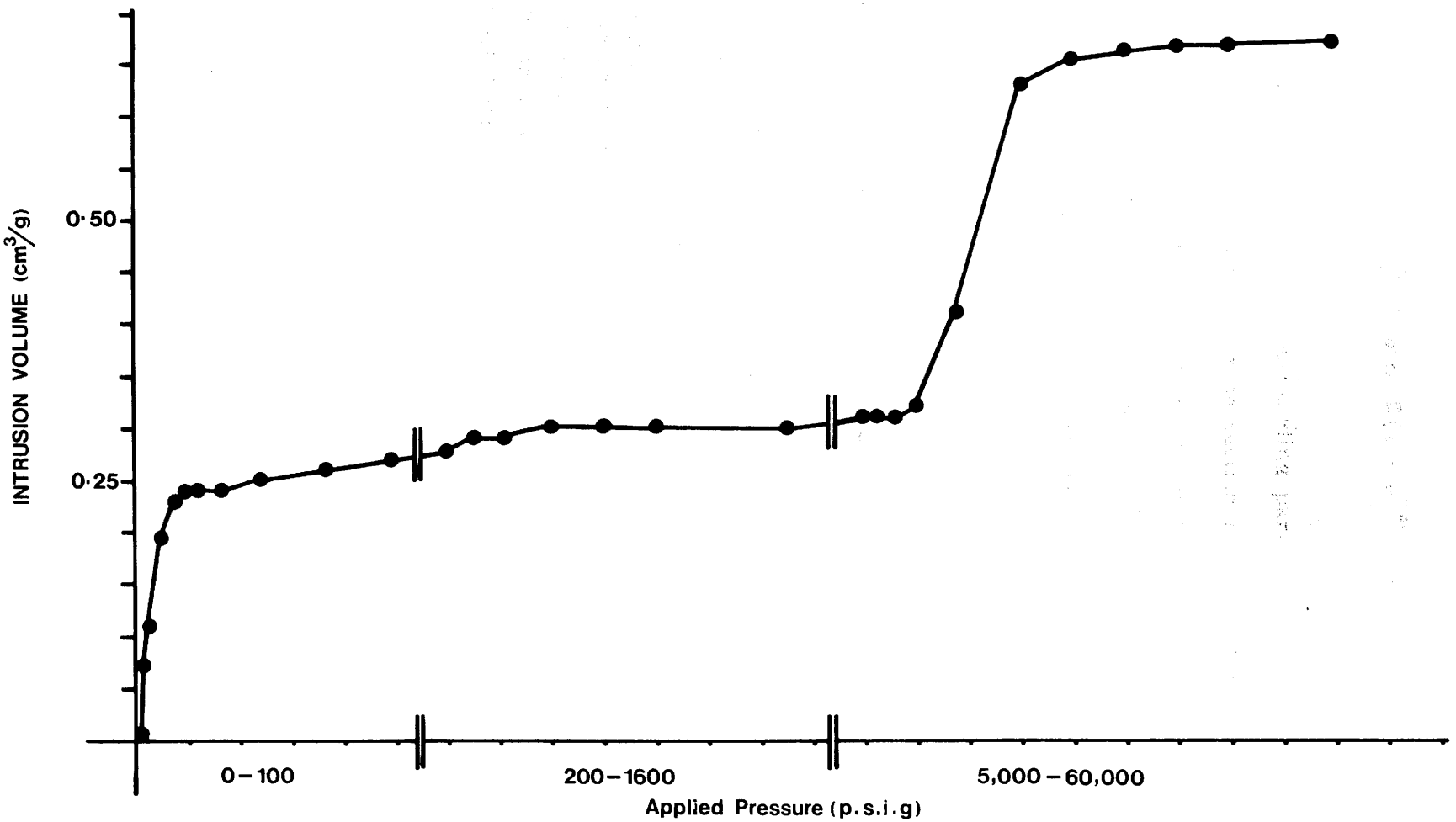

Figure 3·3(b) – Mercury Intrusion Volume versus Applied Pressure for Catalyst RC2

The determination is based on the following equation:-

$$R = \frac{m}{M} N \Phi \sigma E(1 - e^{-\lambda t})$$

where Φ = flux of bombarding particles

σ = capture cross section for target nuclide

λ = decay constant of γ-emitting nuclide

t = irradiation time

E = efficiency of detector

R = counting rate at end of irradiation

m = mass of sample

M = atomic weight of elemental species analysed

N = Avogadro number

Samples of RC1 and RC2, weighing 0.103g and 0.096g respectively, were irradiated in a fixed neutron flux for 45 seconds along with standard samples which contained known quantities of chlorine and platinum. For each of the catalyst and standard samples, the resultant emitted γ-rays, the energy and half-life of which were characteristic of the ^{38}Cl and ^{197}Pt nuclides formed during the irradiation period, were counted for 10 minutes using a Ge(Li) detector. The specific weights of chlorine and platinum in catalysts RC1 and RC2 were obtained (table 3.6) by comparing the ^{38}Cl and ^{197}Pt activities of the catalyst samples, at the end of the irradiation period, with those of the standard samples.

TABLE 3.6: Platinum and Chlorine Contents of Catalysts RC1 and RC2

	RC1	RC2
Weight % Platinum	0.31	1.08
Weight % Chlorine	0.77	1.26

3.3 ANALYSIS OF SPENT CATALYSTS

After each experiment several samples of the spent catalyst charge were recovered from the reaction chamber and subsequently examined. This section is confined to a description of the analytical techniques used in the spent catalyst analysis. Selected results from the analysis are referred to, where appropriate, throughout the ensuing chapters.

3.3.1 Neutron Activation Analysis

This enabled comparisons to be made between the chlorine contents of the spent catalyst samples and those of the corresponding fresh samples. The neutron activation analysis of the spent catalyst samples was identical to that of the fresh catalysts which has been described previously (section 3.2.5).

3.3.2 Surface Carbon Analysis

The residual surface carbon content of the spent catalyst samples was analysed using a simple combustion technique. Individual samples of spent catalyst were heated to 1100°C in an oxygen atmosphere. Pyrolysis of the surface carbonaceous residues occurred leading to carbon dioxide formation. Gas chromatographic analysis provided a quantitative measure of the carbon dioxide formed, from which the % weight of carbon on the catalyst was obtained.

CHAPTER FOUR
EXPERIMENTAL

- oOo -

4.1 MATERIALS

4.1.1 N-Heptane

All non-radiolabelled n-heptane used throughout the course of this study was puriss p.a. n-heptane as supplied by Fluka. The purity, as measured by gas chromatography, was >99.5%. with a water content of <0.05%. It was used without further purification.

4.1.2 [14-C] Labelled N-Heptane

1-[14-C] n-heptane was prepared from 1-[14-C] n-heptyl bromide by a simple Grignard reaction followed by decomposition with dilute acid to afford the alkane:-

$$C_7H_{15}Br \xrightarrow[\text{Dry } Et_2O]{Mg} C_7H_{15}MgBr \xrightarrow{HCl} C_7H_{16} + MgBrCl$$

Dry magnesium turnings were added to a solution of 1-[14-C] n-heptyl bromide (I.C.I.plc) in sodium dry ether. A small crystal of iodine was added and the mixture heated to initiate the reaction. After the formation of the Grignard reagent, a small sample was quenched by addition of dilute (10%) hydrochloric acid and the mixture extracted with ether. The dried ether solution was distilled to remove the ether then subjected to preparative g.l.c. to isolate the pure n-heptane. This was diluted with inactive n-heptane before use.

4.1.3 Hydrogen

Cylinder hydrogen (B.O.C.Ltd.) was used without further purification.

4.1.4 Helium

Cylinder helium (B.O.C.Ltd.) was used without further purification.

4.1.5 Methane

Cylinder methane (B.O.C.Ltd.) was used as a quenching gas in the gas flow proportional counting system. No purification was made before use.

4.2 THE HIGH PRESSURE MICROCATALYTIC REFORMING SYSTEM

4.2.1 Introduction

The initial part of this study was concerned with the design, construction and calibration of a microcatalytic reforming system capable of operating at temperatures of $\leqslant$500°C and pressures of $\leqslant$20 atm. The desire to operate under these conditions, which simulated those used in an industrial reactor, necessitated that strong building materials be employed and, in accordance with this, stainless steel was used wherever possible. A simplified diagram of the high pressure microcatalytic reforming system is shown in Fig.4.1.

The system consisted of three sections:

i) the feed system
ii) the reactor system
and iii) the analytical system

As such, it was designed to accommodate both continuous flow and non-continuous flow experiments.

4.2.1.1 Continuous Flow Studies

During continuous flow studies the feed system was used to introduce a continuous supply of a hydrogen/hydrocarbon reactant mixture to the reactor system (Fig.4.1). The method by which this was achieved is described in section 4.4.2. Thus, the reactants were flowed over the surface of the catalyst, in an uninterrupted manner, throughout the duration of the continuous flow experiment.

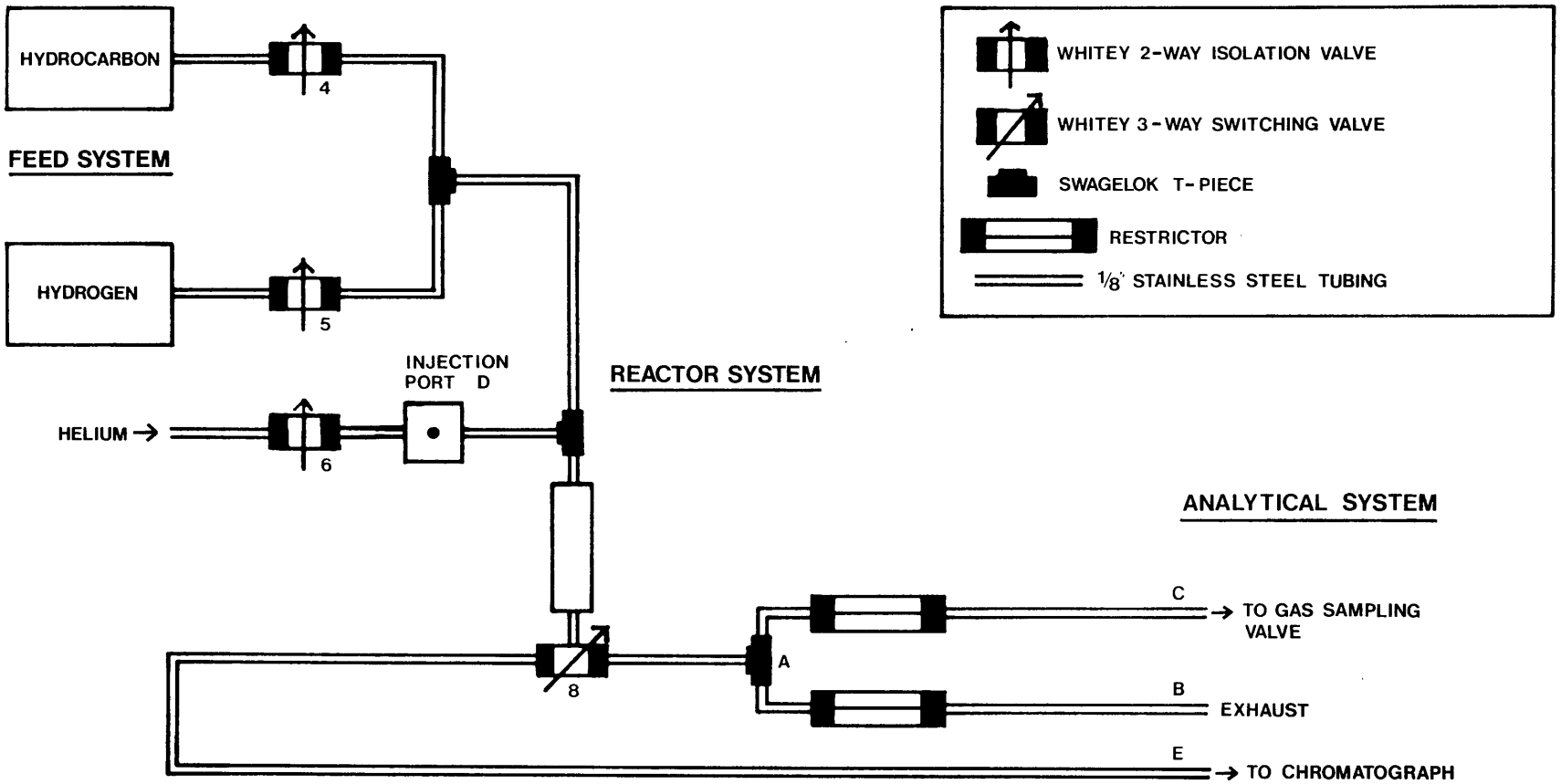

Figure 4.1 – Simplified Diagram of High Pressure Microcatalytic Reforming System

On elution from the reactor system, the gas stream was split into two unequal fractions via a 'T' junction (Fig.4.1.A), the larger fraction being vented to the atmosphere via a restricted exhaust (B). The lesser fraction, which was also ultimately vented (C) but via a finer restrictor, passed through a gas sampling facility which enabled the product gas stream, at any given instant during the continuous flow experiment, to be analysed.

All continuous flow experiments were performed using a non-radiolabelled hydrocarbon feedstock.

4.2.1.2 Non-Continuous Flow Studies

By manipulating isolation valves 4 and 5 (Fig.4.1) the reactor system was disconnected from the continuous flow feed system which allowed non-continuous flow studies, involving either unlabelled or [14-C] radiolabelled hydrocarbon reactant, to be carried out. Under these conditions, using valves 6,8 (Fig.4.1) and 12 (Fig.4.9), the helium chromatographic carrier gas was diverted via the catalyst chamber en route to the chromatograph. The manual injection of liquid hydrocarbon into the carrier gas stream, via a heated injection port situated upstream of the chromatograph (Fig.4.1.D), enabled 'pulse-flow' experiments to be performed. The analysis of product mixtures by gas sampling was not relevant to this type of experiment as any products formed, during passage of the injected pulse through the catalyst chamber, were automatically introduced into the chromatographic columns by the carrier gas stream (E).

Alternatively, the catalyst chamber and injection port were completely isolated from the rest of the microcatalytic reforming system by closing valves 4,5,6 and 8. In this way, liquid hydrocarbon reactant was injected into a 'static' helium filled catalyst chamber. Valves 6 and 8 were then released to

allow the helium chromatographic carrier gas to flow through the catalyst chamber and flush the reaction products directly onto the chromatographic column for analysis (E).

4.2.1.3 Restrictors

These components, which were incorporated into both the feed and reactor sections of the microcatalytic reforming system, were important for maintaining the stability of reactant and product flow rates during continuous flow studies.

A restrictor is essentially a device which regulates the flow of a gas and which is suitable for use under high pressure conditions. A restrictor is not merely a crimp, susceptible to expansion under the influence of a high pressure gas flow, but rather a piece of calibrated crimped tubing which, by its design, experiences equal internal and external pressures. The possibility of expansion, or indeed further compression, of the calibrated restriction, which would have an adverse effect on the stability of the flow rate across it, is thus eliminated. A further benefit of using restrictors as opposed to conventional crimped tubing restrictions is considered in section 4.2.2.

A diagram of a restrictor is shown in Fig.4.2 and the apparatus and procedure used in their construction is described in appendix I.

4.2.2 THE FEED SYSTEM

This section of the microcatalytic reforming system was designed to feed a constant and steady stream of gaseous hydrogen/hydrocarbon reactant mixture to the reactor system during continuous flow studies. To achieve this, separate hydrogen and hydrocarbon component gas streams were combined via a 'T' junction. A schematic diagram of the feedsystem is shown in Fig.4.3.

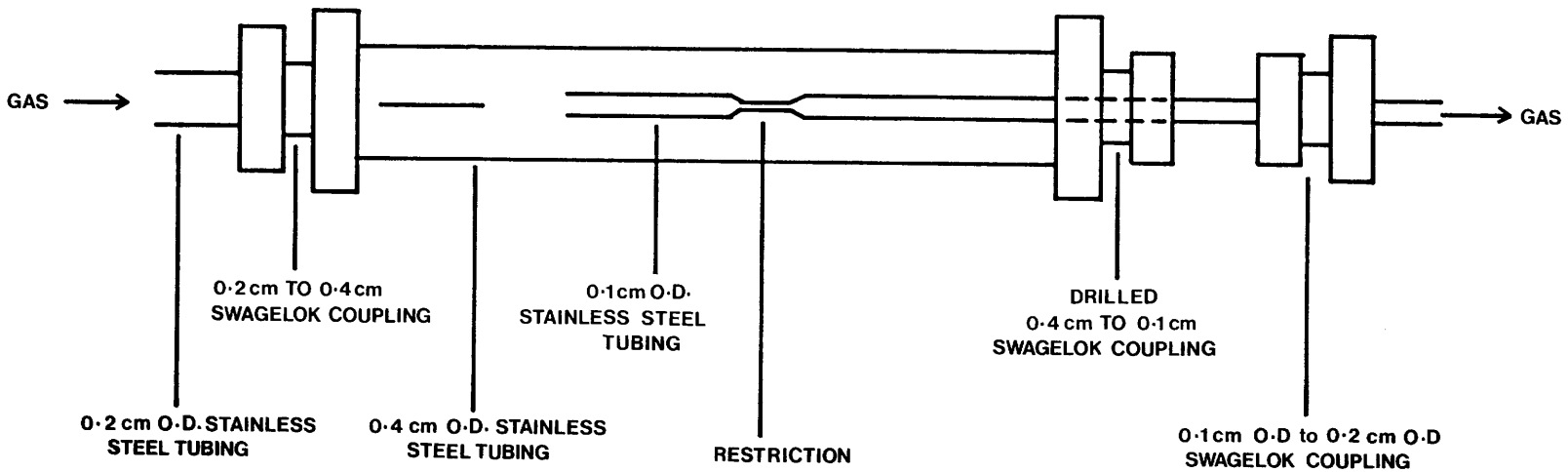

Figure 4·2 – Diagram of a Restrictor.

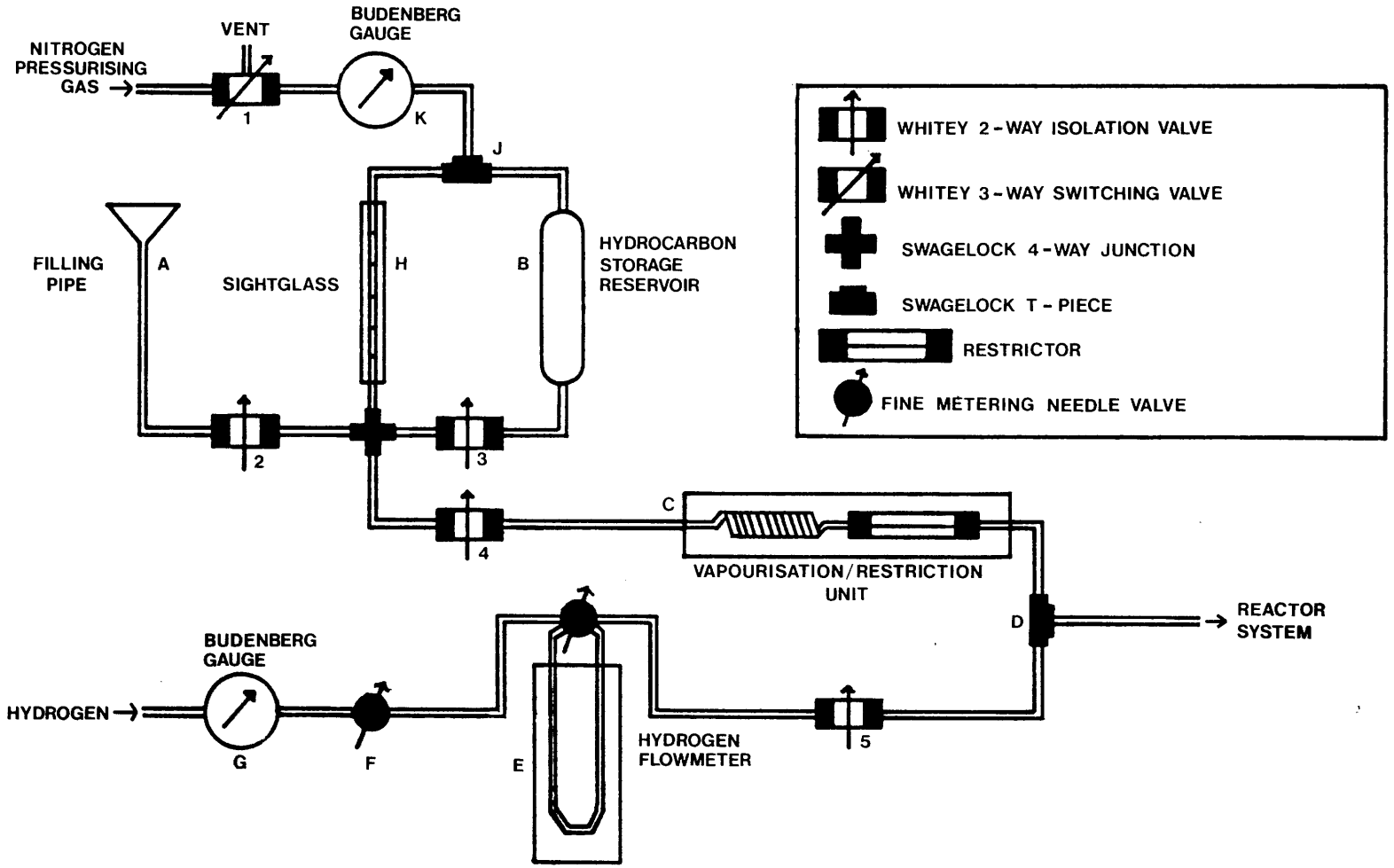

Figure 4.3 – Schematic Diagram of Feed System.

Under atmospheric pressure, liquid hydrocarbon feedstock was directed through a funnelled filling pipe (A) into a 75 ml. stainless steel storage reservoir (B). After isolation from the filling pipe (valve 2), the reservoir was pressurised by introducing a controlled pressure of nitrogen gas into the volume above the level of the liquid hydrocarbon. Under the influence of high pressure nitrogen, a constant flow of hydrocarbon was channelled through the pipework connecting the storage reservoir to a vapourisation/restriction unit (C).

The vapourisation/restriction unit contained a feed vapouriser and a restrictor in series. The former consisted of approximately 30 cm. of 0.3 cm.i.d. stainless steel tubing wound into a spiral and, together with the restrictor, was surrounded by a tubular quartz furnace. The temperature of the furnace was controlled by an external Simmerstat device and was monitored by a thermocouple permanently fixed to the inside wall of the furnace. To minimise heat loss the furnace was enclosed within a box constructed from 1 cm. thick "Sindanyo" insulating board. Using the Simmerstat, the vapourisation/restriction unit was maintained at a temperature of ca.290°C, this being sufficiently in excess of the hydrocarbon feedstock boiling point to ensure that vapourisation was rapid and complete. After passage through the restrictor, calibrated to admit a flow of 1 ml/min. at a pressure differential of 60 p.s.i, the gaseous hydrocarbon flowed on to a 'T' junction (D) where the reactant gas mixture was generated by blending the gaseous hydrocarbon with a stream of hydrogen gas which emanated from the hydrogen limb of the feed system.

A prerequisite for the stable mixing of the hydrogen and hydrocarbon gas streams, in a fixed and well defined ratio, was that the flow rate of both streams could be readily, and accurately, controlled and measured. Therefore, although the hydrogen limb of the feed system was less elaborate than that of the hydrocarbon, with the hydrogen being drawn directly from a cylinder, it did incorporate flow control and measurement facilities.

The flow rate of hydrogen gas through the feed system was measured by directing the gas stream through a U-tube capillary flow meter which was filled with dodecane (Fig.4.3.E). The flow meter operated on the following principle. A small restriction was placed on the hydrogen stream across the two arms of the U-tube manometer which were partially filled with dodecane (Fig.4.4). This was done by adjusting a Nupro fine metering needle valve to a suitable fixed setting. Although the restriction was such that the gas flow was constrained to only a minor extent, a small pressure differential (ΔP) was established across the restriction and, consequently, the dodecane columns in each arm of the manometer adopted different levels (Δh). Increasing the pressure difference across the restriction resulted in a corresponding increase in gas flow. The dodecane columns responded by assuming a new Δh value which was representative of the new gas flow.

Before its installation into the hydrogen limb of the feed system, the flow meter was calibrated by combining it, in series, with a graduated bubble flow meter. The bubble flow meter enabled the relationship between absolute hydrogen flow and the height differential (Δh) response of the dodecane columns in the hydrogen flow meter to be correlated. A plot of hydrogen flow versus flow meter Δh response is shown in Fig.4.5.

A Hoke fine metering needle valve (Fig.4.3.F), situated between the hydrogen cylinder and the flow meter, was used to control the hydrogen stream during continuous flow studies. Adjustment of the valve produced a simultaneous change in the relative levels of the dodecane columns, which thus allowed the Δh value which corresponded to the desired hydrogen flow to be established and maintained.

The hydrogen pressure between the cylinder and the Hoke needle valve was continuously monitored using a Budenberg gauge (0-300 p.s.i.g) (G).

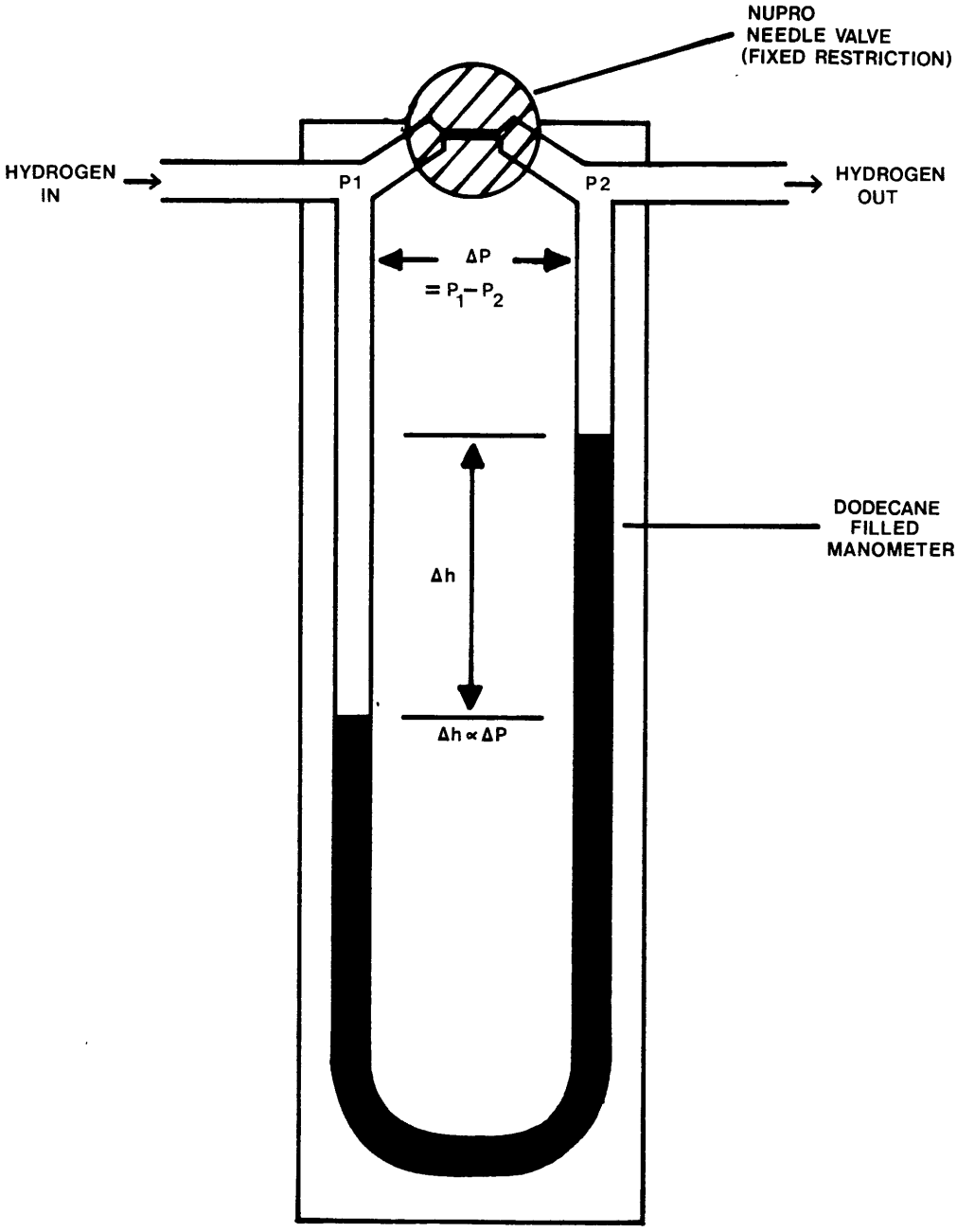

Figure 4.4 – Diagram of Hydrogen Flow Meter

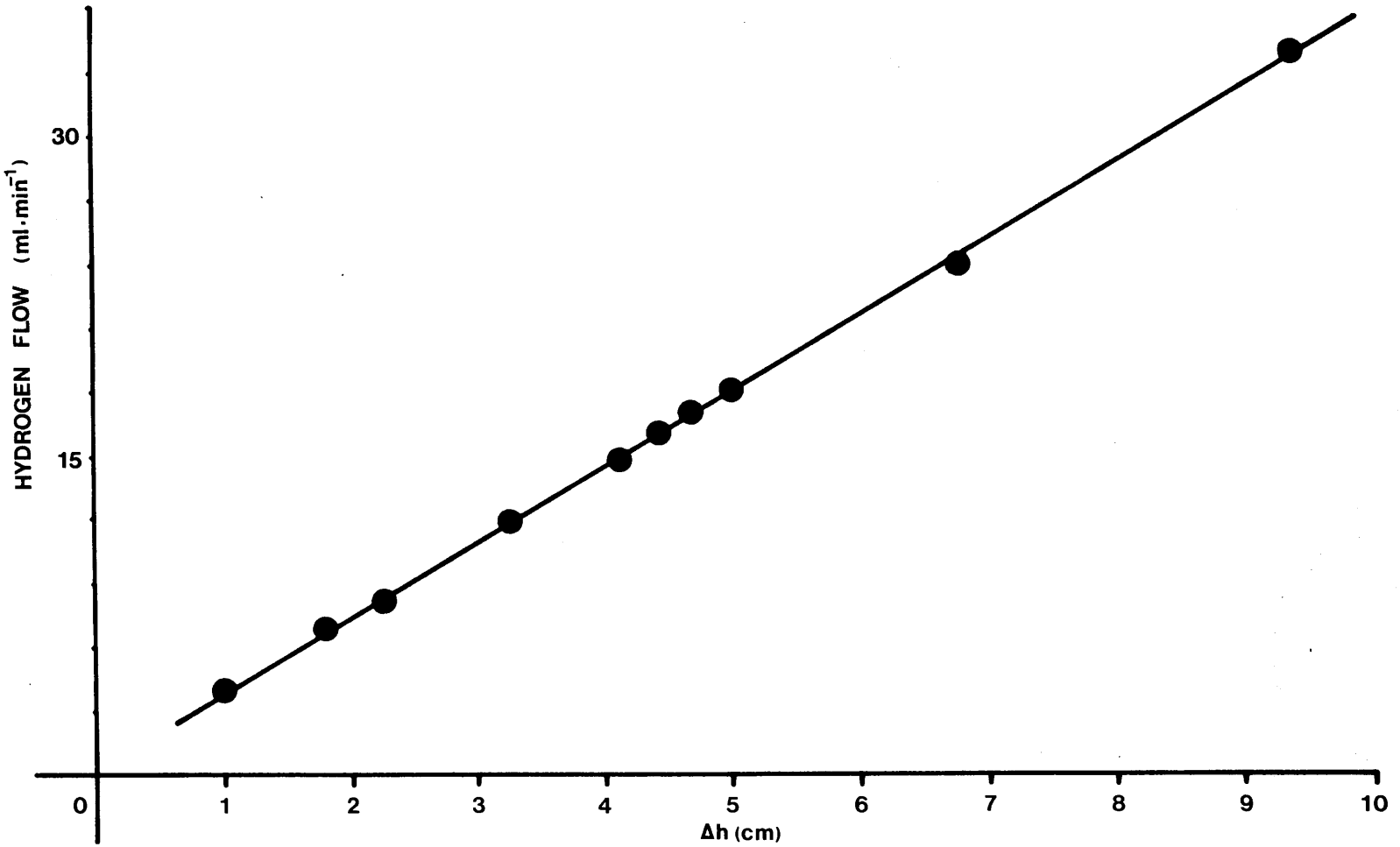

Figure 4·5 – Hydrogen Flow Rate versus Flow Meter Δh·

In the case of the hydrocarbon feedstock, a calibrated sightglass (i.d.1.5 mm) (Fig.4.3.H) permitted the rate of displacement of liquid hydrocarbon from the storage reservoir (B) to be calculated. The sightglass, which measured approximately 18 cm. in length, was tightly secured by two Swagelok couplings in a position adjacent to, and level with, the liquid hydrocarbon storage reservoir.

During continuous flow studies the sightglass and storage reservoir were operated in parallel with one another. Accordingly, the hydrocarbon limb of the feed system was split, temporarily, into two branches (Fig.4.3.J), both of which were identical except that one branch incorporated the storage reservoir whilst the other embodied the sightglass. Thus, the single stream of liquid hydrocarbon feedstock that flowed into the feed vapouriser, was generated by combining two initial contributory hydrocarbon streams of equivalent flow rate. One stream emerged from the storage reservoir whilst the other originated from that branch of the hydrocarbon feed system containing the sightglass. The flow rates of these two streams were equivalent because the two branches of the hydrocarbon feed system were pressurised to the same degree by the nitrogen gas.

It was possible, through closure of isolation valve 3 (Fig.4.3), to halt the issue of liquid hydrocarbon from the storage reservoir. In these circumstances all hydrocarbon fed to the vapouriser was drawn from that which was contained within the sightglass branch of the feed system. Disconnecting the storage reservoir in this manner, did not affect the overall flow rate of liquid hydrocarbon through the feed system. This depended solely on the pressure differential that existed across the fixed restrictor, which remained constant, and it was independent of the pathway along which the liquid hydrocarbon was channelled en route to the restrictor.

Under these conditions, the transparent sightglass enabled the descending level of the liquid hydrocarbon meniscus within the sightglass branch of the feed system to be visually monitored.

As the internal diameter of the graduated sightglass was known, the volume of liquid hydrocarbon displaced, per unit time, could be calculated. Therefore, the sightglass provided a rapid and convenient means of ascertaining the liquid hydrocarbon feed rate. Once the measurement was complete, the liquid hydrocarbon storage reservoir, which held the vast bulk of the liquid hydrocarbon, was reinstated as a feedstock source by reopening valve 3 (Fig.4.3).

During such measurements, although the descent of the liquid hydrocarbon through the sightglass occurred in a steady and continuous manner, the level of the hydrocarbon meniscus was subject to a slight, but continuous, rapid oscillation (±2 mm) about a mean level. This phenomenon was attributed to a corresponding oscillation of the hydrocarbon "boiling front" in the feed vapouriser tubing, as illustrated in Fig.4.6.

The boiling front is the term used to describe the region of interface between the liquid and gaseous phases of the hydrocarbon stream which is undergoing vapourisation. The vapourisation of liquid hydrocarbon at boiling front 1 (Fig.4.6) momentarily cools the walls of the stainless steel tubing adjacent to it. Therefore, the liquid hydrocarbon has to progress further along the vapouriser tubing to a hotter region in order to vapourise, which thus creates a new boiling front, 2. In the meantime the cooled tubing adjacent to boiling front 1 is reheated by the surrounding furnace, and the original boiling front is re-established. In this way, the boiling front in the feed vapouriser tubing migrates continually back and forth between two limits which results in a corresponding fluctuation in the level of the hydrocarbon meniscus in the sightglass.

Some difficulty was experienced, therefore, in accurately reading the instantaneous level of the liquid hydrocarbon meniscus in the sightglass, which could, potentially, have led to erroneous calculated flow rate values. In practice, however, the instantaneous level of the hydrocarbon in the sightglass was estimated by taking

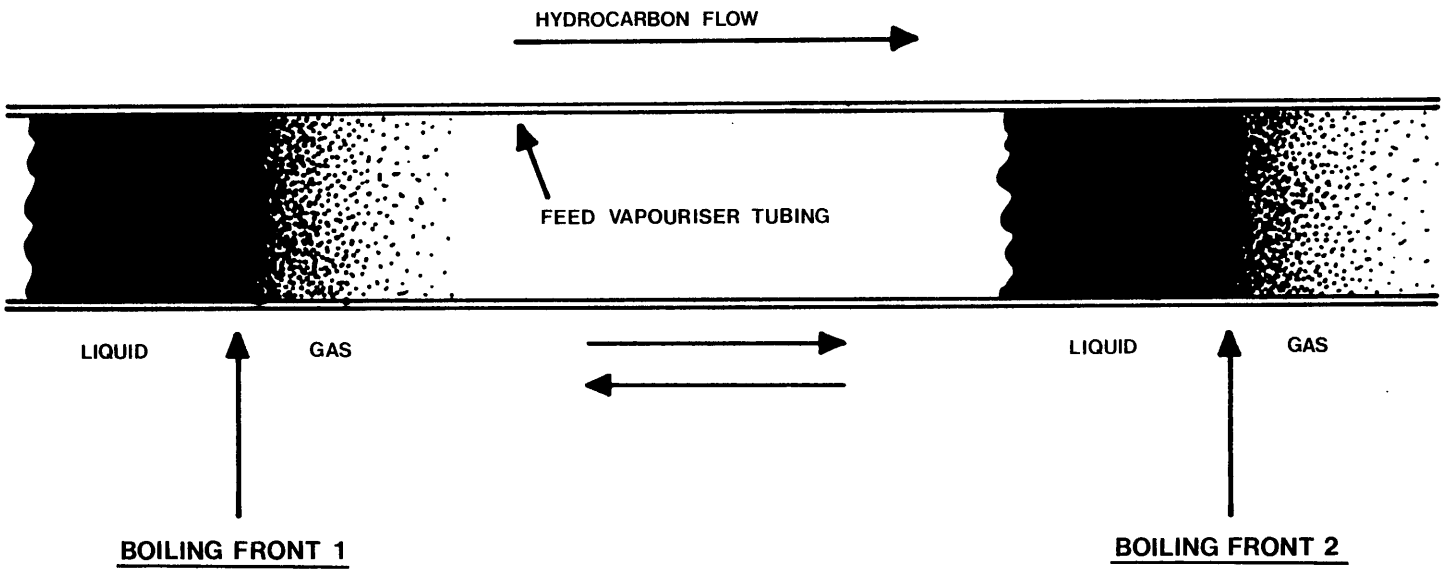

Figure 4.6 – Oscillating Hydrocarbon Boiling Front.

a value midway between the upper and lower limits of the fluctuation in meniscus level. Furthermore, during each flow rate measurement the level of liquid hydrocarbon within the sightglass was allowed to drop ca.10 cm. This large drop ensured that any error associated with reading the initial and final levels of the meniscus was likely to have a minimal effect on each calculated flow rate value. Moreover, to ensure further accuracy, the value actually taken as the feed rate of hydrocarbon during a continuous flow experiment was that obtained by averaging the results of several sightglass measurements which were performed at regular intervals throughout the duration of the experiment.

A further benefit of using a restrictor in series with the feed vapouriser (Fig.4.3.C), as opposed to a conventional crimp, was that, because of the large internal volume of the restrictor (constructed from 0.4 cm.i.d.tubing, Fig.4.2), the fluctuation in the vapourisation process was dampened. This helped to ensure that the flow of gaseous hydrocarbon downstream from the restrictor was steady and uniform.

By maintaining the feed vapouriser at a temperature which was high enough to ensure the complete vapourisation of the liquid hydrocarbon, an increase in hydrocarbon flow rate was induced by increasing the pressure exerted by the nitrogen pressurising gas. This pressure, which was measured by a Budenberg gauge (0-300 p.s.i.g) (Fig.4.3.K), was increased by suitable adjustment of the nitrogen cylinder-head primary control valve. Alternatively, a pressure release valve, 1, used in conjunction with the primary control valve, enabled the nitrogen pressure to be decreased instantaneously, thereby effecting a corresponding abatement in the hydrocarbon feed rate.

The initial step in establishing a hydrogen/hydrocarbon gas stream of a fixed and well defined composition during continuous flow studies, was to fix the hydrogen flow rate at the desired value in the absence of the hydrocarbon. To achieve this, hydrogen was

introduced to the section of the system between the cylinder and the Hoke needle valve control (Fig.4.3) with the latter remaining closed. The needle valve was then gradually opened until the hydrogen flowmeter displayed the Δh value that corresponded to the desired hydrogen flow. The hydrogen flow rate through the overall system was then confirmed by attaching a bubble flowmeter to exhausts E and F (Fig.4.7), in turn, and summing these two component hydrogen flows. The pressure within the hydrocarbon limb of the feed system was then set at an arbitrary value (gauge K, Fig.4.3) which was in excess of that exerted by the hydrogen stream (gauge D, Fig.4.7). Thus, when valve 4 (Fig.4.3), which maintained the hydrocarbon limb of the feed system in a state of isolation, was released, gaseous hydrocarbon flowed into, and mixed with, the hydrogen stream.

The gaseous mixture was passed through the reactor 'bypass' (section 4.2.3.3) and vented in the manner described previously (section 4.2.1.1). Using the gas sampling valve (section 4.2.4.2), samples of the mixture were repeatedly injected into the gas chromatograph for analysis. Application of the appropriate hydrocarbon response factor (section 4.2.4.1) to the resultant chromatograms, which was done automatically by the integrator, enabled the molar quantity of hydrocarbon in each injected sample to be determined. Consideration of the volume of the injected gas samples and of the total flow rate of gaseous mixture through the system, which was measured in an identical way to that of the single hydrogen component discussed above, enabled the feed rate of hydrocarbon reactant through the reactor bypass to be calculated. The feed rate of the hydrocarbon was then gradually adjusted, in the manner described, until the desired hydrocarbon flow rate, and therefore, the desired hydrogen/ hydrocarbon ratio, was achieved.

The chromatographic sampling of the hydrogen/hydrocarbon reactant mixture provided a means of verifying the hydrocarbon feed rate values obtained from the sightglass measurements. Furthermore, through consideration of the variation in the molar hydrocarbon content of successive injected gas samples, it afforded a very convenient way

of monitoring the compositional stability of the reactant gas blend before diversion of the continuous flow reactant mixture through the catalyst chamber.

4.2.3 THE REACTOR SYSTEM

4.2.3.1 General Description

A diagram of the reactor system is shown in Fig.4.7. The reaction chamber itself (A) consisted of a 30 cm. section of 0.4 cm. i.d. glass lined stainless steel tubing. This chamber, which was fixed between two stainless steel Swagelok couplings, was encompassed by a ceramic (pyrophyllite) electrical heating furnace (C) which was, in turn, lagged with 'Tyglas' thermal insulating material. The temperature of the furnace was regulated using a Simmerstat controller and was monitored via a thermocouple permanently fixed in the centre of the furnace.

Catalyst samples (0.25g) were maintained in position, midway along the reaction vessel tube, by glass wool.

During continuous flow operations, the pressure within either the reaction chamber or the bypass (section 4.2.3.2) was monitored by a Budenberg gauge (0-300 p.s.i.g) (Fig.4.7.D). The gauge was connected to either of these two alternative routes by switching valve 9.

Switching valves 10 and 11 (Fig.4.7) were used in conjunction with valves 4,5,6 and 8 (Fig.4.1) when interchanging between continuous flow and non-continuous flow experiments (section 4.2.1.2). Valve 10 connected the chromatograph to the continuous flow gas sampling system or, alternatively, enabled a direct route between the chromatograph and the reaction chamber to be created. Switching valve 11 permitted the reaction chamber to be depressurised or flushed out with carrier gas after a continuous flow experiment.

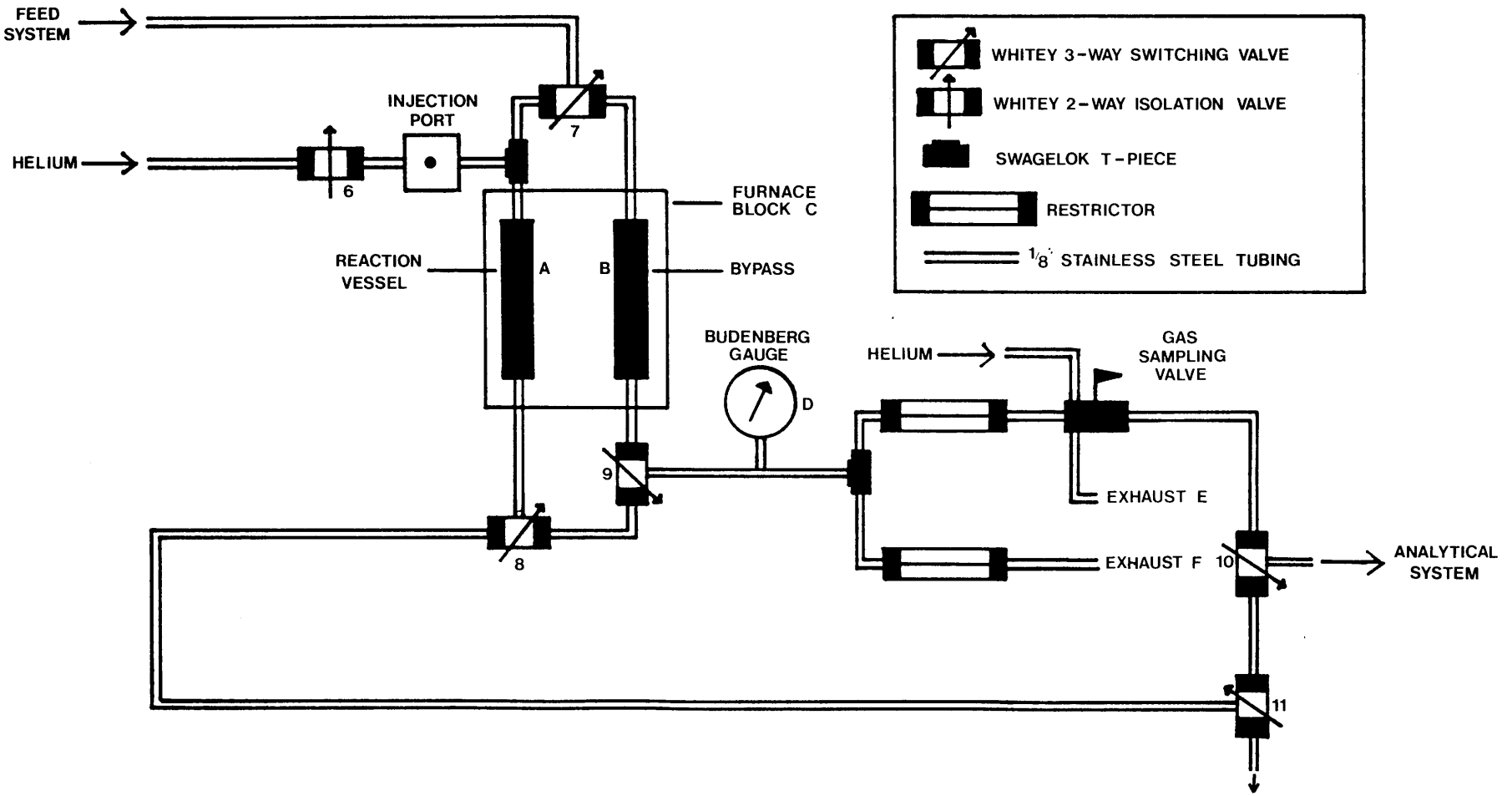

Figure 4·7 – Schematic Diagram of Reactor System.

Where appropriate, the pipework connecting the reactor system to the feed and analytical systems was maintained at an elevated temperature (180°C). This was achieved by binding the stainless steel tubing with electrical heating tape (Electrothermal), the temperature being controlled by Simmerstat and/or Variac transformers. Lagging the pipework, in this manner, eliminated the possibility of any condensation of hydrocarbon taking place after the initial vapourisation of the liquid hydrocarbon reactant had occurred. Thermocouples, placed between the heating tape and the outside wall of the stainless steel tubing, enabled the temperature to be monitored using a Comark type 1602 electronic thermometer.

4.2.3.2 Significance of Reaction Vessel and Catalyst Bed Dimensions

An illustration of the reaction vessel used in this study, containing a sample of catalyst, is shown in Fig.4.8.

The dimensions of the reaction vessel, and of the catalyst bed, are of great significance in any catalytic study involving flowing reactant gases. The diameter of the catalytic reaction vessel is a major factor in controlling both the rate, and mechanism, of the mass and heat transfer processes taking place during the passage of gas phase reactant molecules through the catalyst bed. Hence, unlike a large industrial reaction vessel where the turbulent motion of gas phase reactant molecules is prevalent in gas phase mixing, in a reaction tube of smaller diameter, such as the one used in this study where only laminar flow takes place, the mixing of the gas phase proceeds through the radial diffusion of gas molecules from the centre of the tube, or catalyst bed, to the walls of the vessel, and vice versa. The rate of this radial mixing is governed by the following expression:

$$t = (dT)^2/8Dr$$

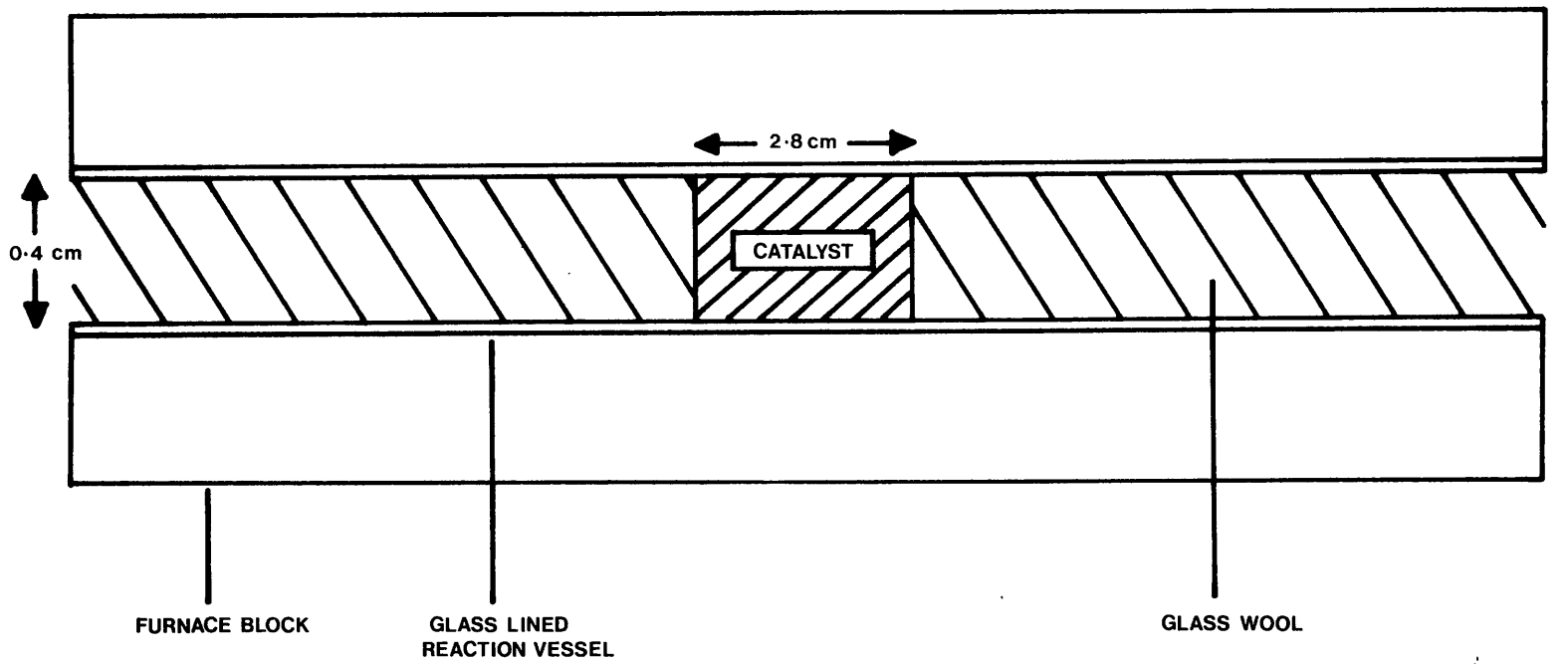

Figure 4·8 – Reaction Vessel Containing Catalyst.

Where t = time taken for a molecule to move from the centre of the reaction tube to the wall (independent of flow rate for laminar flow)

dT = tube diameter

Dr = radial diffusivity

Therefore, as the reaction vessel diameter becomes smaller the rate of radial mixing increases.

Moreover, the rapid radial diffusion operative in small diameter reaction vessels ensures that 'static' or 'stationery' gaseous regions, which can form at the walls of the reaction vessels and around the catalyst particles (wall effects), do not delay the progress of individual molecules through the catalyst bed. Therefore, provided that the catalyst bed is of sufficient length to allow at least one complete radial mixing stage (theoretical plate) to occur (i.e. bed length >> reaction chamber diameter), the concentration of gas phase reactant molecules, and the residence time of individual molecules, within the catalyst bed, is likely to be uniform.

Furthermore, in tubular reaction vessels of small diameter, heat transfer occurs by convection in which the gas phase molecules themselves transport the heat, and it is, therefore, as rapid as mass transfer. Hence, even in the presence of exothermic and endothermic reactions, the temperature gradient across the diameter of the catalyst bed is likely to be negligible when the catalyst vessel is of small diameter.

In the present study, therefore, the dimensions of the reaction vessel, (diameter 0.4 cm.), and of the catalyst bed, (vol.0.35 cm^3, bed length 2.8 cm. = 7 x reaction vessel diameter) (Fig.4.8), were chosen to ensure that the observed product distributions from the continuous flow and pulse-flow experiments, were not influenced by mass and heat transfer limitations.

4.2.3.3 The Bypass

A means whereby, during continuous flow studies, the reaction vessel containing the catalyst could be bypassed, was incorporated into the reactor system. Thus, within the furnace block there existed a further tubular vessel (Fig.4.7.3). This vessel was situated parallel to the reaction vessel and was identical to it in all respects except that it contained no catalyst. Switching valve 7, situated upstream of the furnace block, was used to direct the stream of reactant gases, emanating from the feed system, either over the catalyst or through the bypass. Similarly, with switching valve 8 suitably orientated, switching valve 9 connected either of the two alternative routes to the analytical system. Therefore, as described in section 4.2.2, during continuous flow studies the bypass enabled the desired hydrogen/hydrocarbon reactant flow rate and ratio to be established before the diversion of the reactant stream over the catalyst.

A further benefit of the bypass route was that, during continuous flow studies, it enabled 'blank' experiments to be conveniently performed in situ. Such experiments afforded some indication of the contribution made by non-catalytically produced products to the observed experimental catalytic product distributions. In the case of the pulse-flow and static experiments, blank runs were performed without utilising the bypass facility. In these cases blank runs were carried out as separate experiments using the procedures laid down in section 4.2.1.2, but with a reaction vessel from which all traces of catalyst had been removed. In the non-continuous flow experiments, blank experiments also enabled the reproducibility of the microsyringe injection procedure and associated chromatographic analysis to be examined (section 5.2.2).

4.2.4 THE ANALYTICAL SYSTEM

A schematic diagram of the analytical system is shown in Fig.4.9.

4.2.4.1 Gas Chromatographic Analysis

The chromatographic analysis of product mixtures was carried out using a Pye Unicam PU 4500 thermal conductivity chromatograph equipped with a Pye Unicam PU 4810 computing integrator for the identification, measurement and display of chromatographic peaks. A single 4m x 0.2 cm.i.d. stainless steel column packed with Chromosorb 101 (mesh size 60-100) was used for product separation. Helium was used as the carrier gas.

Unfortunately a flame ionisation chromatographic instrument equipped with a linear temperature programmer, which had been shown to produce the best resolution of potential products, was unsuitable. This was because a non-destructive method of chromatographic detection, such as thermal conductivity detection, was required in order to permit the subsequent radioanalysis of the separate product compounds during [14-C] radiolabelling experiments.

It was found, in general, that reaction products could not be resolved to a satisfactory degree by operating the PU 4500 chromatograph under isothermal conditions. Therefore, in the absence of any automatic temperature programming facility, a temperature programme consisting of three isothermal temperature periods was developed. Thus, in almost all instances, the separation and elution of product compounds was achieved by introducing the product mixtures to the chromatographic column preheated to 110°C. This initial temperature was held constant for the first six minutes of each chromatographic run. The column oven was then rapidly heated to an intermediate temperature of 160°C. After a further fifteen minutes at 160°C

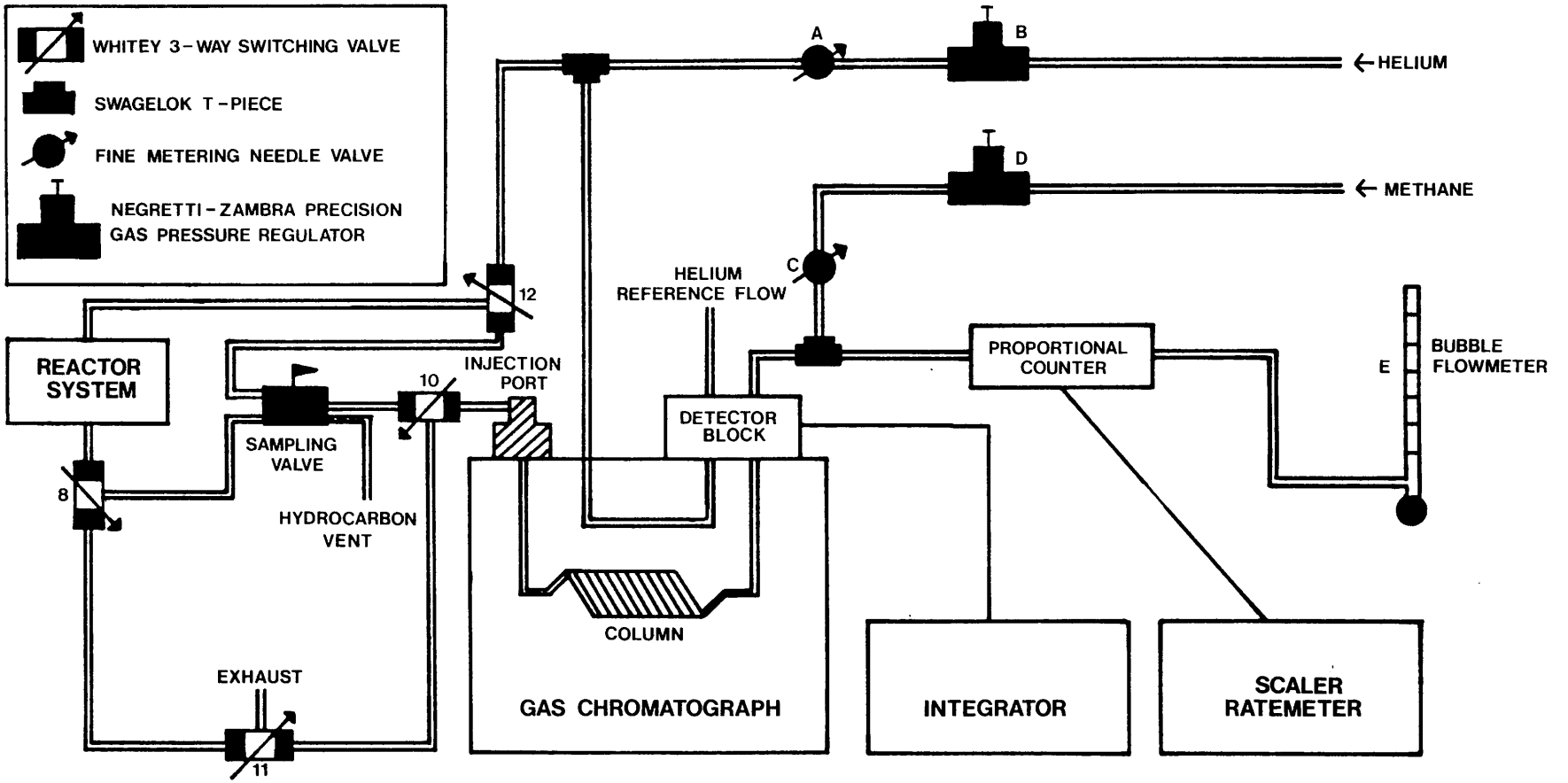

Figure 4.9 -Schematic Diagram of Analytical System.

the temperature was finally increased to 225°C. Maintaining the oven at this temperature, for a further short time period, ensured the elution of any remaining products to complete the chromatogram.

Before the injection of any product samples into the chromatograph, and with the column oven at 110°C, the helium carrier gas flow rate was stabilised at 40 $ml.min^{-1}$ by adjusting a Nupro fine metering needle valve (Fig.4.9.A) used in association with a Negretti Zambra precision gas pressure regulator (B). This flow rate remained constant during the initial isothermal period of the chromatographic runs. However, increasing the temperature of the column oven, in the stepwise manner described, produced a corresponding decrease in the helium flow rate. Thus, during the 160°C and the 225°C isothermal periods the carrier gas flow rate dropped to 32.4 $ml.min^{-1}$ and 24.2 $ml.min^{-1}$ respectively.

A consequence of the stepwise decrease in helium flow rate during a chromatographic run was that the resultant chromatograms, generated by the integrator, exhibited non-horizontal baselines. A sharp, positive deviation away from the stable baseline level traced during the initial isothermal period, was incurred immediately after each temperature increase. During each ensuing isothermal period the baseline gradually descended back to its original level.

Figure 4.10 illustrates the anomalous nature of the baselines generated by the chromatographic temperature programme.

The extent to which the baseline deviated from the initial horizontal level depended only on the size of the associated temperature increment and the integrator sensitivity settings. These parameters were not generally varied between chromatograms which ensured that a non-horizontal baseline trace, identical in character and magnitude of irregularity, was common to all chromatograms. This reproducibility permitted the computing

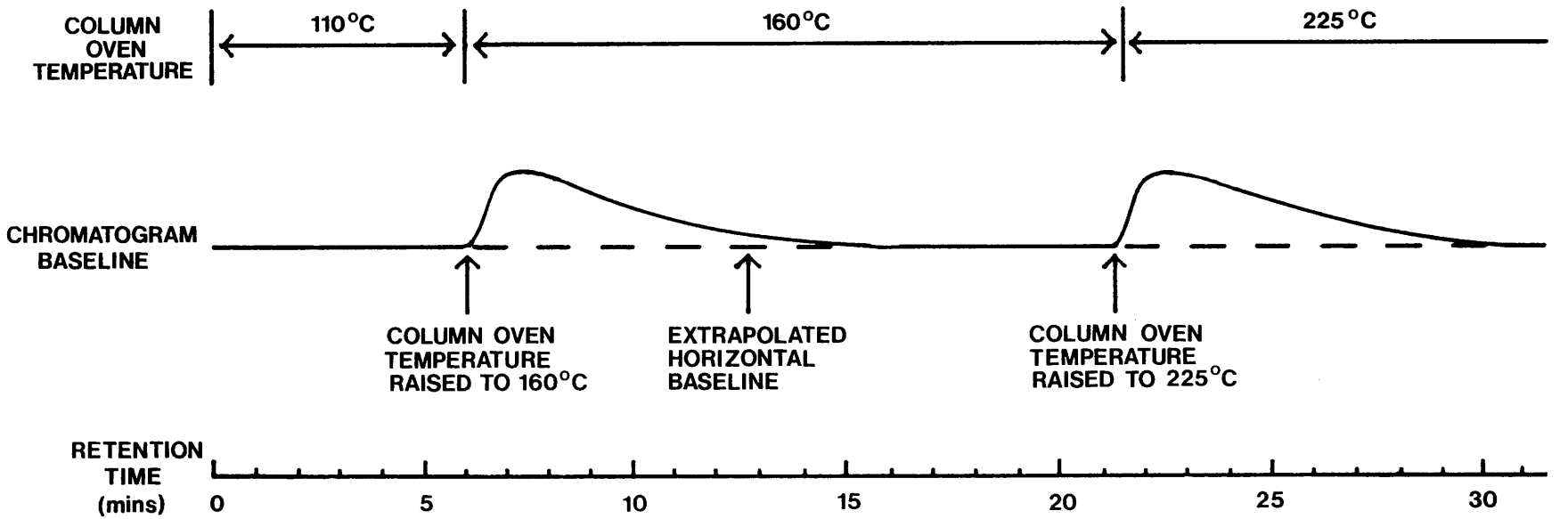

Figure 4·10 –Chromatogram Baseline Generated by Temperature Programme.

integrator to be programmed such that the automatic integration of peaks appearing during the intermediate and final isothermal periods of a chromatographic analysis was performed on the basis of peak area above the deviant baseline and not peak area above the extrapolated horizontal baseline.

The retention times and response factors of all potential reaction products, and of the hydrocarbon reactant, were determined by making unique injections of a known quantity of each compound into the chromatographic column via a chromatographic injection port. Injections were made using a graduated liquid-tight or, where appropriate, gas-tight microsyringe. Before each injection the column oven was preheated to 110°C and the helium carrier gas flow rate stabilised at 40 $ml.min^{-1}$. In all instances the chromatographic temperature programme was commenced upon injection. The calibration procedure was repeated several times for each individual compound and, therefore, all retention times and response factors quoted represent average values. The retention times and response factors of all compounds relevant to this study are given in table 4.1.

The response factors were found to be independent of the integrator sensitivity settings. These settings merely allowed the size of the peaks appearing on the chromatograms to be controlled. Thus, for equivalent repeated injections of a given compound into the chromatograph, each resultant integrator printout reported an "area units" value that was within experimental error of all the other area units values, regardless of the sensitivity at which the corresponding chromatogram had been recorded.

Although the chromatographic conditions employed during the course of this study were developed to produce an optimum separation of product compounds, the resolution of peaks appearing on chromatograms was still often incomplete. This was particularly so in the case of the iso and normal isomers of a given hydrocarbon species where some degree of peak coalescence was generally

Table 4·1 – Chromatographic Retention Times and Response Factors.

COMPOUND	RETENTION TIME (MINS)	RESPONSE FACTOR (AREA UNITS × 10^{-12} · MOL^{-1})
METHANE	0·92	1·64
ETHANE	1·25	1·95
PROPANE	2·05	4·72
ISO – BUTANE	3·67	12·50
BUTANE	4·50	14·60
BUTENE	5·25	14·60
ISO – PENTANE	7·47	4·20
PENTANE	7·98	7·24
PENTENE	8·75	7·24
ISO – HEXANE	10·35	6·00
HEXANE	11·20	13·30
HEXENE	11·95	13·30
ISO – HEPTANE	14·75	21·60
HEPTANE	15·48	23·20
HEPTENE	16·25	23·20
TOLUENE	22·80	18·70

observed. In such cases, a divisory peak boundary was automatically defined by the integrator before integration was performed (Fig.4.11[a]). This boundary was dropped vertically to the baseline from the point on the chromatographic trace between the two peak maxima where the peak gradient was zero. Moreover, in all instances of fused peaks, the individual peak areas were reapproximated manually, using the triangulation method of measurement (Fig.4.11[b]), in order to confirm the reliability of the integrator analysis.

4.2.4.2 The Gas Sampling System

An air tight Valco 8 port injection gas sampling valve (high temperature model) was used to inject fixed volumes of the product gas mixture into the chromatograph during the continuous flow studies. The valve incorporated two identical 4 ml. gas sampling loops, A and B, which were used alternately (Fig.4.12). Thus, in position 1 the post-reactor gas stream was vented to the atmosphere via sample loop A with the helium chromatographic carrier gas being directed through sample loop B. The contents of sample loop A, at any given instant, could be flushed by the helium carrier gas, onto the chromatographic column by manually switching to position 2. When required, a further product sample could be delivered to the chromatograph from sample loop B by returning the valve to position 1.

The entire gas sampling valve was maintained at a temperature of approximately 180°C by electrical heating tape (Electrothermal) in order to eliminate hydrocarbon condensation.

4.2.4.3 The Gas Proportional Counting System

The radiochromatographic analysis of [14-C] labelled product mixtures was performed using a gas flow proportional counter operating in series with the gas chromatograph (**75**) (Fig.4.9). The chromatograph provided a means of separating and detecting eluted compounds which was non-destructive. Thus, the [14-C]

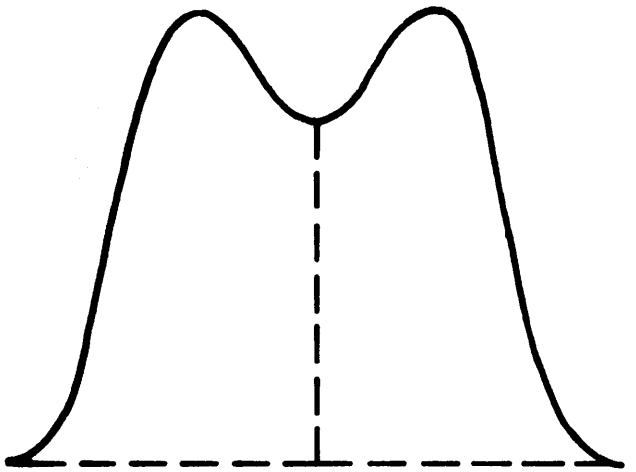

Figure 4·11 (a) – Divisory Peak Boundary Defined by Integrator

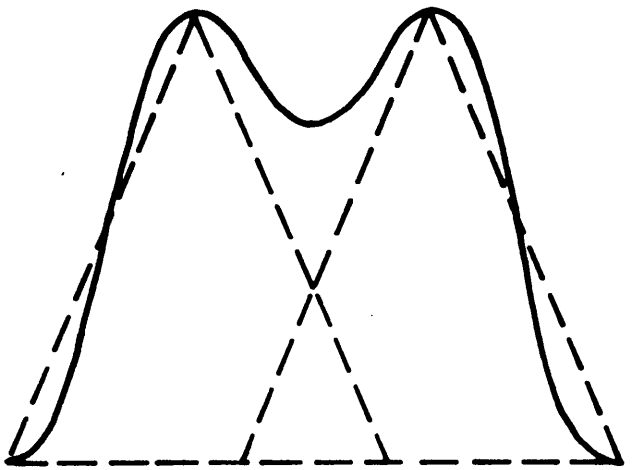

Figure 4·11 (b) – Triangulation Method of Peak Integration

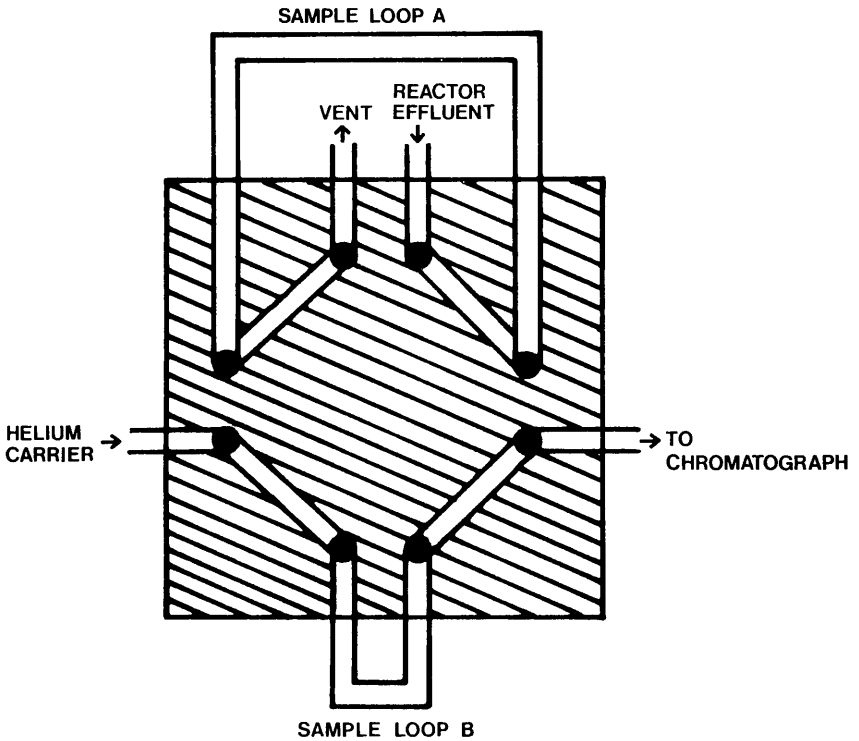

POSITION 1

LOOP A COLLECTION

LOOP B INJECTION

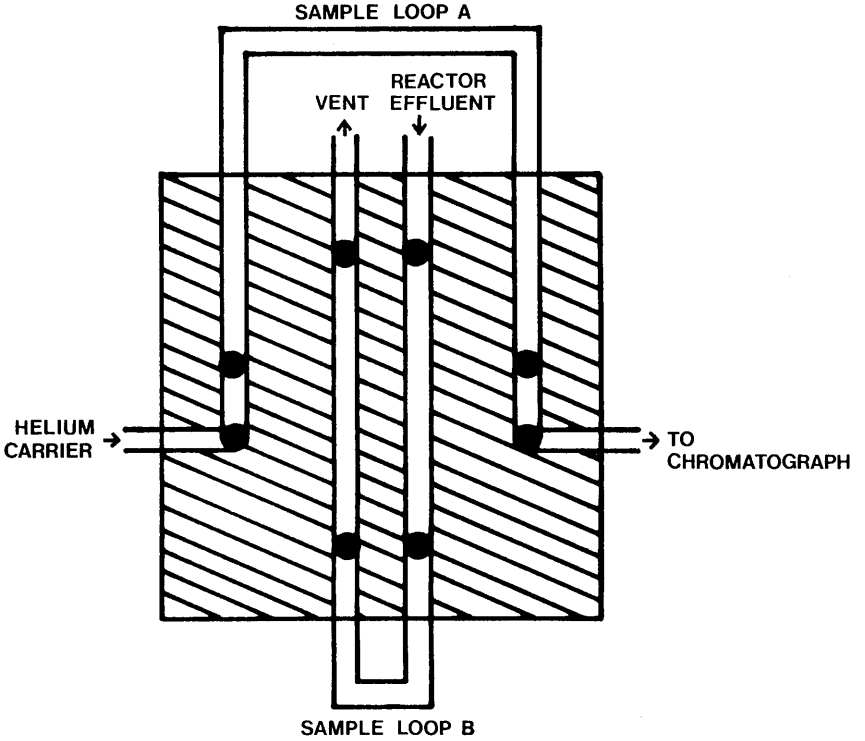

POSITION 2

LOOP A INJECTION

LOOP B COLLECTION

Figure 4·12 – Positions for the Gas Sampling Valve.

content of each successive eluted species could be analysed uniquely during its subsequent passage through the gas proportional counter.

The gas proportional counter, which was constructed primarily from brass and teflon, was similar in design to that described by Schmidt-Bleek and Rowland (**76**) (Fig.4.13). The anode, which consisted of a length of 0.01 cm. diameter stainless steel wire, was suspended in a central position along the length of the cylindrical shaped void enclosed by the brass cathode casing. The anode and cathode were isolated from one another by teflon insulating joints. The proportional counter was connected to a scaler ratemeter (ESI 5350) via a pre-amplifier (ESI 425) and operated using the optimum ratemeter settings described previously (**77**).

Before entering the gas proportional counter, the effluent helium stream from the chromatograph was blended with methane gas to generate a suitable counting gas medium for the radioanalysis of eluted compounds. A helium/methane gas ratio of 10:1 was used throughout the present study. The methane flow, like that of the helium described earlier, was controlled by a Nupro fine metering needle valve used in association with a Negretti Zambra precision gas pressure regulator (Fig.4.9.C and D). Thus, with the column oven initially at 110°C, the desired 10:1 ratio was established by first stabilising the helium flow through the analytical system at 40 $ml.min^{-1}$, as indicated by the bubble flow meter (E). The methane flow was then gradually increased, by adjustment of the methane needle valve, until the required combined flow rate of 44 $ml.min^{-1}$ was achieved.

In order to maintain the 10:1 helium/methane ratio throughout the duration of a radiochromatographic analysis, compensation had to be made to allow for the stepwise decrease in helium flow rate. Thus, as each of the column oven temperature

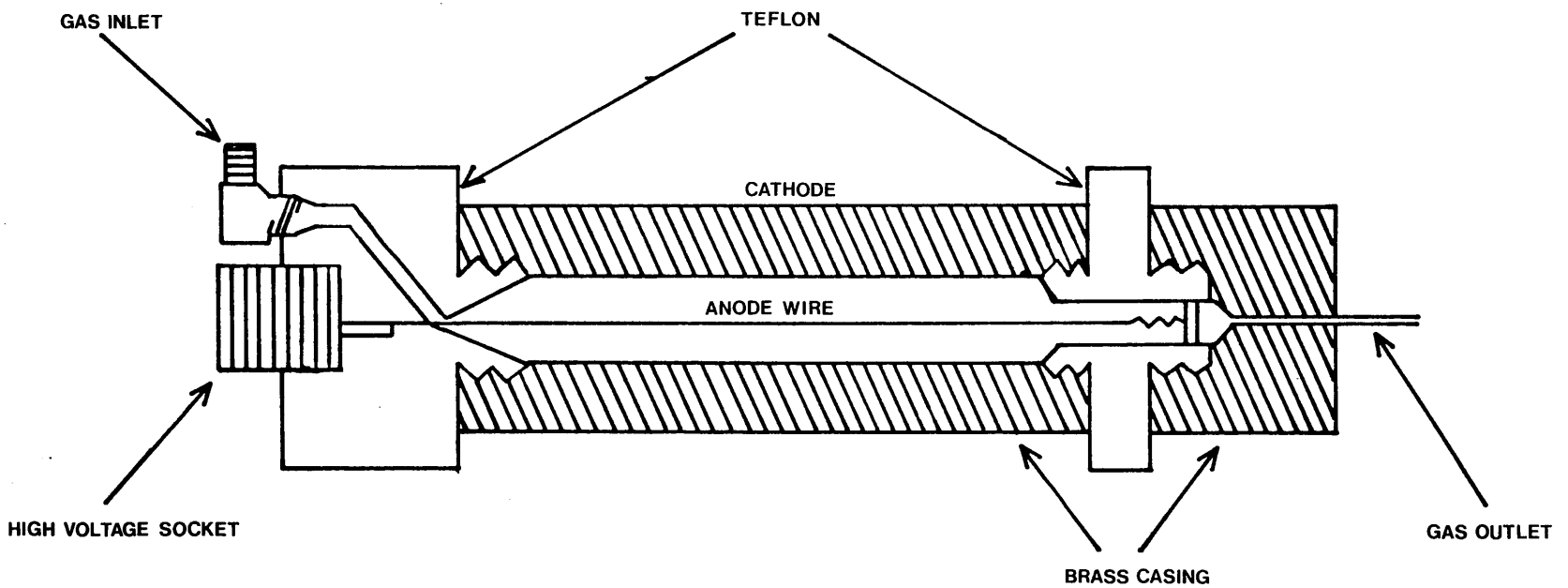

Figure 4·13 – The Gas Proportional Counter.

increments were made, as described previously, the methane flow was curtailed by the appropriate amount through simultaneous adjustment of the methane needle valve. Thus, during the intermediate and final isothermal periods of a radiochromatographic run, the combined helium and methane flow rate through the gas proportional counter was maintained at 35.6 $ml.min^{-1}$ and 26.6 $ml.min^{-1}$, respectively.

Using an external ß-emitting [60-Co] radiation source, the "voltage plateau" of the gas proportional counter was established for each of the three helium/methane counting gas flow rate values. This is the voltage region in which the counting rate induced by a given radiation source is independent of the applied voltage. With the [60-Co] source resting in position on the external wall of the cathode, the applied voltage was gradually increased, from an arbitrary low starting voltage, in small 5 or 10 volt increments. At each voltage setting the count rate was determined over an appropriate time period. The resultant graphs of count rate versus applied voltage are shown in Fig.4.14.

The mid point of the "voltage plateau" reveals the "best working voltage" of the gas proportional counter for a particular set of conditions. Thus, although the count rate produced by the [60-Co] source increased with decreasing counting gas flow rate, the lengths and positions of the voltage plateau were independent of the flow rate of the counting gas mixture and consequently the applied voltage was maintained at a value of 2.25 kV throughout the course of each radiochromatographic run.

The reproducibility of the gas proportional counting system was examined, under operating conditions, by regularly performing a series of consecutive one minute counts and recording the distribution of count rate values obtained. This was done using the external [60-Co] radiation source with each of the three counting gas flow rate values being considered independently.

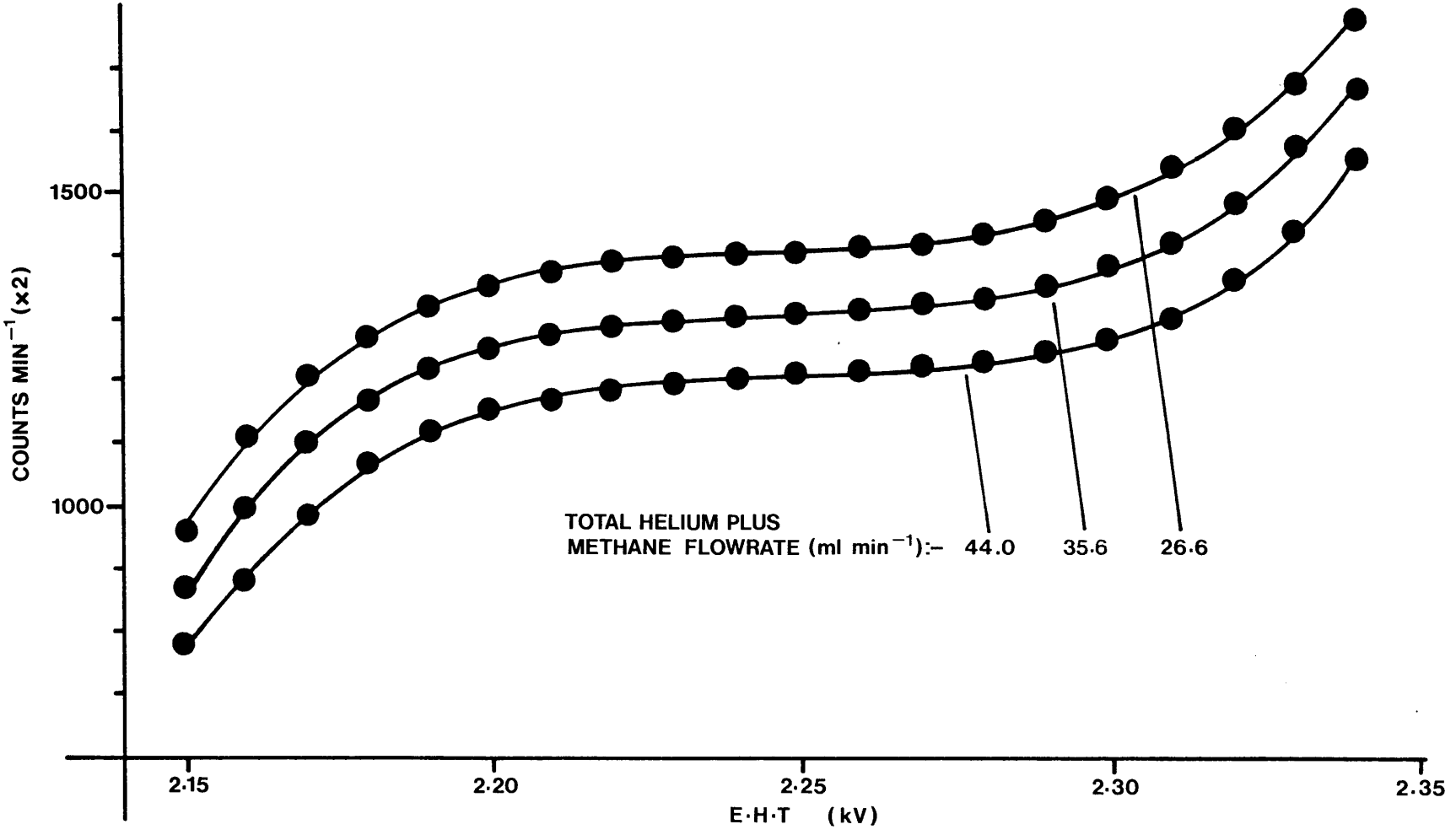

Figure 4.14 – Gas Proportional Counter Voltage Plateau (Helium to Methane Ratio 10:1)

Although, as stated, the count rate increased with decreasing counting gas flow rate, all count rate values recorded for a given flow rate were generally within the expected inherent error, $\pm \sqrt{n}$ counts.min^{-1}, of a mean value, n counts.min^{-1}. This indicated that the counting system was stable under all conditions employed.

In a similar way, but in the absence of the [60-Co] source, the background count rate associated with each counting gas flow rate value was determined. Background readings were collected at frequent time intervals during the radiolabelling experiments and, as in the presence of the [60-Co] source, count rate values obtained for a given counting gas flow rate generally fell within $\pm \sqrt{n}$ counts.min^{-1} of a mean background count rate, n counts.min^{-1}.

For each of the three counting gas flow rate values the count rate generated by the external [60-Co] source, and the background count rate, were as follows:

Table 4.2 - Variation in [60-Co] and Background Count Rates with Counting Gas Flow Rate.

Counting Gas Flow Rate (ml/min)	[60-Co] Source (c.p.m)	Background (c.p.m)
44.0	600 ± 24	90 ± 9
35.6	650 ± 25	97 ± 10
26.6	700 ± 26	104 ± 10

The failure of several consecutive count rate readings to fall within the expected limits, was indicative of a departure from the desired 10:1 helium/methane counting gas ratio. This situation was rectified by making the appropriate adjustments to the methane needle valve until the expected count rate, and therefore, by implication, the correct counting gas blend, was reinstated.

During the radiochromatographic analysis of product mixtures, counting was commenced upon injection of the product sample into the chromatograph and was continued, without interruption, until all product species had been eluted from the chromatographic columns and had passed through the gas proportional counter. In this way, the total number of counts associated with an injected product sample could be determined. Moreover, throughout the counting period the instantaneous counts value was noted and recorded at 30 second intervals. This permitted the number of counts accumulated during any small time interval, (t_2-t_1), of the analysis to be computed. The counts associated with individual product species or groups of products could, therefore, be ascertained by correlating the scaler rate meter data with the accompanying chromatogram. Thus, the counts detected during a retention time interval (t_2-t_1) pertained to any products eluted during that same period.

All count rate values recorded during a radiochromatographic analysis were normalised with respect to the sensitivity of the gas proportional counter that was associated with the column oven temperature of 160°C. In addition, in all cases, the appropriate background count rate was multiplied by the relevant counting time interval and subtracted from the detected counts value.

CHAPTER FIVE

TREATMENT OF RESULTS

- oOo -

5.1 PROCEDURE FOR THE CALCULATION OF YIELD, CONVERSION, CARBON MASS BALANCE AND SELECTIVITY

The yield,conversion, carbon mass balance and selectivity values quoted throughout this text (as percentages) are defined as follows:

Yield:- the number of moles of hydrocarbon reactant converted into an individual product species relative to the number of moles of hydrocarbon reactant introduced to the catalyst. Thus, for a product i, the yield is expressed by the relationship,

$$\text{yield} = \frac{ni\ (Mi)}{N\ (X)} \qquad \ldots\ldots\ldots\ (1)$$

where ni = the number of carbon atoms in product species i,

Mi = the number of moles of product species i,

N = the number of carbon atoms in the hydrocarbon reactant molecule,

and X = the number of moles of hydrocarbon reactant introduced to the catalyst.

Conversion:- the total number of moles of hydrocarbon reactant transformed into products relative to the number of moles of hydrocarbon reactant introduced to the catalyst. This was obtained by summing all the individual product yields. Thus, for j product species,

$$\text{conversion} = \sum_{i=1}^{i=j} \frac{ni\ (Mi)}{N\ (X)} \qquad \ldots\ldots\ldots\ (2)$$

Carbon Mass Balance:- the number of moles of carbon atoms eluted from the reaction vessel relative to the number of moles of carbon atoms introduced to the reaction vessel. This was derived using a modified form of equation (2) which included a term to account for the elution of unreacted hydrocarbon reactant,

$$\text{carbon mass balance} = \frac{[\sum_{i=1}^{i=j} ni\ (Mi)] + N(Y)}{N\ (X)} \quad \ldots\ldots\ldots(3)$$

where Y = the number of moles of hydrocarbon reactant eluted from the catalyst.

Thus, the values obtained for the conversion and yield provide a measure of, respectively, the total catalyst activity and its activity with respect to individual product components, whilst the carbon mass balance figures relate to the capacity of the catalyst to retain surface carbon.

The selectivity values of the catalyst with respect to individual product species were obtained by dividing the appropriate yield values by the conversion,

$$\text{selectivity} = \frac{ni\ (Mi)}{\sum_{i=1}^{i=j} ni\ (Mi)} \quad \ldots\ldots\ldots(4)$$

During continuous flow experiments (section 4.2.1.1) the number of moles of hydrocarbon reactant fed to the catalyst, per unit time (Xt), was calculated from a series of sightglass measurements as described in section 4.2.2. Chromatographic analysis of the post reactor gas stream via the gas sampling valve (section 4.2.4) permitted the molar quantity of each individual eluted compound present within a fixed volume of this gas stream, equivalent to the sample loop volume, to be determined. Measurement of the

overall gas flow rate through the system (section 4.2.2) enabled the time taken for the gas sample loop to be filled by the post reactor gas stream to be calculated. Thus, the rate of elution of any compound from the reaction vessel, and hence the time dependent numerator values in equations (1), (2) and (3), could be derived from any time-on-stream value during a continuous flow experiment.

The chromatographic analysis of a gaseous hydrogen/hydrocarbon reactant mixture which was passed through the reactor bypass in the absence of any catalyst (section 4.2.2), revealed that a slight, but continuous, random fluctuation of the hydrogen/hydrocarbon reactant ratio about a preset value occurred during continuous flow operations. It was necessary, therefore, to minimise any influence that such deviations away from the preset reactant ratio would have on the derived yield, conversion and carbon mass balance values, thereby ensuring that the values actually obtained, for any given time-on-stream, were truly representative of the performance of the catalyst at that time and under the preset reactant ratio conditions. Accordingly, all individual yield, conversion and carbon mass balance values quoted in the following chapter were generated by averaging the results of between six to twelve consecutive sample loop injections. The samples were taken in rapid succession during a sampling period which was relatively very short ($\leq$6 hours) when compared to the total reaction time ($\leq$130 hours). The resultant averaged values were considered to be indicative of the state of the catalyst at the time-on-stream value which corresponded to the mid-point of the sampling period.

In the non-continuous flow experiments (section 4.2.1.2) the (X) values relevant to equations (1), (2) and (3) were defined simply by the quantity of hydrocarbon reactant material introduced to the reaction vessel via the injection port. For each injection, the yield, conversion and carbon mass balance values were calculated by applying equations (1), (2) and (3) to the integral areas of the peaks obtained in the associated chromatogram.

All yield and conversion values quoted in the following chapter relate only to catalytically generated product species and are exclusive of any contribution made by gas phase pyrolysis products. The yields of the latter species were determined from appropriate blank experiments (section 4.2.3.3) using equation (1) and were subtracted from the overall experimental yields to obtain the catalytic yield and conversion values. This subtraction was not performed, however, in the derivation of carbon mass balance values.

5.2 ERRORS

5.2.1 Errors on Continuous Flow Results

The absolute error associated with each of the averaged product yield values obtained during the continuous flow experiments was derived using the following relationships:-

$$\sigma_1 = \sqrt{\sum_{z=1}^{z=q} \frac{(Mit(z) - \overline{Mit})^2}{(q - 1)}} \qquad \ldots\ldots\ldots(1)$$

where $Mit(z)$ = the rate of formation of product species i as calculated from sample loop injection z,

q = the number of sample loop injections,

$\overline{Mit}$ = the mean rate of formation of product species i calculated from q sample loop injections.

σ_1 represents the absolute error on each individual $Mit(z)$ value. The absolute error on the mean value, $\overline{Mit}$, was calculated using:-

$$\sigma_2 = \frac{\sigma_1}{\sqrt{q}} \qquad \ldots\ldots\ldots(2)$$

Hence, the relative error, S_1, on each of the averaged yield values, $\frac{ni\ \overline{Mit}}{N\ Xt}$ was obtained using the equation:-

$$S_1 = \sqrt{\left(\frac{\sigma_3}{Xt}\right)^2 + \left(\frac{\sigma_2}{\overline{Mit}}\right)^2} \qquad \ldots\ldots\ldots(3)$$

where σ_3 = the absolute error on the hydrocarbon feed rate Xt (σ_3 was calculated using a procedure similar to that employed in the derivation of the σ_1 values but from a series of hydrocarbon feed rate measurements taken during the course of the experiment (section 4.2.2)).

The absolute error, σ_4 , on the yield was then derived:-

$$\sigma_4 = S_1 \cdot \left(\frac{ni.\bar{M}it}{N.Xt}\right) \qquad \ldots\ldots\ldots(4)$$

The absolute errors associated with the conversion and carbon mass balance values were generated by simply combining the appropriate yield errors according to the equation:-

$$\sigma_5 = \sqrt{\Sigma(\sigma_4)^2} \qquad \ldots\ldots\ldots(5)$$

The summation in equation (5) was taken over all product species and all eluted species, respectively, when calculating the errors on the conversion and carbon mass balance values. Similarly, the relative error, S_2, on each of the individual product selectivity values was obtained using the appropriate yield and conversion relative errors thus:-

$$S_2 = \sqrt{\left(\frac{\sigma_4}{\text{yield}}\right)^2 + \left(\frac{\sigma_5}{\text{conversion}}\right)^2} \qquad \ldots\ldots\ldots(6)$$

Hence, the absolute error, σ_6 , on each selectivity figure was evaluated:-

$$\sigma_6 = \frac{S_2 \cdot ni(Mi)}{\sum_{i=1}^{i=j} ni(Mi)} \qquad \ldots\ldots\ldots(7)$$

The absolute error on the sum of several selectivity values was obtained by combining the appropriate individual σ_6 absolute errors in a manner similar to that described previously for the derivation of the carbon mass balance and conversion errors (equation (5)).

The absolute errors σ_1 - σ_6, thus calculated, represented one standard deviation from the mean which corresponds to a confidence interval of approximately 68%. The confidence interval on each of the experimental yield, conversion, carbon mass balance and selectivity values was increased to 95% by multiplying each standard deviation figure by an appropriate student t - distribution factor. The factor applied in any particular calculation was dependent on the number of sample loop injections from which the yield, conversion or carbon mass balance value had been derived.

5.2.2 Errors on Non-Continuous Flow Results

Before each of the non-continuous flow experiments, (section 4.2.1.2), repeated injections of a chosen fixed quantity of the liquid hydrocarbon feedstock were made into the helium carrier gas and passed through the empty reaction vessel as described in section 4.2.3.3. The results obtained from the integration of each resultant chromatogram indicated a very high degree of reproducibility in the microsyringe injection and chromatographic analysis procedure, as described in section 4.2.1.2.

Similarly, as described in section 4.2.4.3, the gas proportional counting system used in the radiochromatographic analysis of non-continuous flow experimental product mixtures was observed to be stable under all analytical conditions.

Consequently, it was not considered necessary to perform error calculations on the results obtained from the chromatographic and radiochromatographic analysis of non-continuous flow product mixtures.

CHAPTER SIX

RESULTS

- oOo -

As stated previously, all yield, conversion, carbon mass balance and selectivity values given in this chapter are expressed in the form of percentages. The error values quoted in tables 6.2 - 6.10 denote a confidence interval of 95%. All error bars represent a confidence interval of 68%.

6.1 Continuous Flow Experiments

A gaseous reactant mixture consisting of hydrogen and n-heptane in a 6:1 molar ratio was flowed continuously, in separate experiments, over 0.25 g samples of the reduced catalysts RC1 and RC2. The experimental conditions used in the continuous flow studies were as follows:-

TABLE 6.1 - Experimental Conditions for Continuous Flow Studies

Temperature (°C)	500
Pressure (atm)	9.50
WHSV (g.n-heptane/g.cat/hr)	2.24
Reaction Time (hours)	<130

Table 6.2 lists the yields of the gas phase pyrolysis products that were formed during blank experiments (section 4.2.3.3) carried out under the temperature, pressure and flowrate conditions given in table 6.1.

TABLE 6.2: Yields of Pyrolysis Products obtained during Blank Continuous Flow Experiments

PRODUCT	YIELD
METHANE	0.17 ± 0.02
ETHANE	1.37 ± 0.27
PROPANE	0.70 ± 0.13
BUTANE	0.20 ± 0.04
PENTANE	0.37 ± 0.08
HEXANE	0.10 ± 0.04

6.1.1 Continuous Flow of Hydrogen/N-Heptane over Catalyst RC1

The hydrogen/n-heptane reactant mixture was passed over a sample of catalyst RC1 for 130 hours under the conditions shown in table 6.1. Throughout this period the effluent gas stream was sampled at regular intervals and the yields of all individual product species calculated. The resultant values, together with the amount of unreacted n-heptane, are recorded in table 6.3 and are presented graphically as a function of time-on-stream in figures 6.1 - 6.6.

The yields of all product species were observed to decrease with time. For each product, however, the most substantial yield loss occurred during the initial stages of the experiment, the loss becoming progressively less rapid with time until eventually a stable yield value was approached. Accordingly, the conversion values, which are presented in the first column of table 6.4, exhibited a similar trend when considered as a function of

Table 6·3 – Yields of Individual Product and Amount of Unreacted N – Heptane versus Time – on – Stream

TIME-ON-STREAM (HRS)	METHANE	ETHANE	PROPANE	ISO–BUTANE	BUTANE	ISO–PENTANE
1·8	0.71 ± 0.38	4.54 ± 2.15	5.38 ± 2.54	1.18 ± 1.07	2.07 ± 0.64	5.35 ± 1.01
8·7	0.52 ± 0.17	2.87 ± 1.00	2.95 ± 0.59	0.46 ± 0.07	1.31 ± 0.20	2.58 ± 0.46
23·5	0.40 ± 0.0	2.79 ± 0.99	2.80 ± 0.56	0.41 ± 0.04	1.28 ± 0.20	2.33 ± 0.38
31·0	0.39 ± 0.11	2.43 ± 0.70	2.60 ± 0.63	0.43 ± 0.12	1.31 ± 0.34	2.55 ± 0.47
48·0	0.40 ± 0.09	2.27 ± 0.79	2.33 ± 0.52	0.34 ± 0.06	1.04 ± 0.17	2.09 ± 0.33
75·0	0.32 ± 0.07	1.50 ± 0.49	1.77 ± 0.34	0.24 ± 0.05	0.88 ± 0.14	1.51 ± 0.34
105·0	0.39 ± 0.09	1.79 ± 0.57	1.88 ± 0.41	0.25 ± 0.05	0.90 ± 0.18	1.52 ± 0.37
125·0	0.39 ± 0.08	1.68 ± 0.50	1.81 ± 0.36	0.25 ± 0.03	0.87 ± 0.14	1.66 ± 0.37

Table 6.3(cont)–Yield of Individual Products and Amount of Unreacted N–Heptane versus Time-on-Stream

TIME-ON-STREAM (HRS)	PENTANE	ISO–HEXANE	HEXANE	ISO–HEPTANE	HEPTANE	TOLUENE
1·8	3.35 ± 0.84	2.58 ± 0.67	1.94 ± 0.31	22.68 ± 5.04	26 56' ± 10.03	18.77 ± 4.20
8·7	2.55 ± 0.48	1.93 ± 0.33	1.58 ± 0.20	19.76 ± 3.08	30.47 ± 6.99	12.08 ± 2.93
23·5	2.62 ± 0.51	1.43 ± 0.22	1.67 ± 0.38	18.86 ± 2.95	40.22 ± 7.89	12.45 ± 2.07
31·0	2.34 ± 0.40	1.31 ± 0.40	1.45 ± 0.20	17.26 ± 2.29	50.07 ± 7.87	11.26 ± 1.54
48·0	2.02 ± 0.32	1.40 ± 0.28	1.46 ± 0.21	16.09 ± 2.58	52.85 ± 9.86	10.60 ± 1.97
75·0	1.82 ± 0.26	0.80 ± 0.15	1.15 ± 0.17	15.15 ± 2.49	60.97 ± 10.12	8.45 ± 1.82
105·0	1.78 ± 0.42	0.70 ± 0.17	1.02 ± 0.18	13.62 ± 2.07	64.50 ± 10.79	7.22 ± 0.98
125·0	1.85 ± 0.52	0.93 ± 0.13	1.04 ± 0.15	14.88 ± 3.59	60.98 ± 11.31	8.07 ± 1.65

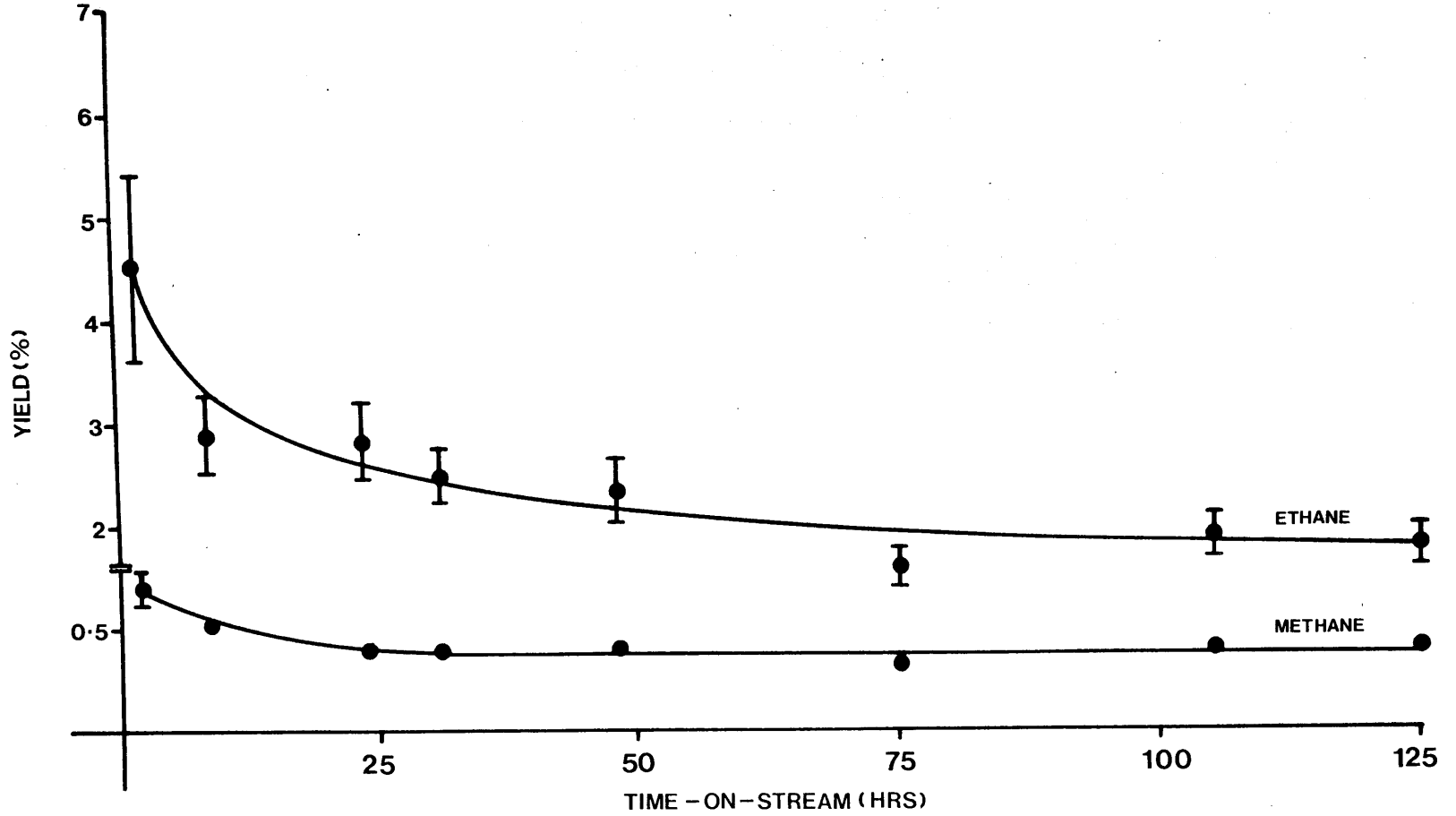

Figure 6·1 – Yield of Methane and Ethane versus Time-on-Stream

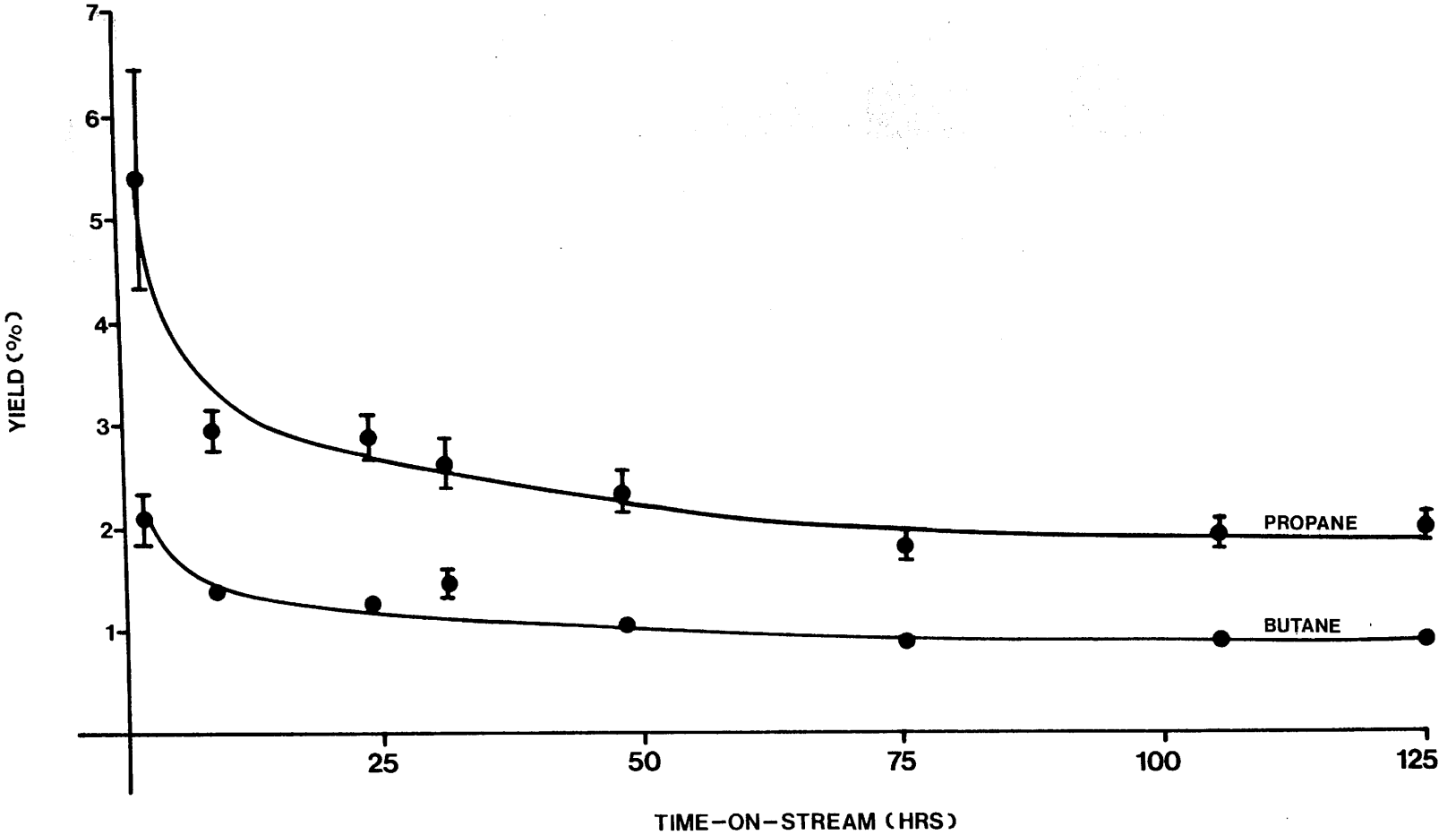

Figure 6.2-Yield of Propane and Butane versus Time-on-Stream

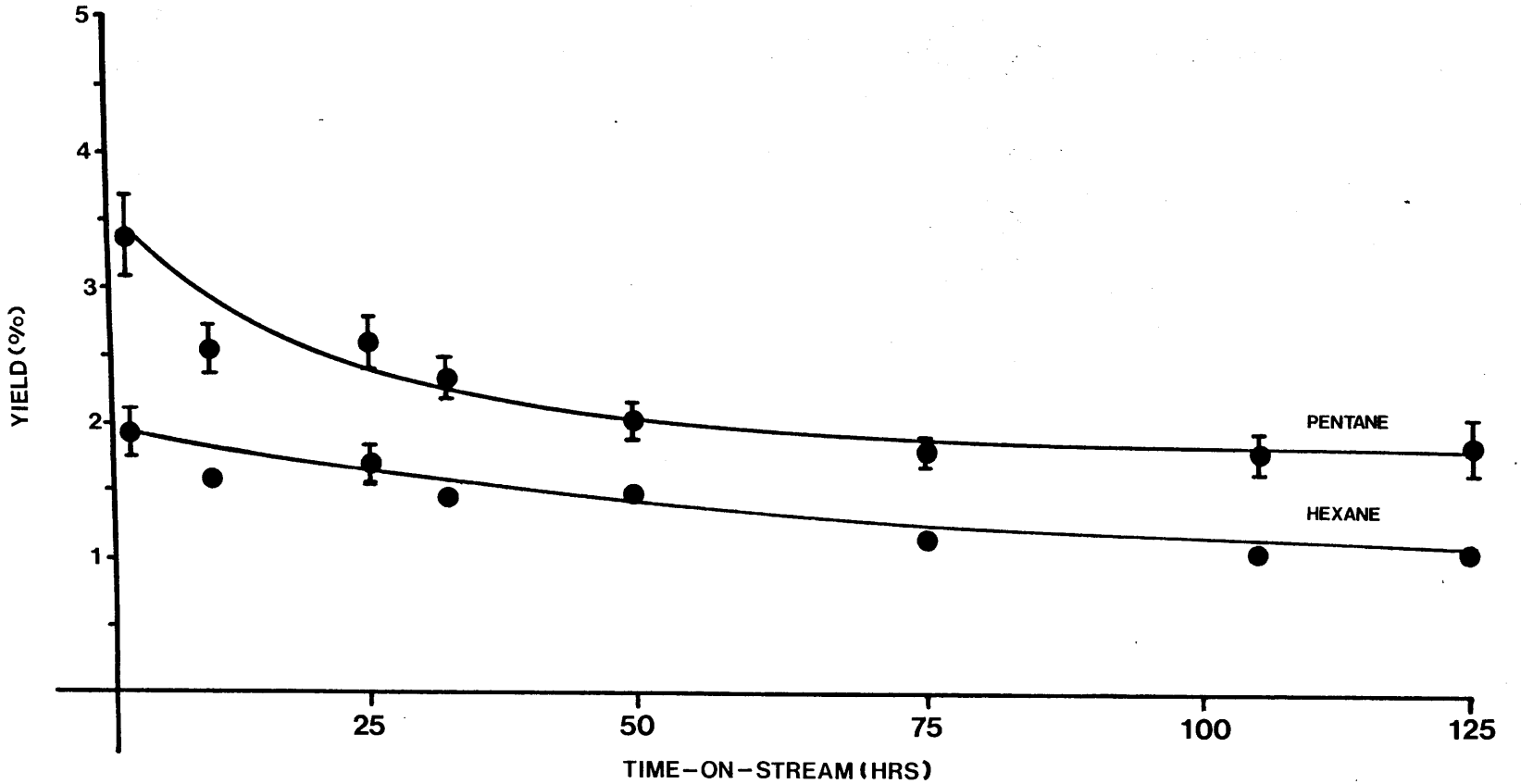

Figure 6·3 – Yield of Pentane and Hexane versus Time-on-Stream

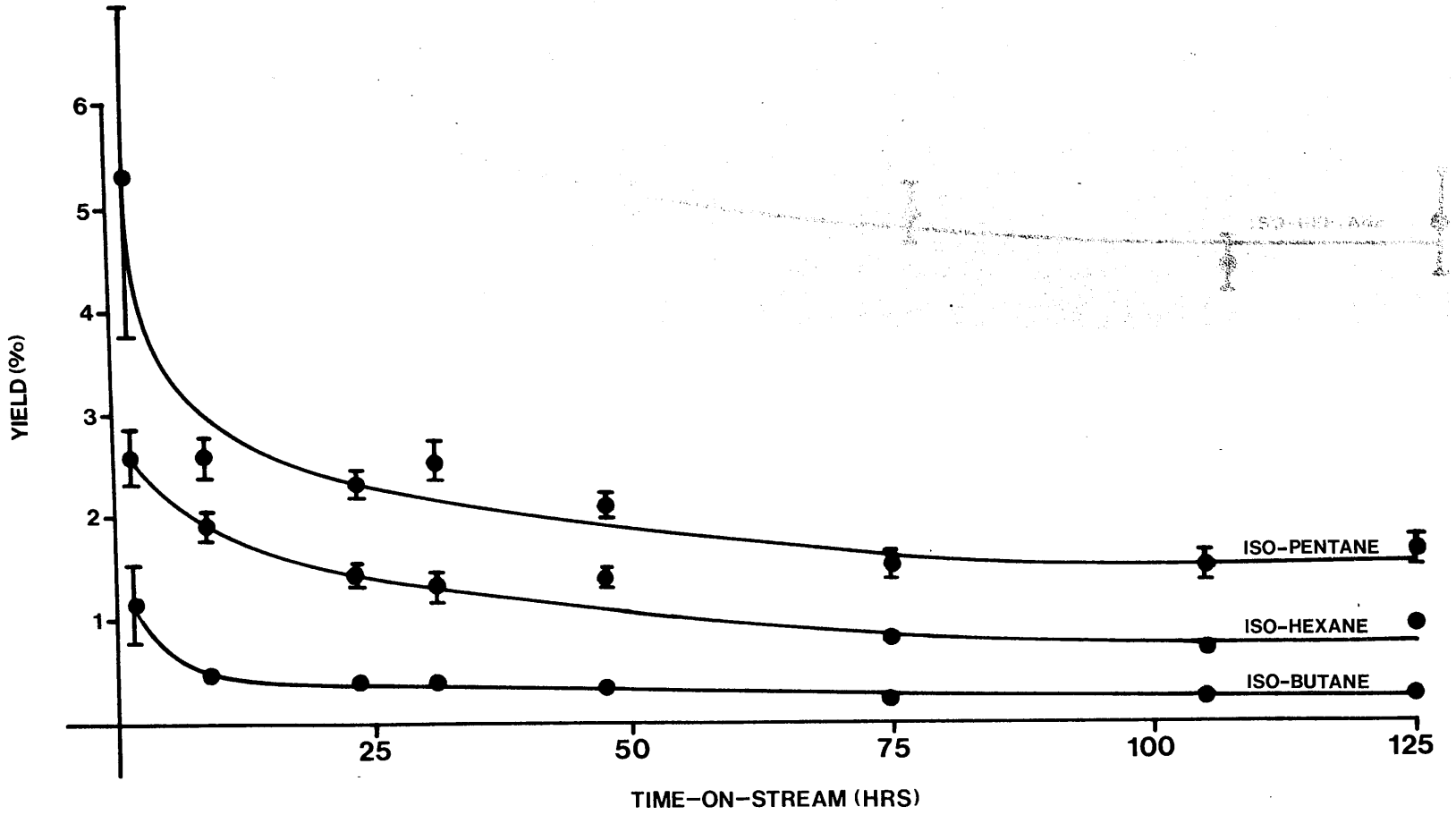

Figure 6.4 - Yield of Iso-Butane, Iso- Pentane, and Iso-Hexane versus Time-on-Stream

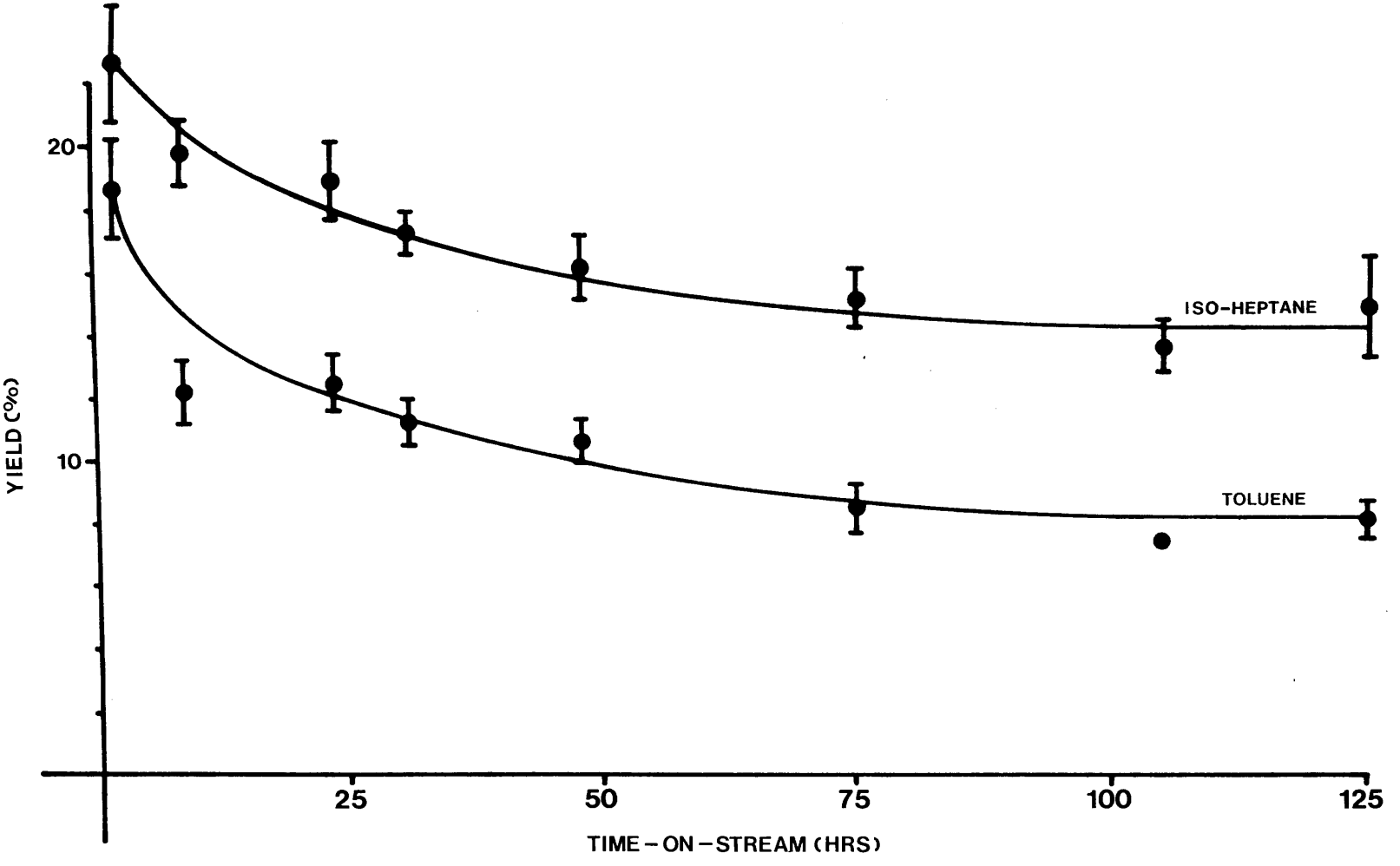

Figure 6.5 –Yield of Iso-Heptane and Toluene versus Time-on-Stream.

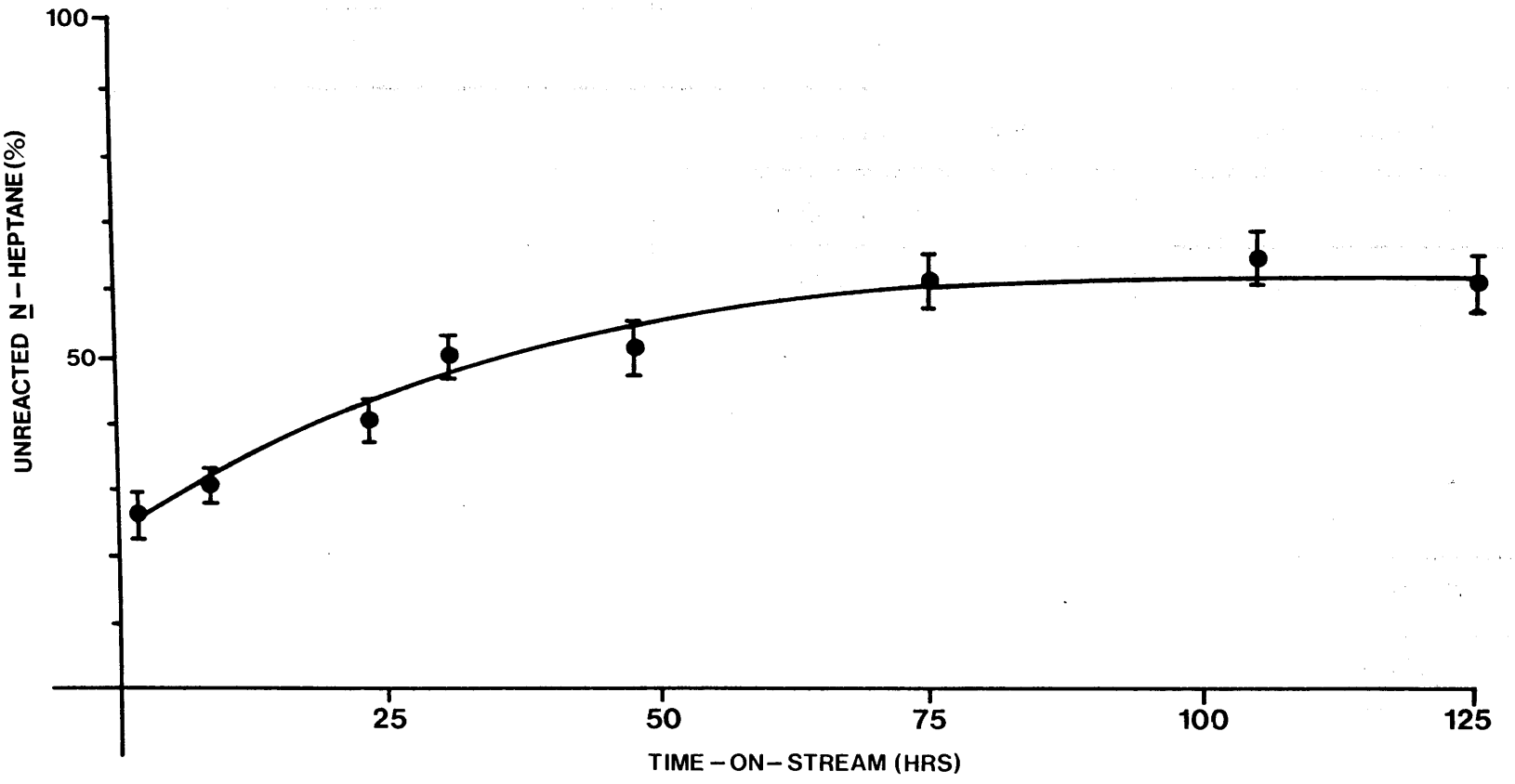

Figure 6.6 - Amount of Unreacted N-Heptane versus Time-on-Stream.

Table 6.4 – Conversion, Unreacted N – Heptane and Carbon Mass Balance versus Time – on – Stream.

TIME – ON – STREAM (HRS)	CONVERSION	UNREACTED N – HEPTANE	CARBON MASS BALANCE
1·8	68.87 ± 7.63	26.56 ± 10.03	98.38 ± 13.17
8·7	48.75 ± 4.47	30.47 ± 6.99	82.16 ± 8.30
23·5	47.36 ± 3.85	40.22 ± 7.89	90.52 ± 8.78
31·0	43.68 ± 3.02	50.07 ± 7.87	96.69 ± 8.43
48·0	40.39 ± 3.48	52.85 ± 9.86	96.18 ± 10.45
75·0	34.00 ± 3.15	60.97 ± 10.12	97.91 ± 10.60
105·0	31.43 ± 2.42	64.50 ± 10.79	98.86 ± 11.05
125·0	33.76 ± 4.02	60.98 ± 11.31	97.68 ± 12.00

time-on-stream as illustrated in figure 6.7.

The data presented thus far is, therefore, consistent with the commonly observed phenomenon that the deactivation of catalysts, including those employed in reforming processes, tends to occur with an initial fast rate which gradually subsides until an almost stable activity is attained.

The values for the amount of unreacted n-heptane are listed in the second column of table 6.4. A plot of this data (Fig.6.6) clearly indicates that the amount of residual unreacted n-heptane appearing in the post reactor gas stream follows largely the opposite trend, with time, to that observed in both the individual product yields and the total conversion. Thus, during the initial stages of the reaction a relatively small amount (25%) of the n-heptane reactant that was fed to the reaction vessel appeared in the reactor effluent. The amount progressively increased, however, until in the later stages of the experiment a larger (60%) more stable proportion was eluted.

The value for the amount of unreacted n-heptane feedstock that is observed at any given time-on-stream is, in principle, governed by two determining factors, namely, the activity of the catalyst at that time, and the extent to which the n-heptane is retained on the catalyst surface in the form of carbonaceous materials. Accordingly, an almost exact inverse correlation was observed to exist between the rate of deactivation of the catalyst (Fig.6.7) and the rate of increase in the amount of n-heptane reactant (Fig.6.6), except during those periods in which high levels of surface retention were indicated. For instance, during the 1.8 - 8.7 hour, and possibly also the 8.7 - 23.5 hour time-on-stream intervals where the inverse correlation was less well defined, the carbon mass balance values, which are shown in the third column of table 6.4, suggest that very significant quantities of carbonaceous materials were being retained.

Figure 6.8 shows the carbon mass balance values plotted as a function of time-on-stream. The graph implies that a sharp

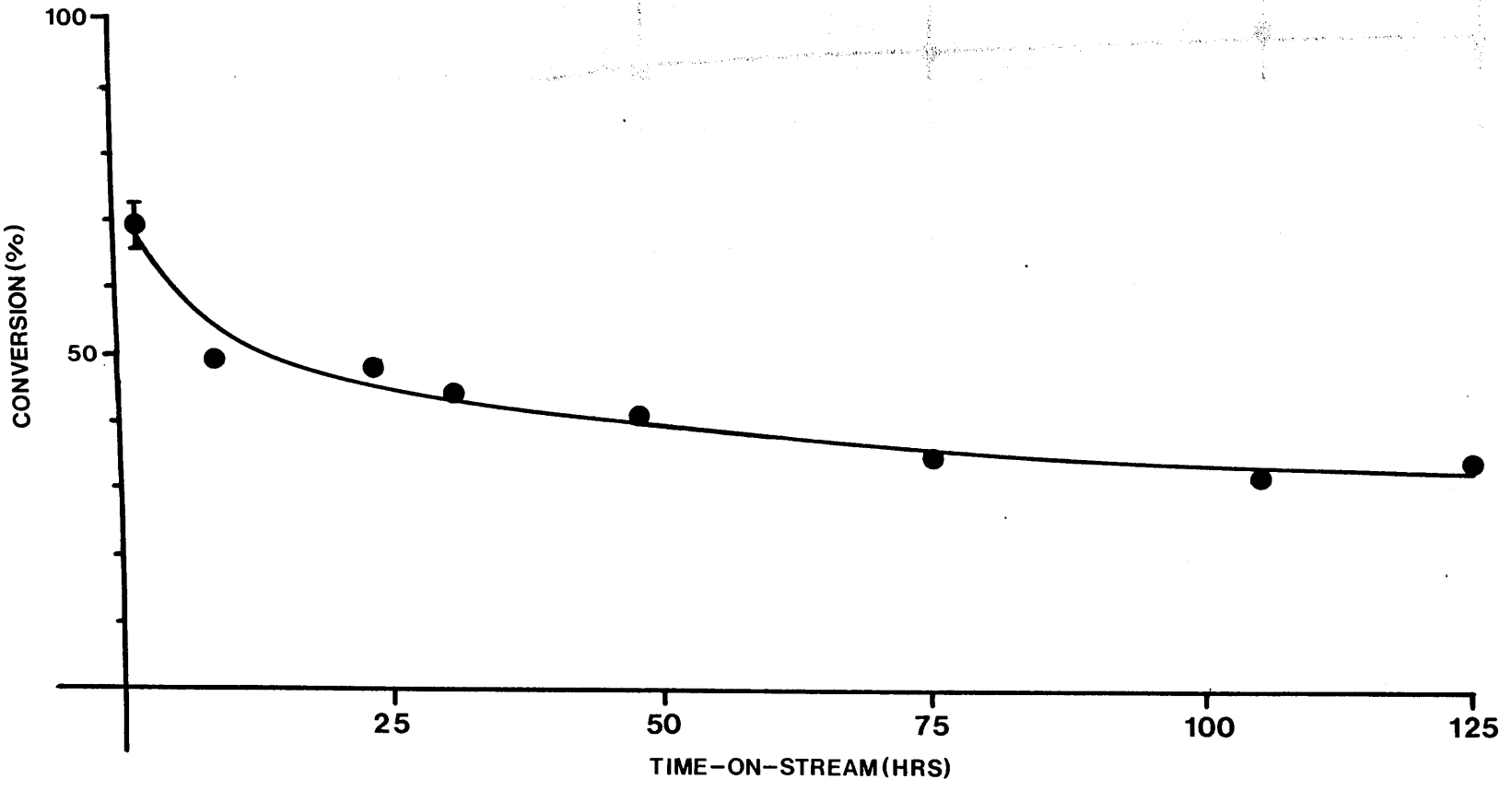

Figure 6·7–Total Conversion versus Time–on - Stream

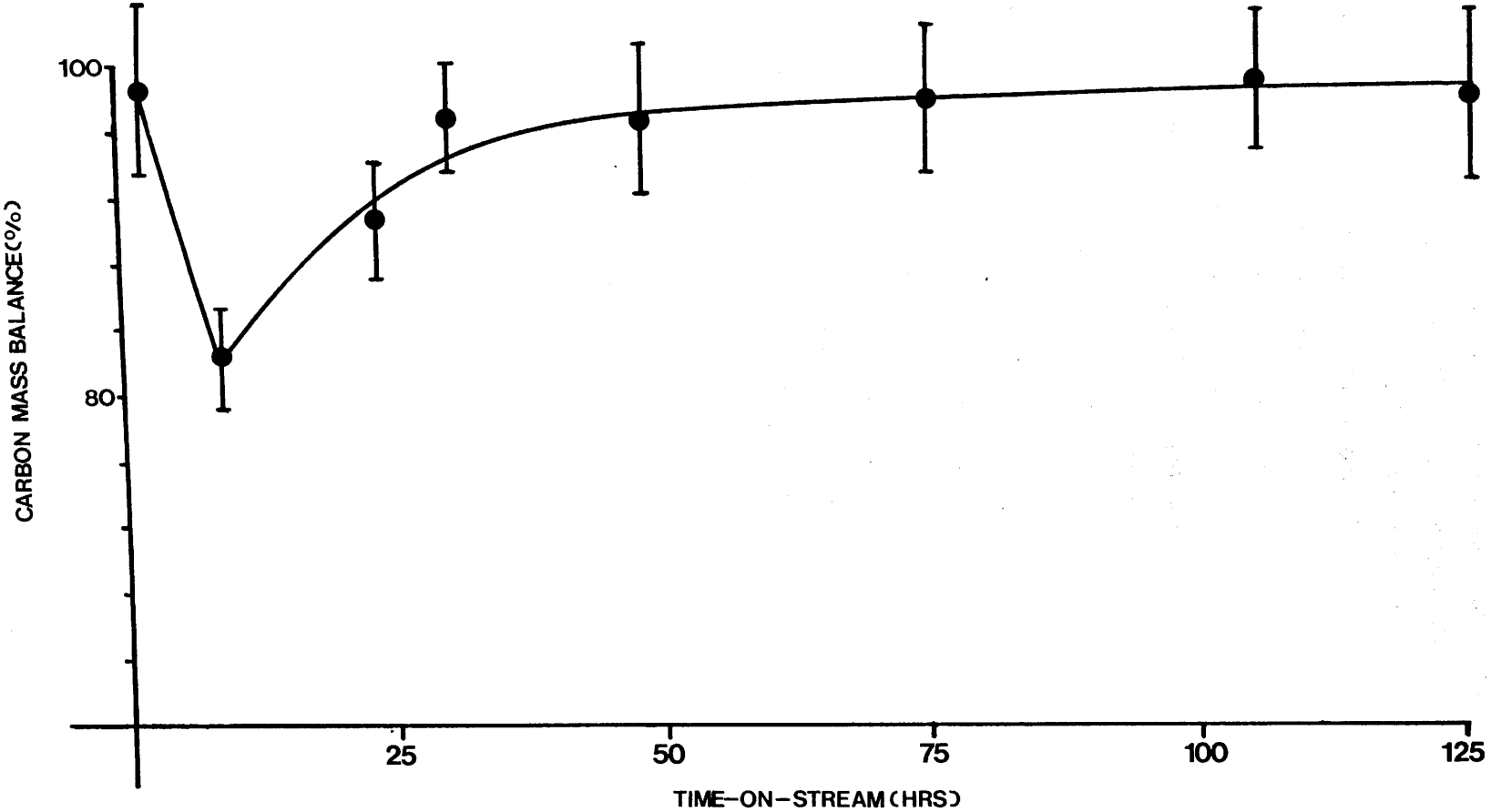

Figure 6.8– Carbon Mass Balance versus Time-on-Stream

increase in the extent of n-heptane retention on the catalyst surface took place during the initial stages of the reaction with a maximum uptake of hydrocarbon occurring after a reaction time of 8.7 hours. Thereafter, the extent of retention gradually lessened, ultimately approaching a situation where there was no further net uptake of carbon by the catalyst. This latter stage is signified by the asymptotic approach of the curve to the carbon mass balance value of 100%. When the graph is interpreted in terms of the weight of residual carbon retained on the catalyst surface at the end of the experiment, a value equivalent to around 900% of the original catalyst weight is inferred. This differs very significantly from a corresponding figure of 0.53% which was obtained from the combustion analysis of the spent catalyst.

The selectivity values of catalyst RC1 with respect to each of the individual product species are listed in table 6.5. The variation with time in the selectivity of the catalyst for each of the major types of reforming reaction was examined by considering the selectivity values for appropriate individual compounds, or groups of compounds, each of which was considered to be representative of a particular reaction type. Thus, the iso-heptane and toluene selectivity values at any given time-on-stream were considered to be indicative of, respectively, the selectivity of the catalyst for the isomerisation and aromatisation processes. Similarly, summing the individual methane, ethane, n-pentane and n-hexane selectivity values at each time-on-stream, enabled any trend in the selectivity of the catalyst with respect to hydrogenolysis to be followed, whilst variations in the selectivity of the catalyst for hydrocracking were monitored by summing the iso-butane, iso-pentane and iso-hexane values.

Table 6.6 gives the selectivities of catalyst RC1 with respect to aromatisation, isomerisation, hydrocracking and hydrogenolysis against the corresponding time-on-stream values. The data contained in table 6.6 is illustrated in figures 6.9 - 6.10. The

Table 6.5 – Selectivity with respect to Individual Products versus Time-on-Stream

TIME-ON-STREAM (HRS)	METHANE	ETHANE	PROPANE	ISO-BUTANE	BUTANE	ISO-PENTANE
1.8	1.04 ± 0.57	6.60 ± 3.20	7.81 ± 3.79	1.72 ± 1.56	3.01 ± 0.99	7.77 ± 1.70
8.7	1.08 ± 0.38	5.89 ± 2.12	6.06 ± 1.33	0.95 ± 0.18	2.71 ± 0.49	5.30 ± 1.06
23.5	0.85 ± 0.16	5.89 ± 2.15	5.92 ± 1.29	0.87 ± 0.12	2.70 ± 0.48	4.94 ± 0.91
31.0	0.89 ± 0.27	5.57 ± 1.65	5.96 ± 1.51	0.98 ± 0.30	3.01 ± 0.81	5.86 ± 1.15
48.0	1.01 ± 0.24	5.63 ± 2.02	5.78 ± 1.38	0.87 ± 0.17	2.58 ± 0.48	5.18 ± 0.94
75.0	0.95 ± 0.23	4.44 ± 1.52	5.22 ± 1.13	0.72 ± 0.18	2.61 ± 0.49	4.45 ± 1.09
105.0	1.25 ± 0.32	5.72 ± 1.86	5.98 ± 1.39	0.81 ± 0.18	2.88 ± 0.62	4.86 ± 1.26
125.0	1.16 ± 0.29	4.99 ± 1.61	5.36 ± 1.25	0.76 ± 0.14	2.58 ± 0.54	4.92 ± 1.26

Table 6·5 (cont)–Selectivity with respect to Individual Products.

TIME–ON–STREAM (HRS)	PENTANE	ISO–HEXANE	HEXANE	ISO–HEPTANE	TOLUENE
1·8	4.87 ± 1.33	3.74 ± 1.06	2.81 ± 0.55	32.93 ± 8.17	27.25 ± 6.81
8·7	5.24 ± 1.11	3.96 ± 0.77	3.24 ± 0.52	40.53 ± 7.34	24.79 ± 6.42
23·5	5.55 ± 1.18	3.02 ± 0.54	3.53 ± 0.86	39.82 ± 7.03	26.29 ± 4.86
31·0	5.37 ± 1.00	3.02 ± 0.96	3.32 ± 0.51	39.53 ± 5.93	25.78 ± 3.96
48·0	5.03 ± 0.91	3.48 ± 0.77	3.61 ± 0.61	39.84 ± 7.25	26.24 ± 5.38
75·0	5.37 ± 0.93	2.37 ± 0.49	3.38 ± 0.60	44.56 ± 8.41	24.87 ± 5.85
105·0	5.67 ± 1.41	2.24 ± 0.60	3.25 ± 0.65	43.33 ± 7.39	23.00 ± 3.60
125·0	5.50 ± 1.67	2.78 ± 0.51	3.11 ± 0.58	44.07 ± 11.86	23.92 ± 5.66

Table 6·6 – Selectivity with respect to Major Reactions versus Time-on-Stream.

TIME-ON-STREAM (HRS)	AROMATISATION	ISOMERISATION	HYDROCRACKING	HYDROGENOLYSIS
1·8	27.25 ± 6.81	32.93 ± 8.17	13.23 ± 2.54	15.32 ± 3.55
8·7	24.38 ± 6.42	40.53 ± 7.34	10.19 ± 1.32	15.45 ± 2.48
23·5	26.29 ± 4.86	39.82 ± 7.03	8.55 ± 1.06	15.82 ± 2.60
31·0	25.78 ± 3.96	39.53 ± 5.93	9.82 ± 1.53	15.15 ± 2.01
48·0	26.24 ± 5.38	39.84 ± 7.25	9.48 ± 1.23	15.28 ± 1.12
75·0	24.87 ± 5.85	44.56 ± 8.41	7.50 ± 1.21	14.14 ± 1.89
105·0	23.00 ± 3.60	43.33 ± 7.39	7.85 ± 1.41	15.89 ± 1.58
125·0	23.92 ± 5.66	44.07 ± 11.86	8.41 ± 1.37	14.76 ± 2.18

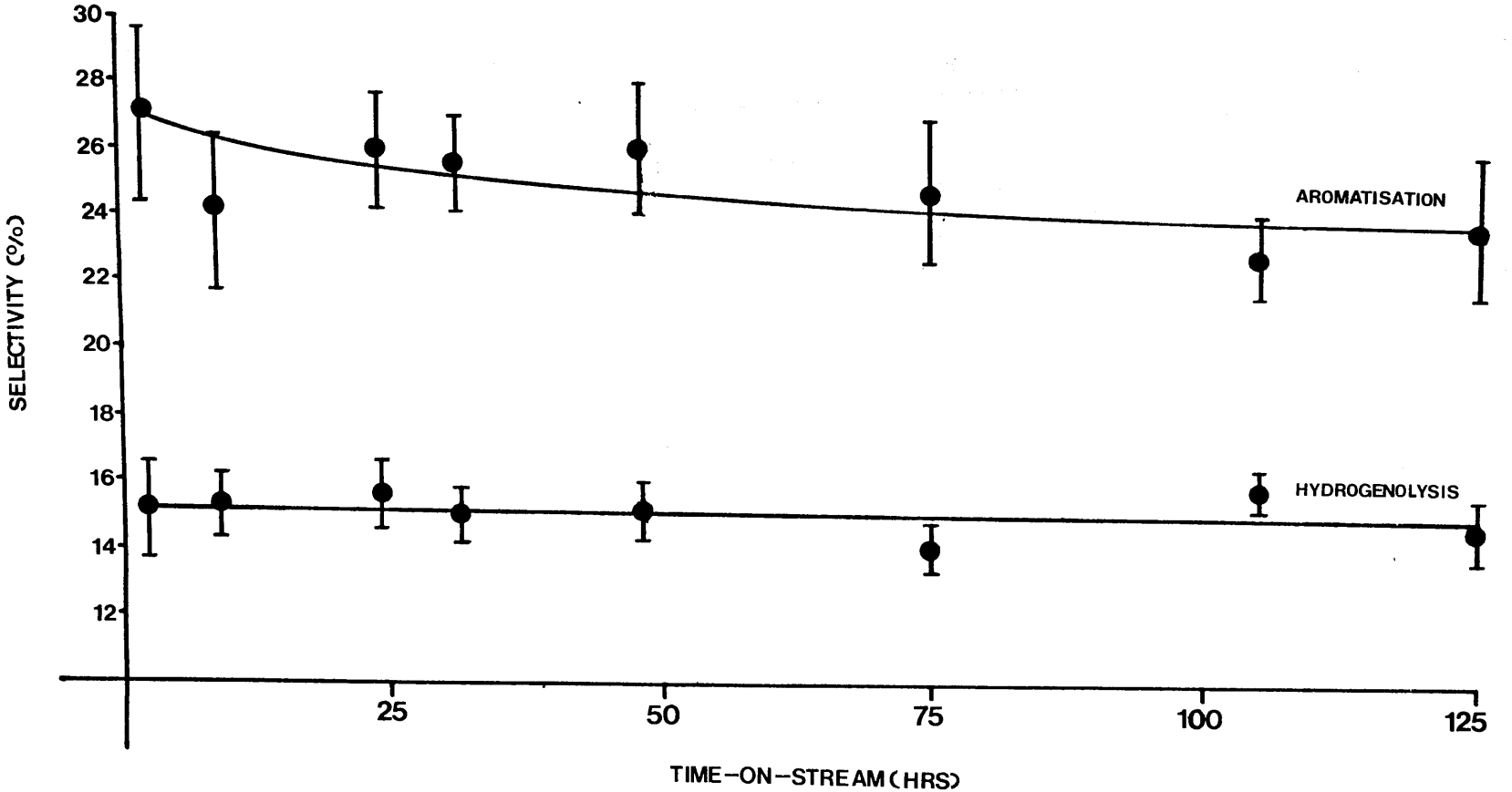

Figure 6.9- Selectivity with respect to Aromatisation and Hydrogenolysis versus Time-on-Stream

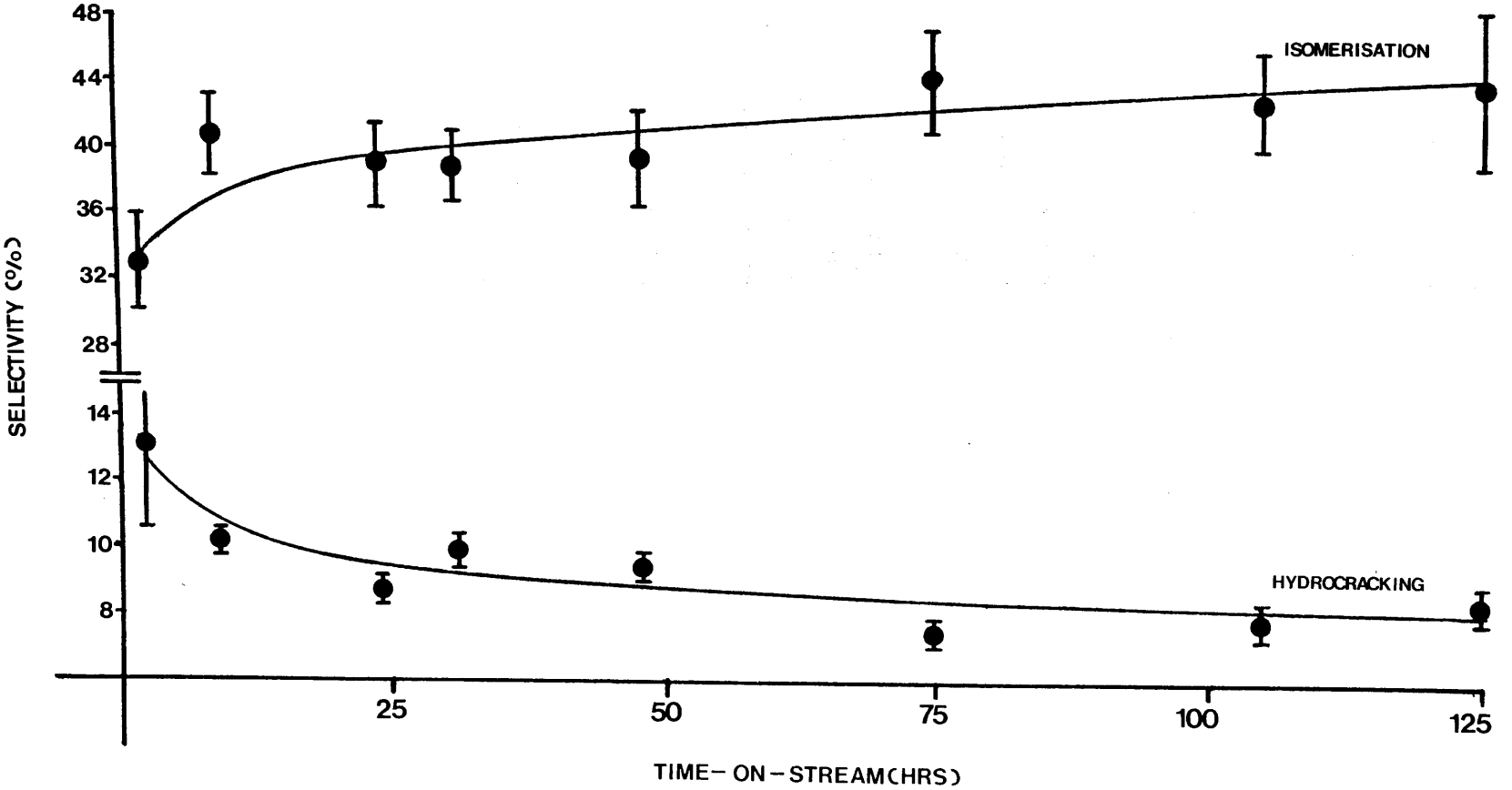

Figure 6.10 - Selectivity with respect to Isomerisation and Hydrocracking versus Time-on-Stream

results reveal that throughout the course of the experiment considerable changes in the selectivity of the catalyst were experienced. Figures 6.9 - 6.10 clearly demonstrate, for example, that a substantial increase in the isomerisation selectivity occurred with a reciprocal decrease taking place in the aromatisation and hydrocracking selectivities. The selectivity of the catalyst with respect to hydrogenolysis remained essentially constant. Moreover, the selectivity changes did not occur linearly with respect to time. Instead, as is particularly apparent from figure 6.10, the most pronounced changes were experienced during the initial stages of the experiment with more stable selectivity values gradually being assumed as the reaction time increased. In this respect the trends observed in the selectivity values are similar to those noted earlier in the total conversion and individual product yield values.

Neutron activation analysis of spent catalyst RC1, after the completion of the continuous flow run, indicated a residual catalyst chlorine content of 0.11% by weight as compared to a corresponding figure of 0.77% by weight for the fresh catalyst.

6.1.2 Continuous Flow of Hydrogen/N-Heptane over Catalyst RC2

The continuous flow experiment described in section 6.1.1 was repeated under identical conditions using catalyst RC2.

The yields of all product species and the amount of n-heptane remaining unreacted are tabulated against the corresponding time-on-stream values in table 6.7 and are presented graphically in figures 6.11 - 6.16. The conversion and carbon mass balance values are given in table 6.8 and are plotted as a function of time-on-stream in figures 6.17 and 6.18 respectively, whilst the selectivities of the catalyst with respect to both the individual product species and the major reaction types are listed in tables 6.9 and 6.10. Figures 6.19 - 6.21 relate to the data contained in table 6.10.

Table 6.7 – Yield of Individual Products and Amount of Unreacted N–Heptane versus Time–on–Stream

TIME–ON–STREAM (HRS)	METHANE	ETHANE	PROPANE	ISO-BUTANE	BUTANE	ISO-PENTANE
1.8	3.18 ± 0.69	8.81 ± 1.48	9.40 ± 2.48	0.92 ± 0.34	3.18 ± 0.63	5.59 ± 1.59
6.8	2.55 ± 0.69	10.25 ± 2.16	7.39 ± 1.73	0.82 ± 0.12	2.84 ± 0.59	5.92 ± 1.45
21.3	1.88 ± 0.18	7.75 ± 0.83	5.18 ± 0.47	0.50 ± 0.20	2.11 ± 0.16	3.52 ± 0.49
46.0	1.70 ± 0.41	6.91 ± 2.26	4.50 ± 1.30	0.35 ± 0.11	1.73 ± 0.33	3.24 ± 0.81
66.5	1.84 ± 0.24	5.85 ± 1.02	3.75 ± 0.40	0.24 ± 0.03	1.62 ± 0.14	2.45 ± 0.43
92.0	2.21 ± 0.28	8.36 ± 1.74	4.88 ± 0.94	0.23 ± 0.10	1.98 ± 0.39	3.44 ± 1.04

Table 6.7(cont)-Yield of Individual Products and Amount of Unreacted N-Heptane versus Time-on-Stream

TIME-ON-STREAM(HRS)	PENTANE	ISO-HEXANE	HEXANE	ISO-HEPTANE	HEPTANE	TOLUENE
1.8	5.71 ± 0.56	5.28 ± 0.82	3.21 ± 0.35	8.21 ± 2.14	10.52 ± 3.69	20.02 ± 5.65
6.7	5.60 ± 1.29	3.48 ± 0.63	2.60 ± 0.56	12.29 ± 2.48	21.55 ± 6.05	20.08 ± 4.46
21.3	5.06 ± 0.50	2.30 ± 0.14	2.56 ± 0.22	13.77 ± 2.14	34.04 ± 5.92	15.69 ± 3.04
46.0	4.14 ± 0.73	1.79 ± 0.32	2.06 ± 0.24	12.54 ± 2.51	37.55 ± 8.90	9.98 ± 3.04
66.5	3.95 ± 0.33	1.53 ± 0.16	2.26 ± 0.22	12.95 ± 1.66	45.56 ± 6.87	9.98 ± 1.86
92.0	4.53 ± 0.73	1.58 ± 0.30	2.36 ± 0.47	14.73 ± 1.48	50.51 ± 6.28	9.38 ± 1.45

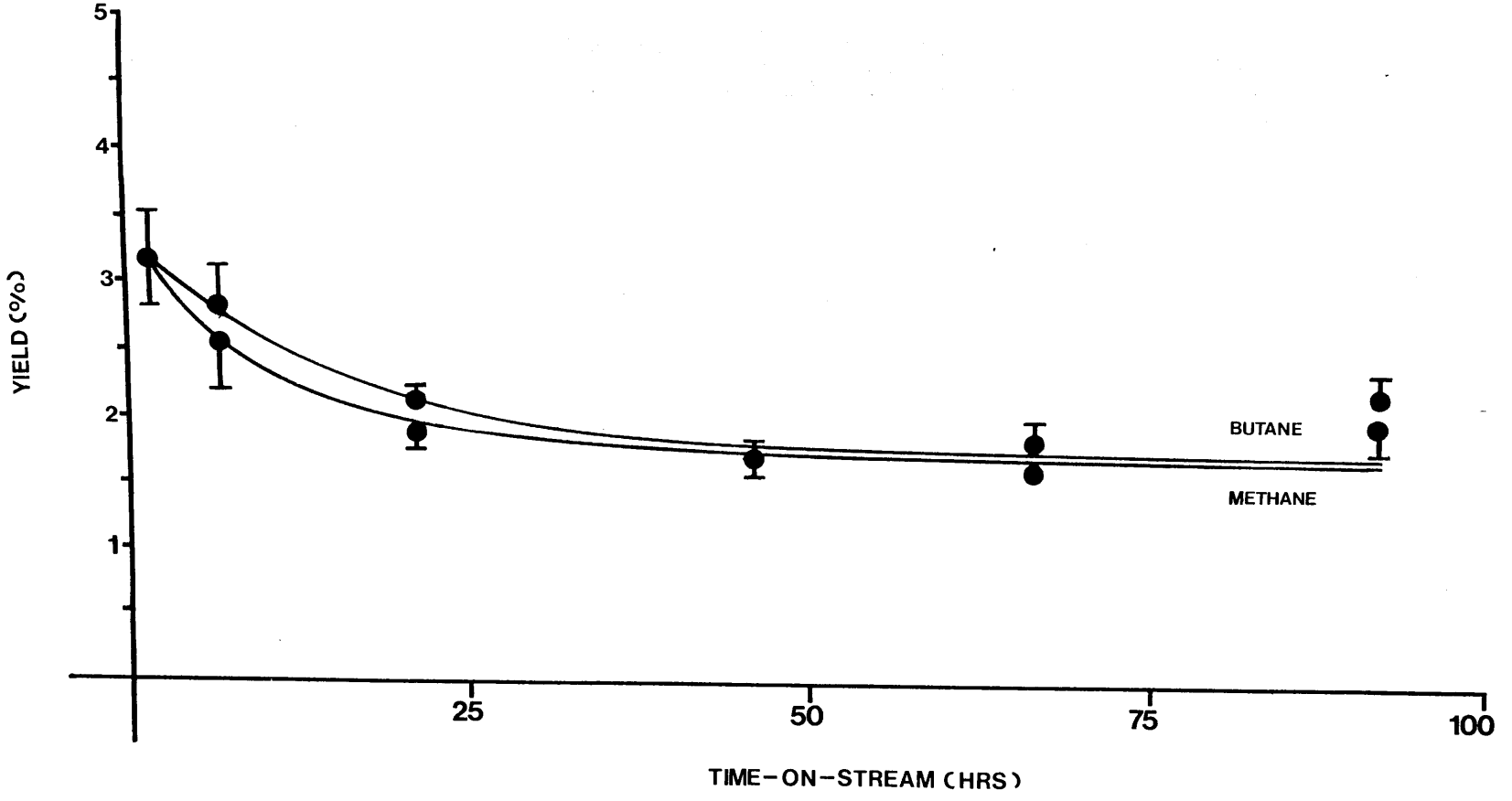

Figure 6.11 - Yield of Butane and Methane versus Time-on-Stream

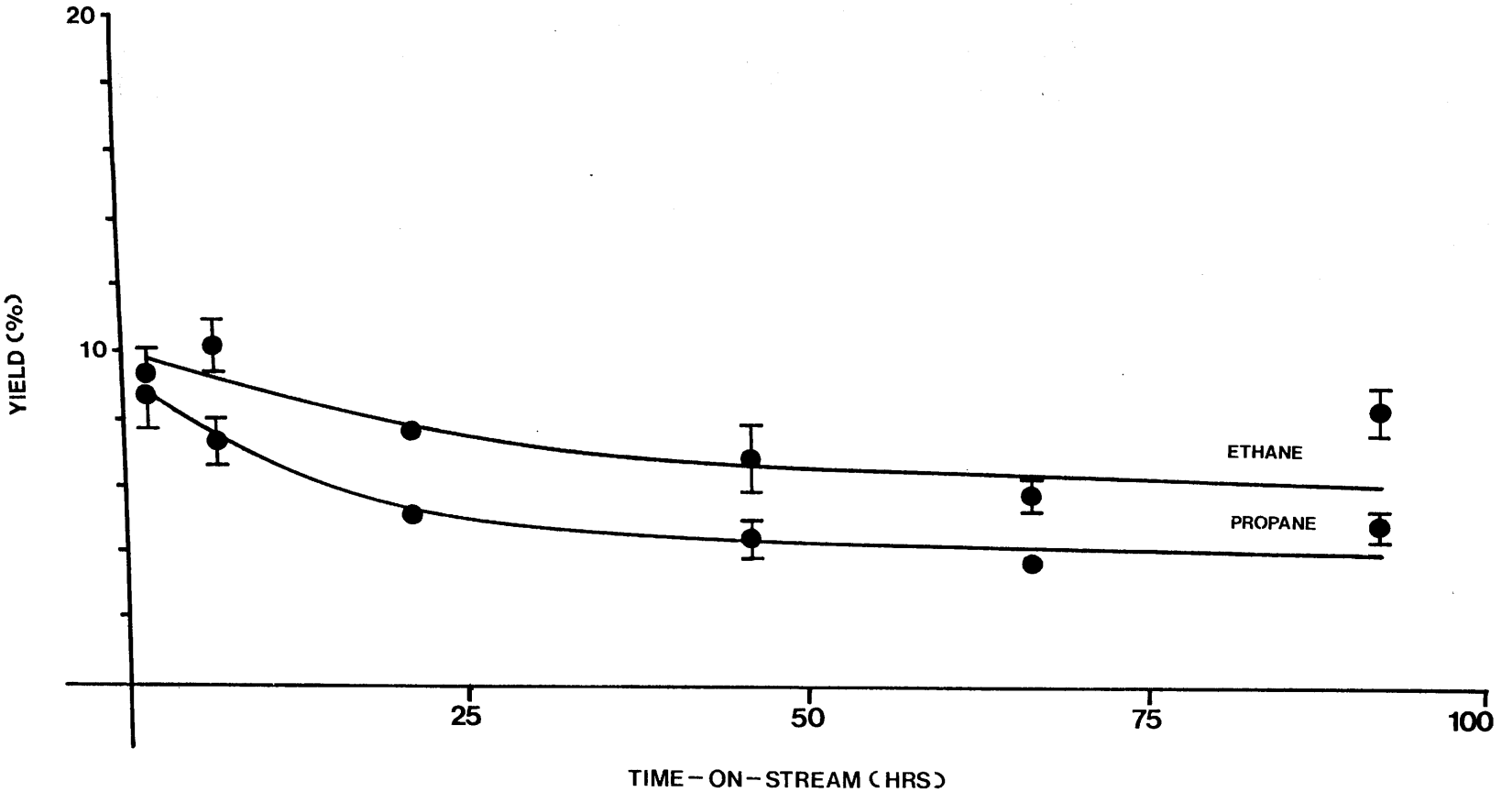

Figure 6.12 - Yield of Ethane and Propane versus Time-on-Stream

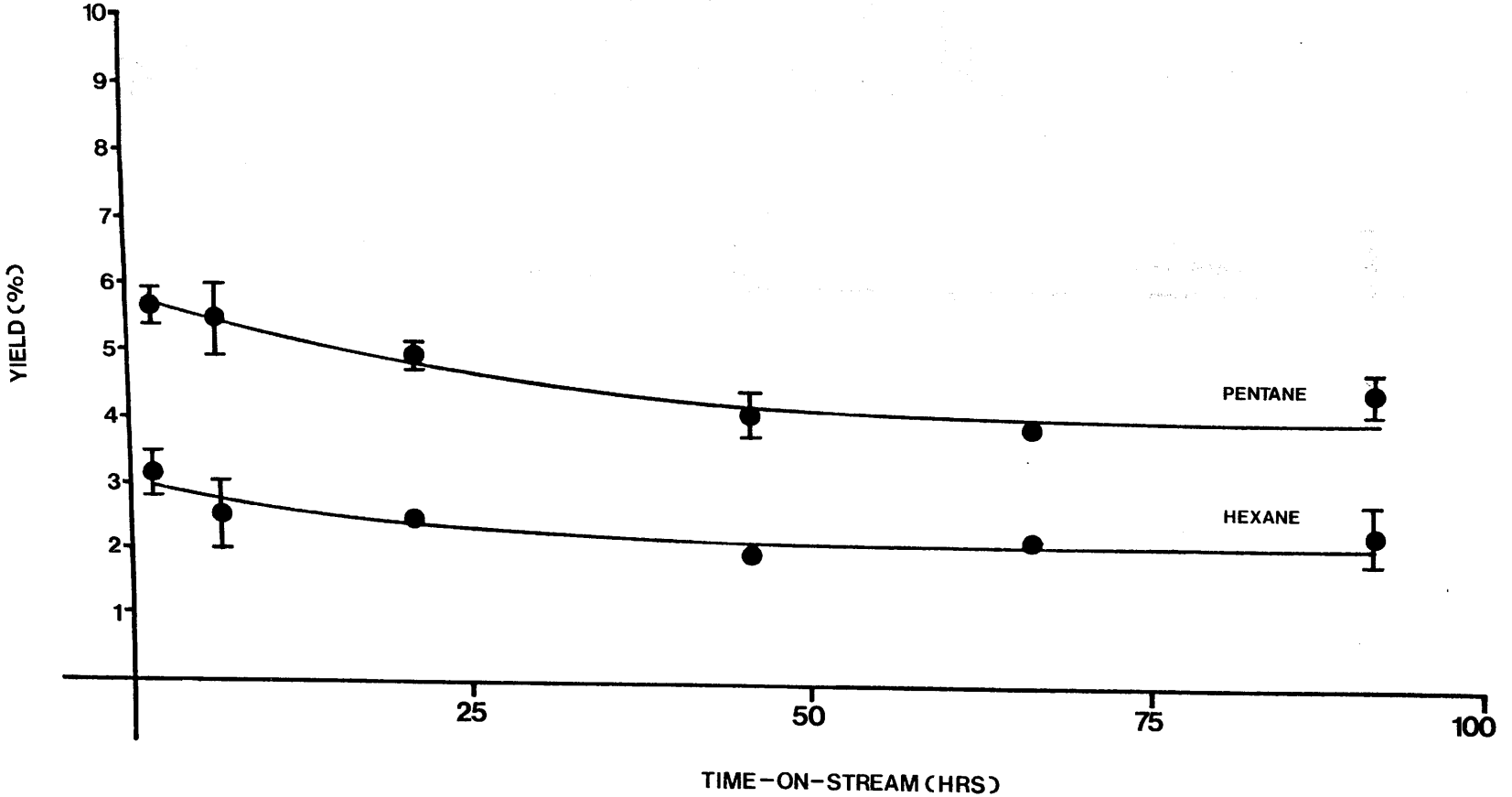

Figure 6.13–Yield of Pentane and Hexane versus Time–on–Stream

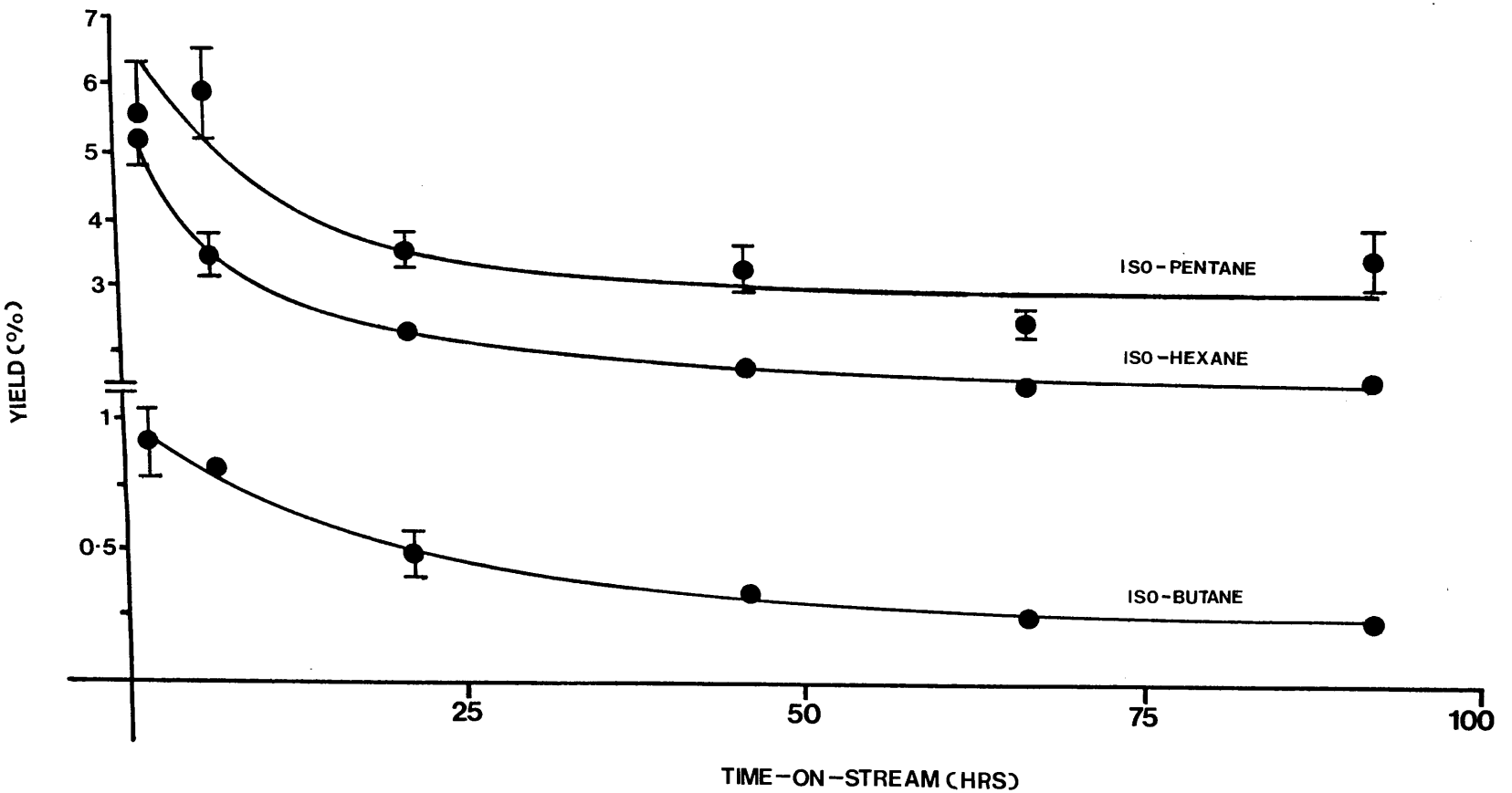

Figure 6.14- Yield of Iso-Pentane, Iso-Hexane, and Iso-Butane versus Time-on-Stream

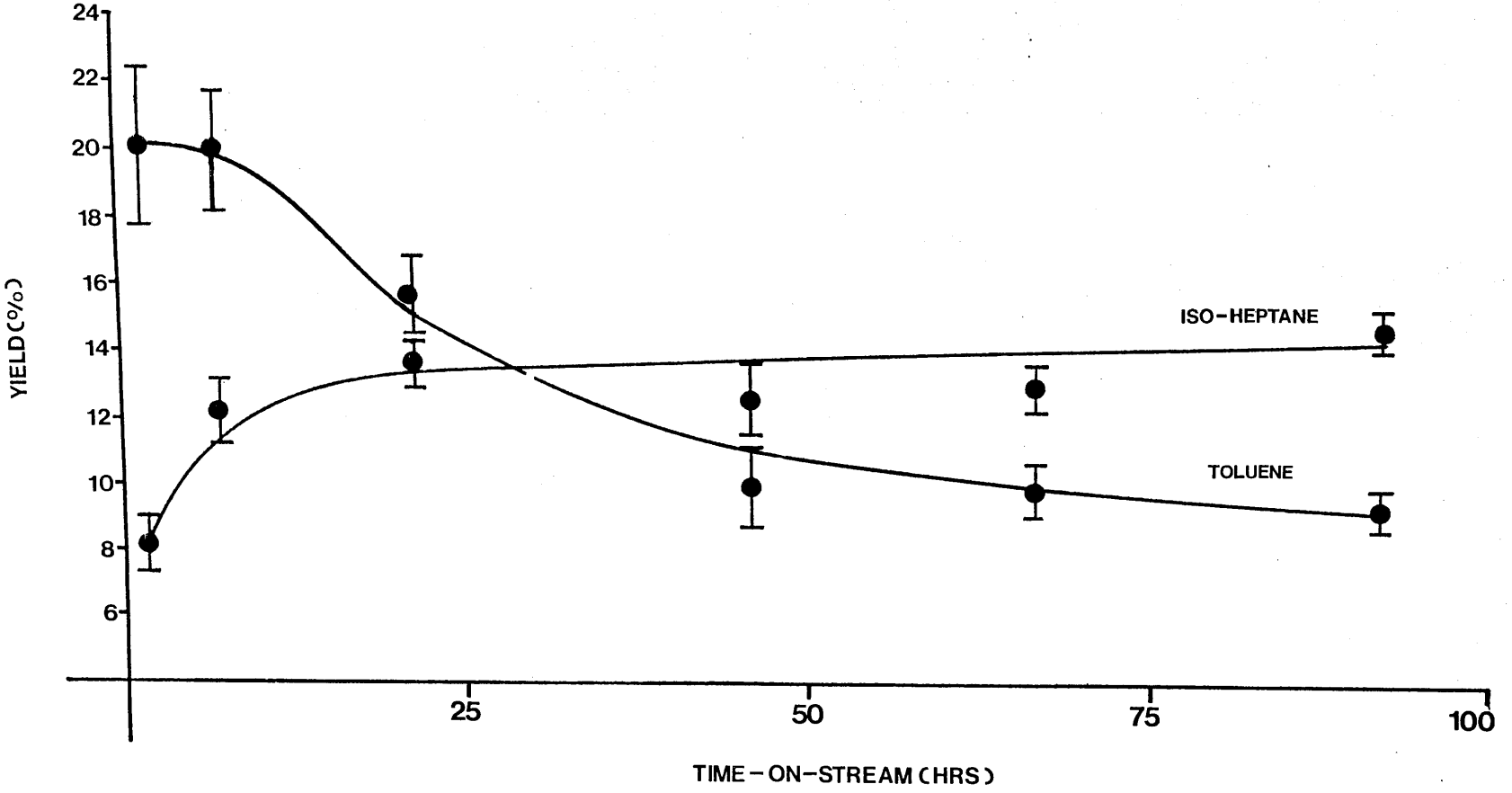

Figure 6.15- Yield of Iso-Heptane and Toluene versus Time-on-Stream

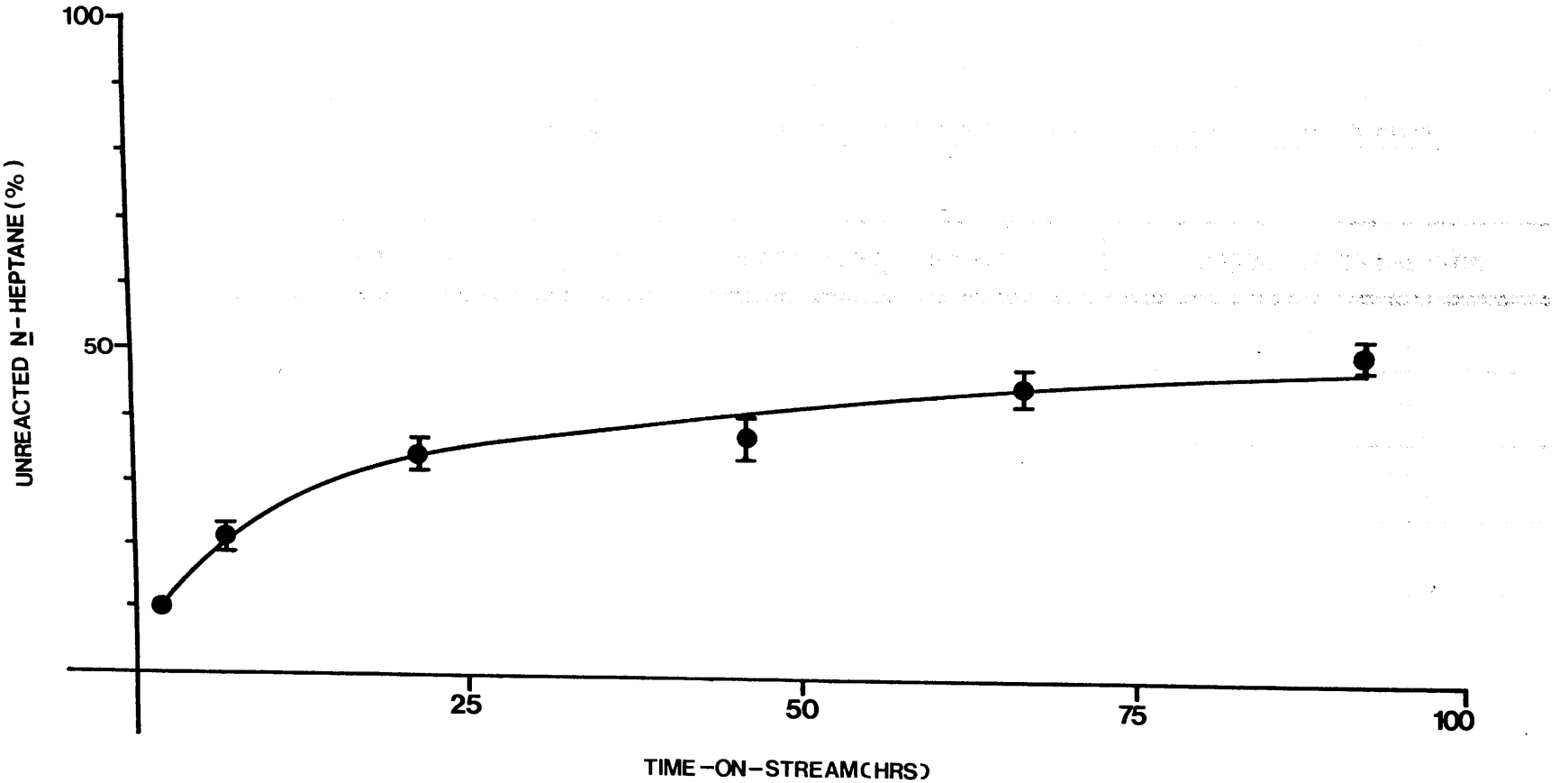

Figure 6.16 – Amount of Unreacted N-Heptane versus Time-on-Stream

Table 6·8 – Conversion, Unreacted N–Heptane and Carbon Mass Balance versus Time–on–Stream

TIME–ON–STREAM (HRS)	CONVERSION	UNREACTED N–HEPTANE	CARBON MASS BALANCE
1·8	73.60 ± 2.97	10.52 ± 1.53	87.07 ± 7.94
6·8	73.82 ± 2.64	21.55 ± 2.55	98.31 ± 8.70
21·3	60.32 ± 1.69	34.04 ± 2.56	97.30 ± 7.10
46·0	48.94 ± 2.17	37.55 ± 3.93	89.43 ± 10.16
66·5	46.43 ± 1.29	45.56 ± 3.08	94.93 ± 7.45
92·0	53.68 ± 1.40	50.51 ± 2.72	107.15 ± 7.06

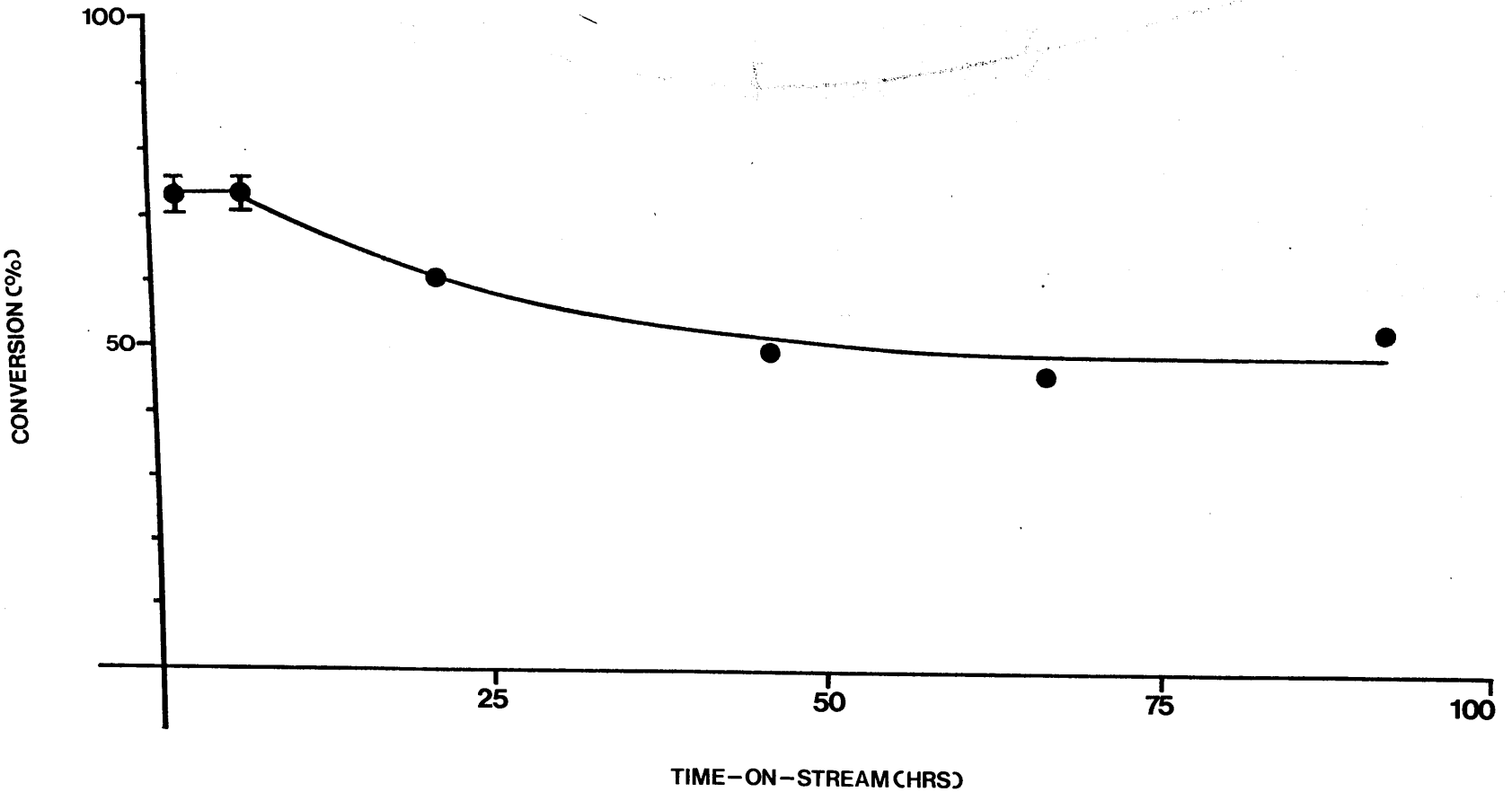

Figure 6.17 – Total Conversion versus Time-on-Stream

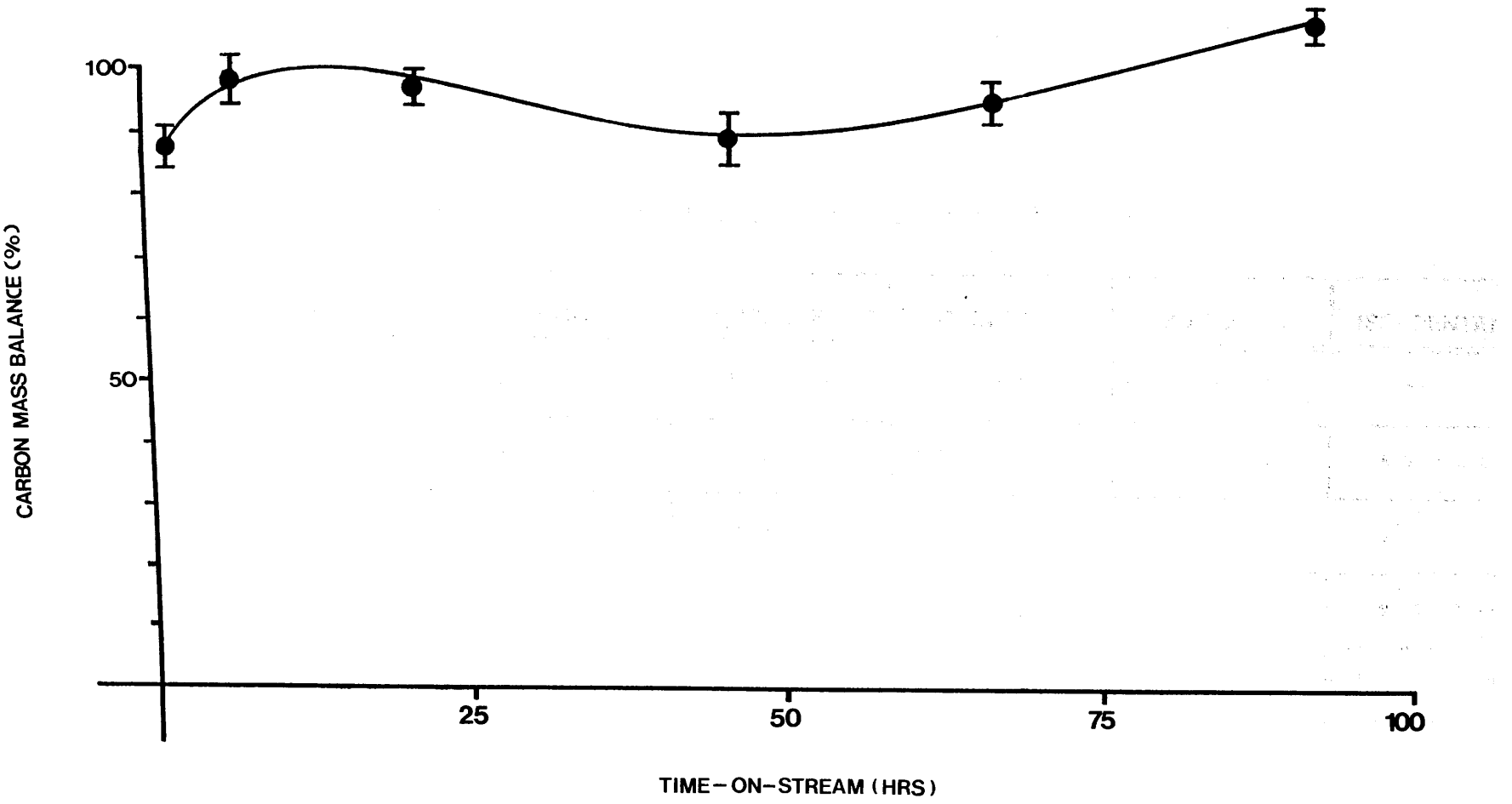

Figure 6.18 - Carbon Mass Balance versus Time-on-Stream

Table 6.9-Selectivity with respect to Individual Products versus Time-on-Stream

TIME-ON-STREAM(HRS)	METHANE	ETHANE	PROPANE	ISO-BUTANE	BUTANE	ISO-PENTANE
1.8	4.32 ± 1.02	11.97 ± 2.31	12.77 ± 3.58	1.25 ± 0.47	4.32 ± 0.95	7.59 ± 2.28
6.8	3.45 ± 0.97	13.88 ± 3.14	10.01 ± 2.49	1.11 ± 0.18	3.85 ± 0.86	8.02 ± 2.07
21.3	3.12 ± 0.36	12.84 ± 1.61	8.59 ± 0.96	0.83 ± 0.34	3.49 ± 0.35	5.84 ± 0.90
46.0	3.47 ± 0.90	14.11 ± 4.82	9.19 ± 2.80	0.71 ± 0.23	3.53 ± 0.76	6.62 ± 1.73
66.5	3.96 ± 0.57	12.60 ± 2.33	8.08 ± 0.99	0.52 ± 0.07	3.49 ± 0.37	5.28 ± 0.98
92.0	4.12 ± 0.57	15.57 ± 3.37	9.10 ± 1.83	0.43 ± 0.18	3.69 ± 0.76	6.41 ± 1.97

Table 6·9 (cont·) – Selectivity with respect to Individual Products.

TIME-ON-STREAM (HRS)	PENTANE	ISO-HEXANE	HEXANE	ISO-HEPTANE	TOLUENE
1·8	7.75 ± 1.06	7.17 ± 1.31	4.36 ± 0.63	11.15 ± 3.09	27.20 ± 8.10
6·8	7.59 ± 1.86	4.71 ± 0.93	3.52 ± 0.81	16.65 ± 3.64	27.20 ± 6.46
21·3	8.39 ± 0.99	3.81 ± 0.34	4.24 ± 0.46	22.83 ± 3.84	26.01 ± 8.09
46·0	8.45 ± 1.71	3.66 ± 0.75	4.21 ± 0.64	25.62 ± 5.73	20.39 ± 6.53
66·5	8.50 ± 0.88	3.30 ± 0.40	4.87 ± 0.56	27.89 ± 3.97	21.49 ± 4.09
92·0	8.44 ± 1.44	2.94 ± 0.58	4.40 ± 0.91	27.44 ± 3.20	17.48 ± 2.76

Table 6·10 – Selectivity with respect to Major Reactions versus Time – on – Stream

TIME – ON – STREAM (HRS)	AROMATISATION	ISOMERISATION	HYDROCRACKING	HYDROGENOLYSIS
1·8	27.20 ± 8.10	11.15 ± 3.09	16.01 ± 2.67	28.40 ± 2.84
6·8	27.20 ± 6.46	16.65 ± 3.64	13.84 ± 2.28	28.40 ± 3.86
21·3	26.01 ± 8.09	22.83 ± 3.84	10.45 ± 1.02	28.59 ± 1.98
46·0	20.39 ± 6.53	25.62 ± 5.73	10.99 ± 1.90	30.24 ± 5.23
66·5	21.49 ± 4.09	27.89 ± 3.97	9.10 ± 1.06	28.36 ± 2.61
92·0	17.48 ± 2.76	27.44 ± 3.20	9.78 ± 2.06	31.07 ± 3.82

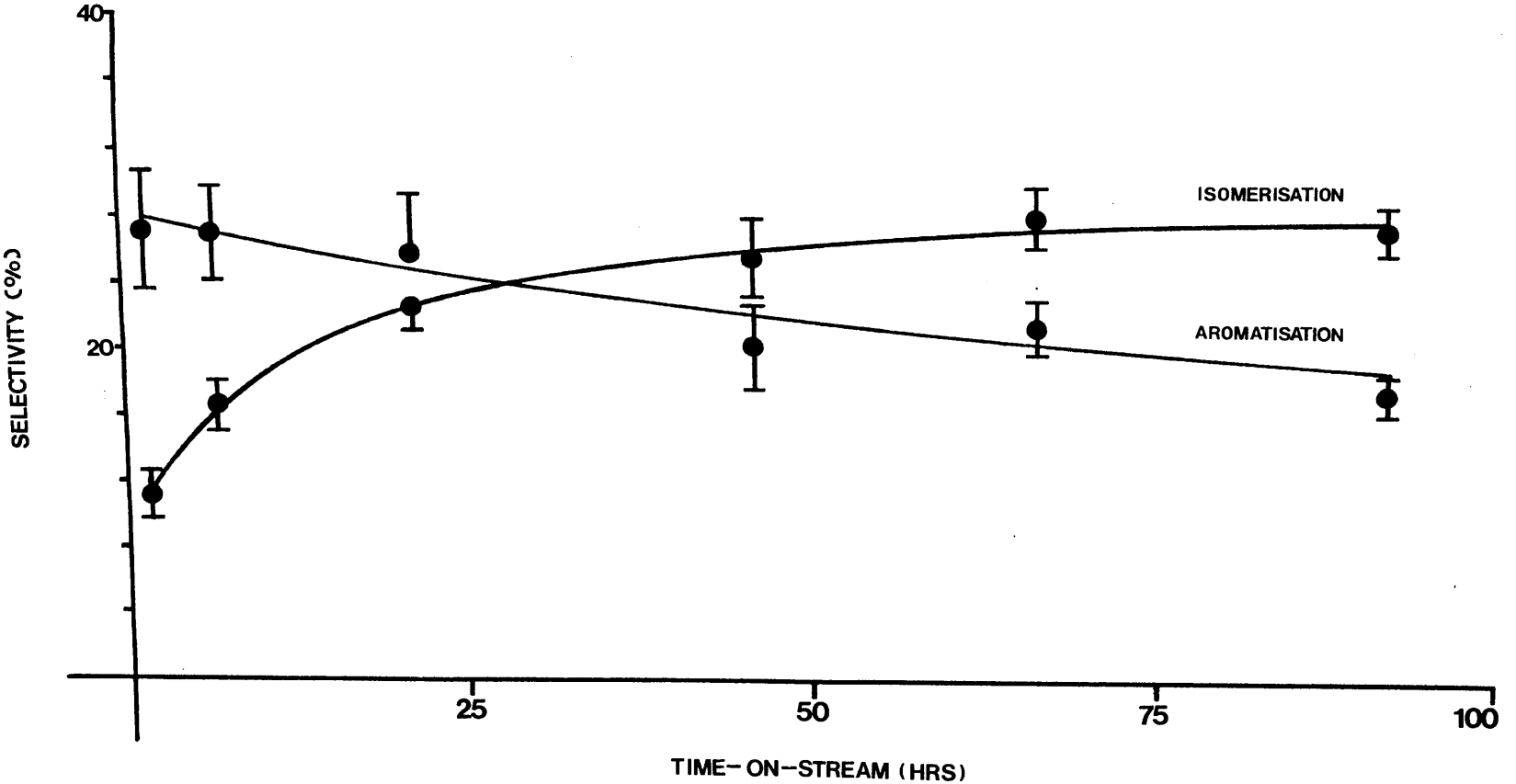

Figure 6.19-Selectivity with respect to Isomerisation and Aromatisation versus Time-on-Stream

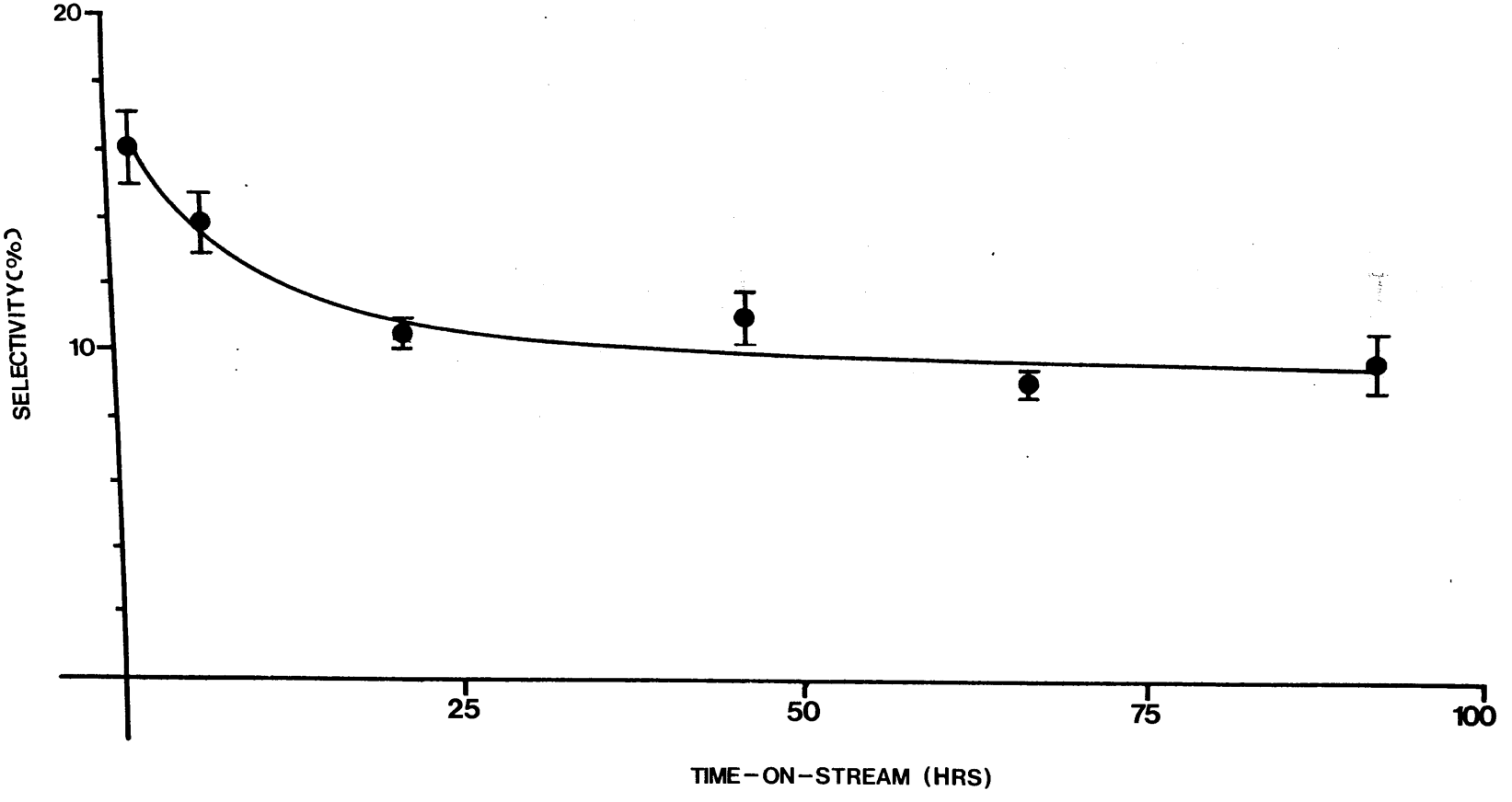

Figure 6.20 - Selectivity with respect to Hydrocracking versus Time-on-Stream

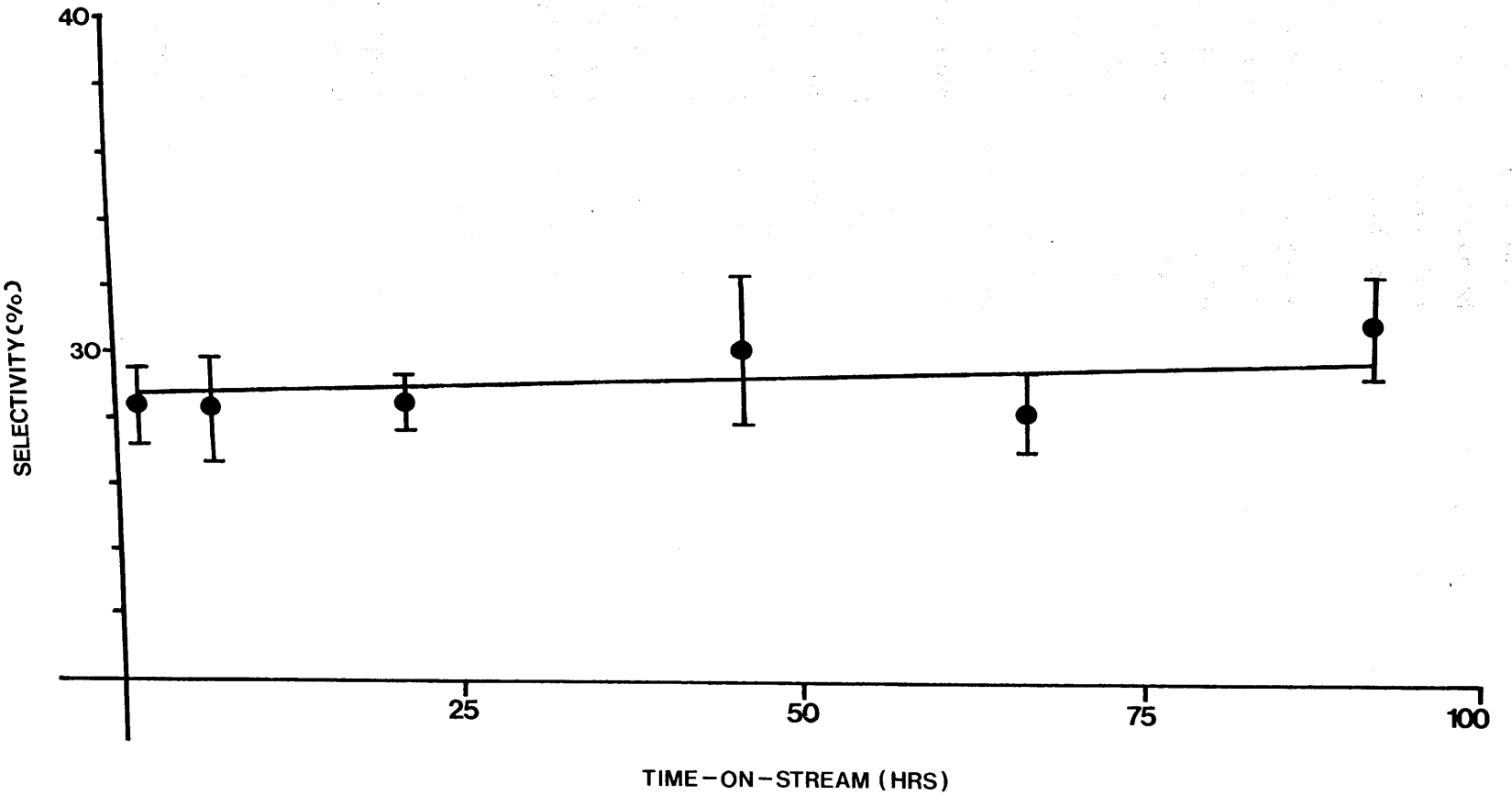

Figure 6.21 - Selectivity with respect to Hydrogenolysis versus Time-on-Stream

On examining figure 6.18 it must be concluded that there is no obvious or discernible trend in the calculated carbon mass balance values. Consequently, it was not considered possible to interpret figure 6.18 in terms of a variation in the extent of carbon uptake by the catalyst surface with time. In considering the remainder of the data, however, it is clear that under a given set of continuous flow conditions strong parallels exist between the performance of catalyst RC2 and that of RC1 (section 6.1.1). For example, at any given time-on-stream the relative yields of the individual products obtained from both catalysts are largely compatible. Moreover, for both catalysts a downward trend is observed in many of the yield and the conversion values with increasing time-on-stream. In addition, the selectivity changes experienced by catalyst RC2 (Figs.6.19 - 6.21) are identical in nature to those described previously for catalyst RC1 (Figs.6.9 - 6.10), with once again the most marked changes in selectivity taking place during the initial stages of the reaction.

However, despite the obvious similarities that exist between the two sets of experimental data, several differences must also be pointed out. Perhaps the most striking of these is that, in the case of catalyst RC2, the yield of the iso-heptane product actually increased during the course of the experiment (Fig.6.15) and yet, as noted, there was a simultaneous decrease in the overall catalyst activity (Fig.6.17). This contrasts with the decrease in iso-heptane yield that occurred in the corresponding experiment carried out over catalyst RC1 (Fig.6.5). Furthermore, although the total conversion for catalyst RC2, like that of catalyst RC1, exhibited an overall decrease with time, in contrast to catalyst RC1 there appears to have been no deactivation during the very initial stages of the reaction. It is also notable that whilst the initial hydrocracking and aromatisation selectivities of the two catalysts were very similar, catalyst RC2 exhibited a higher hydrogenolysis and lower isomerisation selectivity than RC1. Moreover, throughout the course of the experiment the magnitude of the selectivity changes experienced by the two catalysts were different, particularly in the case of the isomerisation and aromatisation reactions (tables 6.6, 6.10).

The residual chlorine content of spent catalyst RC2 was measured by neutron activation analysis at a value of 0.47% by weight. This compares with a corresponding figure of 1.26% by weight for the fresh catalyst.

6.2 Non-Continuous Flow Experiments

The experimental procedure used in both the pulse-flow and static non-continuous flow experiments has been described previously (section 4.2.1.2). Both the experiments reported in this section were performed using catalyst RC1 (section 3.2) and were carried out in the absence of reactant hydrogen.

6.2.1 Pulse-Flow of N-Heptane over Catalyst RC1

The retention of surface carbon by catalyst RC1 was examined under pulse-flow experimental conditions. A total of eight 1µl injections of liquid n-heptane were made into a 40 $ml.min^{-1}$ helium flow and pulsed over a 0.25 g sample of the reduced catalyst which was maintained at 500°C. The injections were made at regular 30 minute intervals throughout a 210 minute injection period. The reduced catalyst was treated with a 40 $ml.min^{-1}$ helium flow for 1 hour before the initial n-heptane injection and was left standing in static helium between injections. Blank pulse-flow experiments (section 4.2.3.3) indicated that the gas phase pyrolysis of n-heptane occurred to a negligible extent under the above experimental conditions.

The yields of all individual products, together with the amount of unreacted n-heptane, and the total conversion values are shown in table 6.11 and the first column of table 6.12. These values are plotted against the corresponding injection numbers in figures 6.22 - 6.28. Carbon mass balance and hydrogen mass balance values were calculated for each injection and these are given in the second and third columns, respectively, of table 6.12. The latter were derived using a procedure similar to that used in the derivation of the carbon mass balance

values which has been described previously (section 5.1). The carbon mass balance values are plotted against injection number in figure 6.29.

Appreciable quantities of carbon were retained by the catalyst surface during the pulse-flow experiment. This is clearly illustrated in figure 6.29 which indicates a quantity of residual carbon equivalent to ca.0.1% of the original catalyst weight. In comparison a corresponding figure of ca.1.0% was obtained from the combustion analysis of the spent catalyst (section 3.3.2) although it should be noted that the size of the sample available for combustion analysis (0.05g) was perhaps too small to permit an accurate determination of surface carbon content to be performed. It is further evident from figure 6.29 that the vast bulk of the carbon uptake occurred during passage of the initial n-heptane pulse through the catalyst bed. A comparatively minor quantity was retained during the second pulse. During the remaining six pulses little if any carbon appears to have been laid down on the catalyst surface with the carbon mass balance values approximating to 100%.

It is very interesting to note that the retention of carbon did not coincide with a corresponding decrease in the catalyst activity. Indeed, the conversion values actually exhibited a very substantial and progressive increase over the first three injections (Fig.6.28). Thereafter an essentially stable value was attained. Figures 6.22 - 6.27 reveal that the trend observed in the conversion values was coupled with a corresponding increase in the individual yields of most of the reaction products. In fact, only methane and the unreacted n-heptane reactant decreased in yield with each subsequent injection. In the case of toluene, and also ethane, a prominent increase in yield which occurred over the first few injections was followed by a progressive decrease in yield during the latter injections.

The trends noted in the individual product yield values are largely reiterated when the corresponding selectivity values are

Table 6.11-Yield of Individual Products and Amount of Unreacted N-Heptane versus Injection Number

INJECTION NO.	METHANE	ETHANE	PROPANE	BUTANE	BUTENE	PENTANE	PENTENE	HEPTANE	HEPTENE	TOLUENE
1	32.60	9.59	0.64					15.12		20.65
2	15.35	24.44	7.69	0.78	0.13			7.15		41.05
3	11.33	24.84	11.41	1.85	0.33	0.42	0.49	5.06	1.21	43.04
4	9.96	31.51	13.95	2.34	0.74	1.04	1.73	4.45	3.14	30.02
5	9.00	29.45	15.08	2.82	1.26	1.91	2.45	3.99	7.29	26.26
6	8.67	28.81	15.39	3.21	1.37	2.35	2.75	3.18	9.96	22.84
7	8.29	28.23	15.56	3.36	1.44	2.22	3.38	3.03	12.09	20.05
8	8.12	27.83	16.10	3.38	1.71	2.69	4.29	3.11	13.21	18.07

Table 6-12- Conversion, Carbon Mass Balance and Hydrogen Mass Balance versus Injection Number.

INJECTION NUMBER	CONVERSION	CARBON MASS BALANCE	HYDROGEN MASS BALANCE
1	62.61	77.71	93.30
2	89.98	96.95	91.10
3	95.32	100.29	91.56
4	94.65	99.10	99.54
5	95.77	99.70	100.82
6	95.57	98.75	101.19
7	94.76	97.79	101.19
8	95.55	98.66	102.84

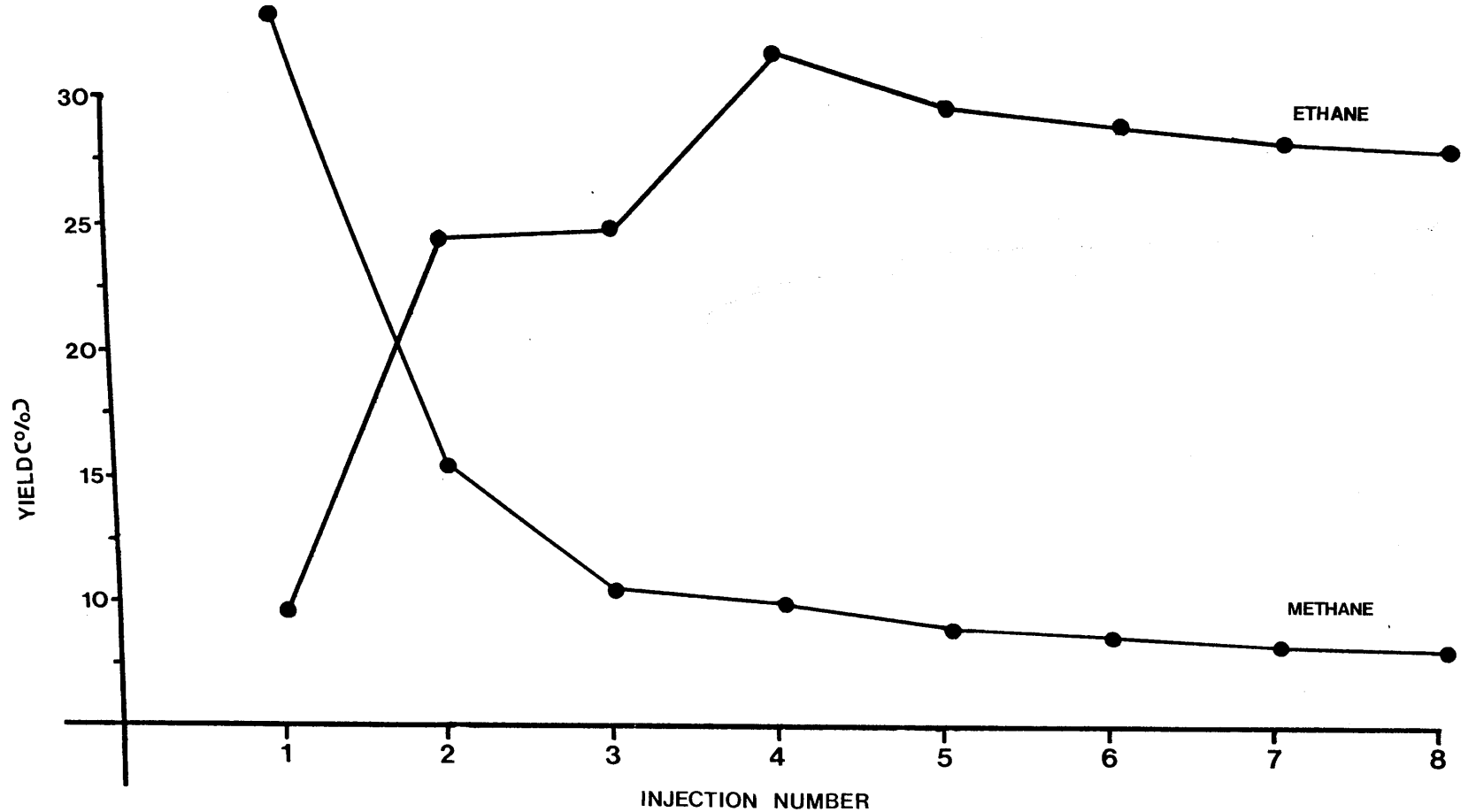

Figure 6.22 – Yield of Methane and Ethane versus Injection Number

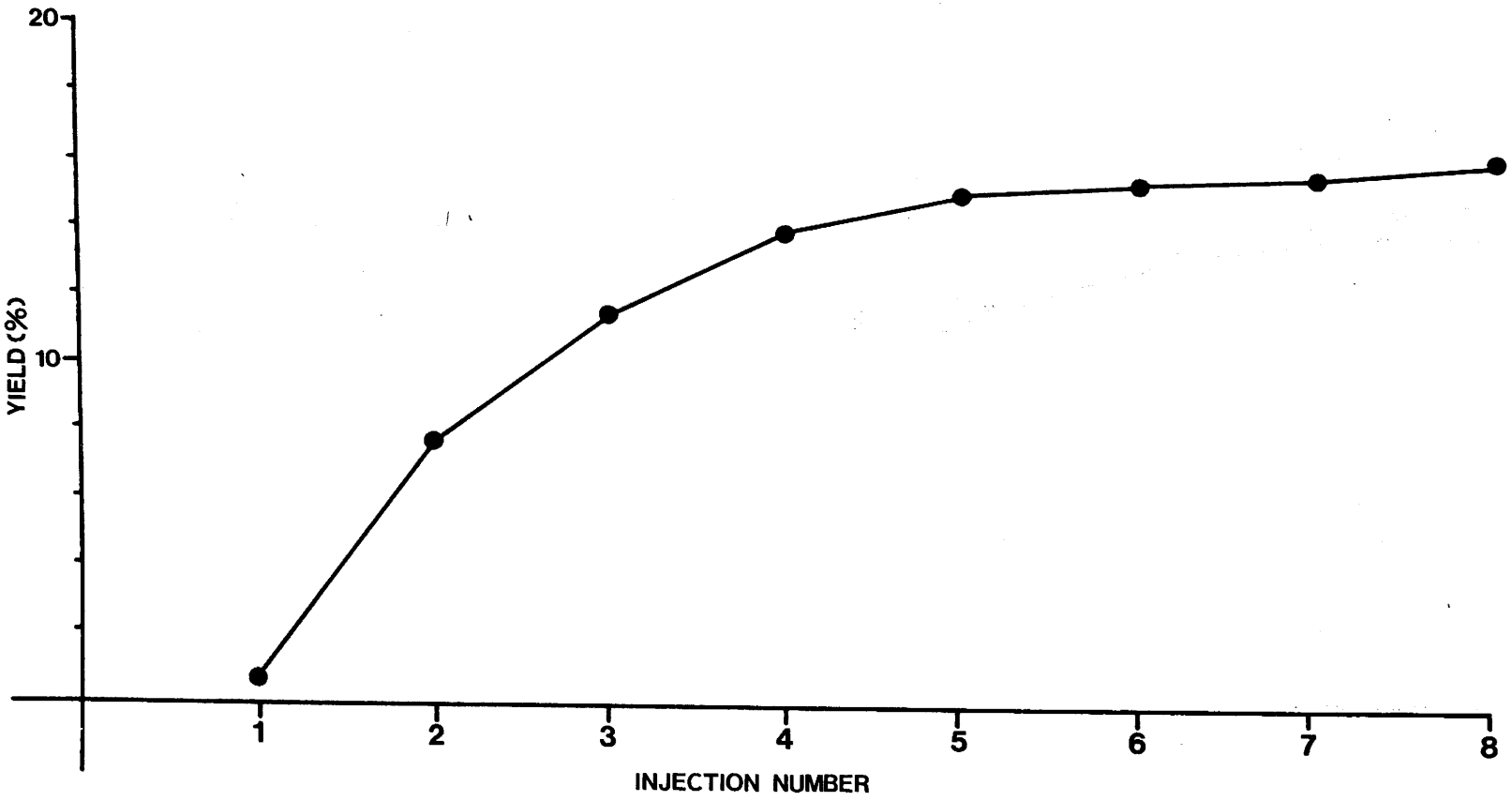

Figure 6·23– Yield of Propane versus Injection Number

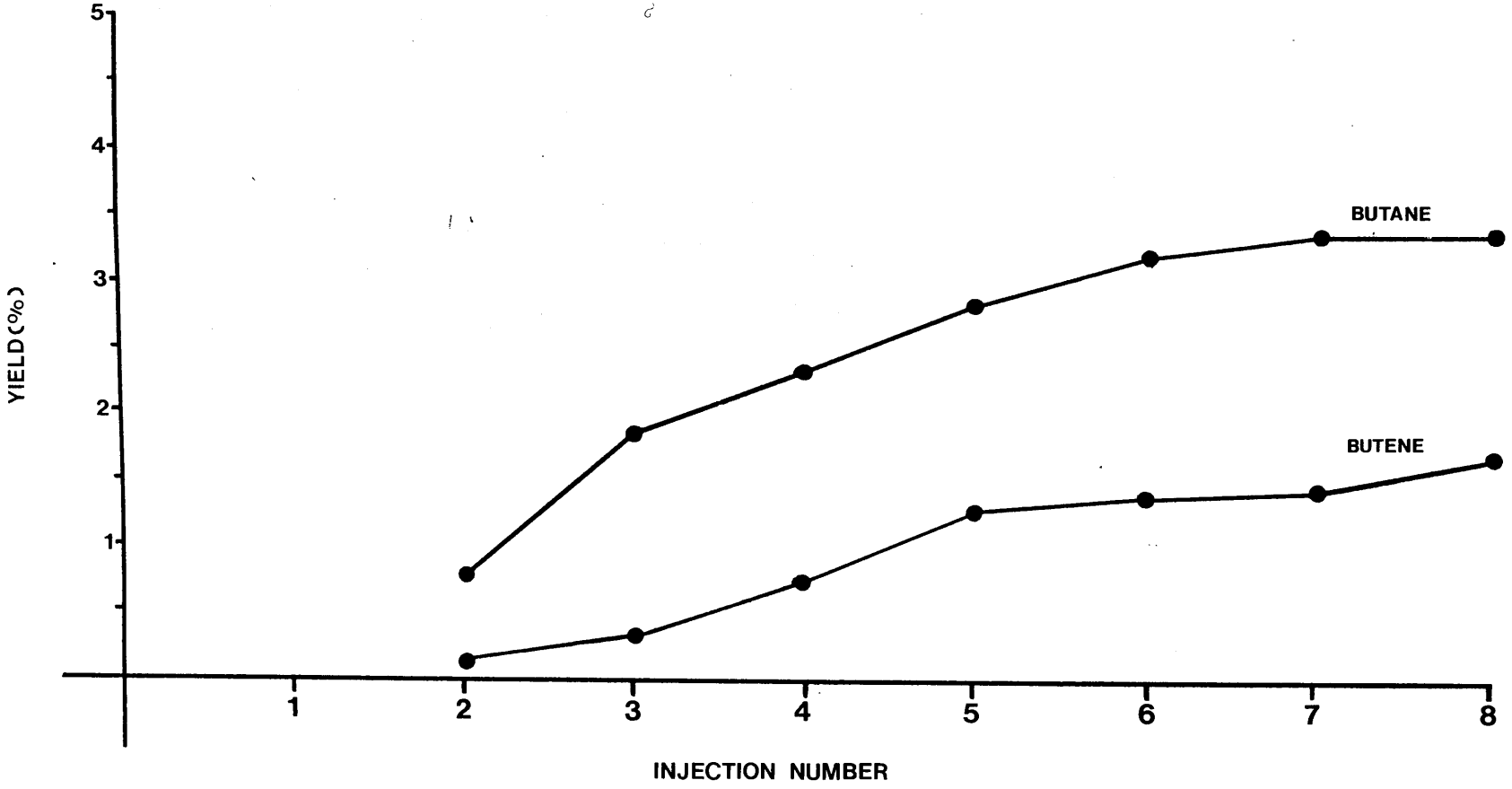

Figure 6.24 – Yield of Butane and Butene versus Injection Number

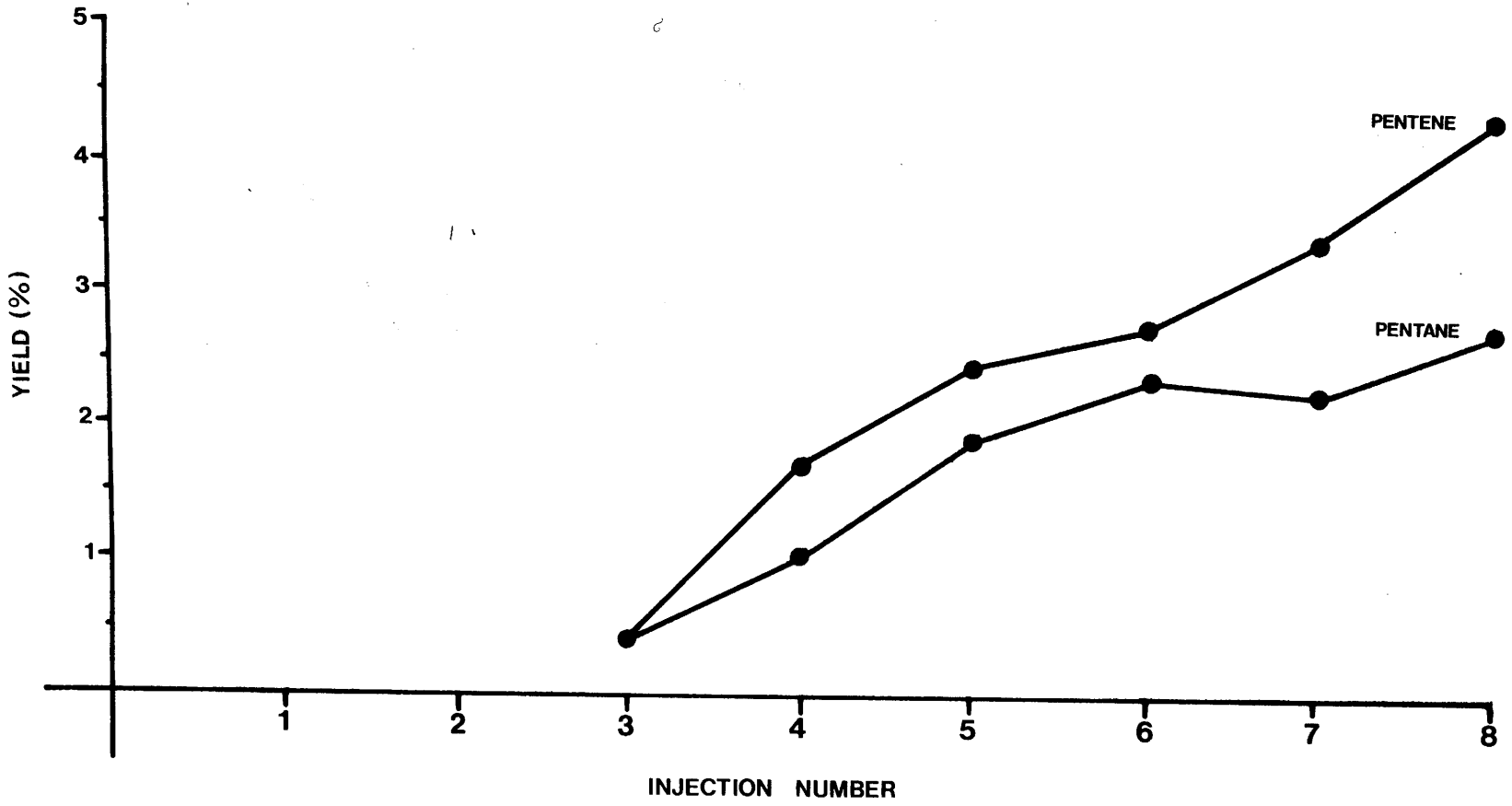

Figure 6.25–Yield of Pentane and Pentene versus Injection Number

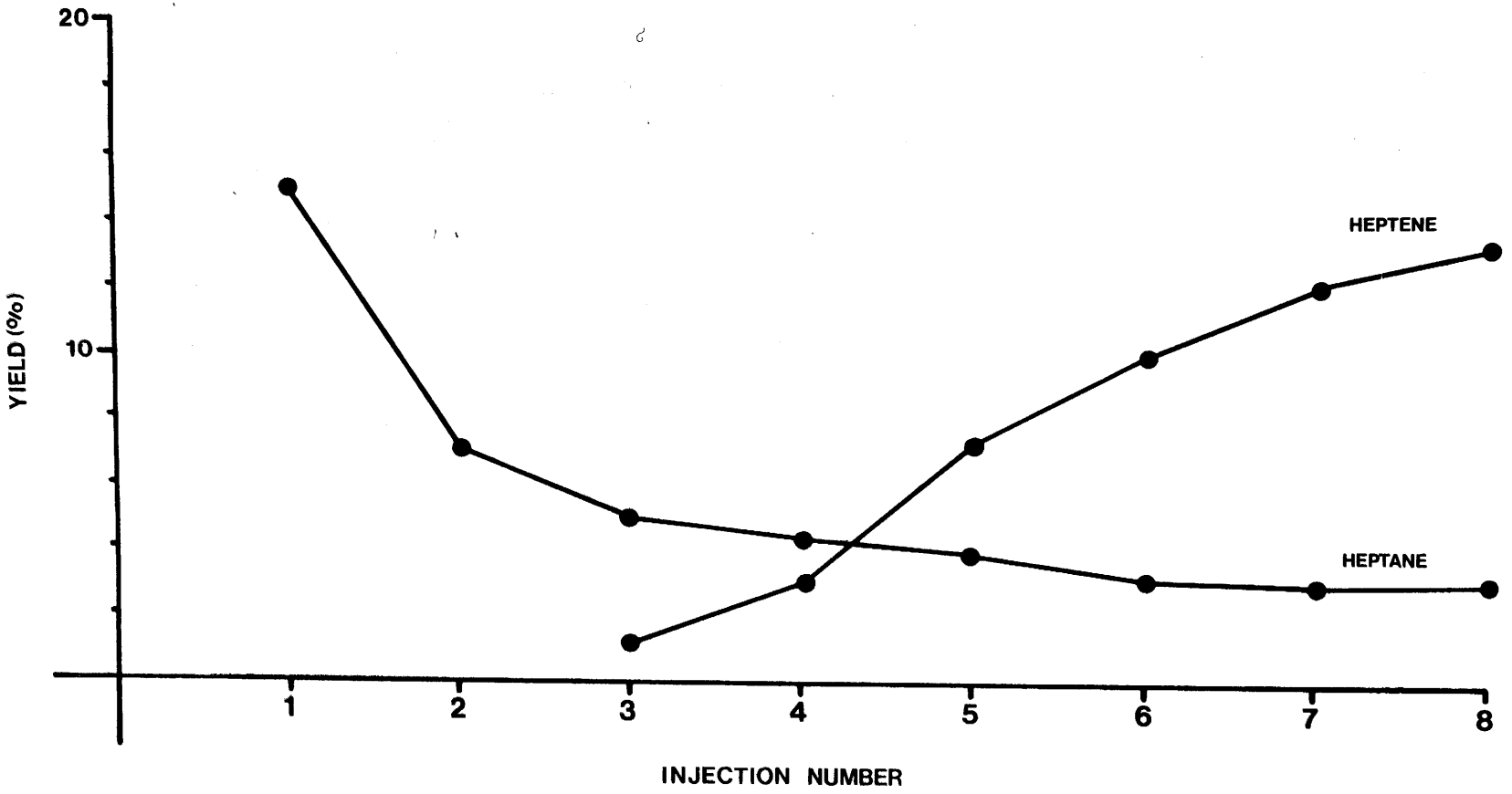

Figure 6.26 - Yield of Heptane and Heptene versus Injection Number

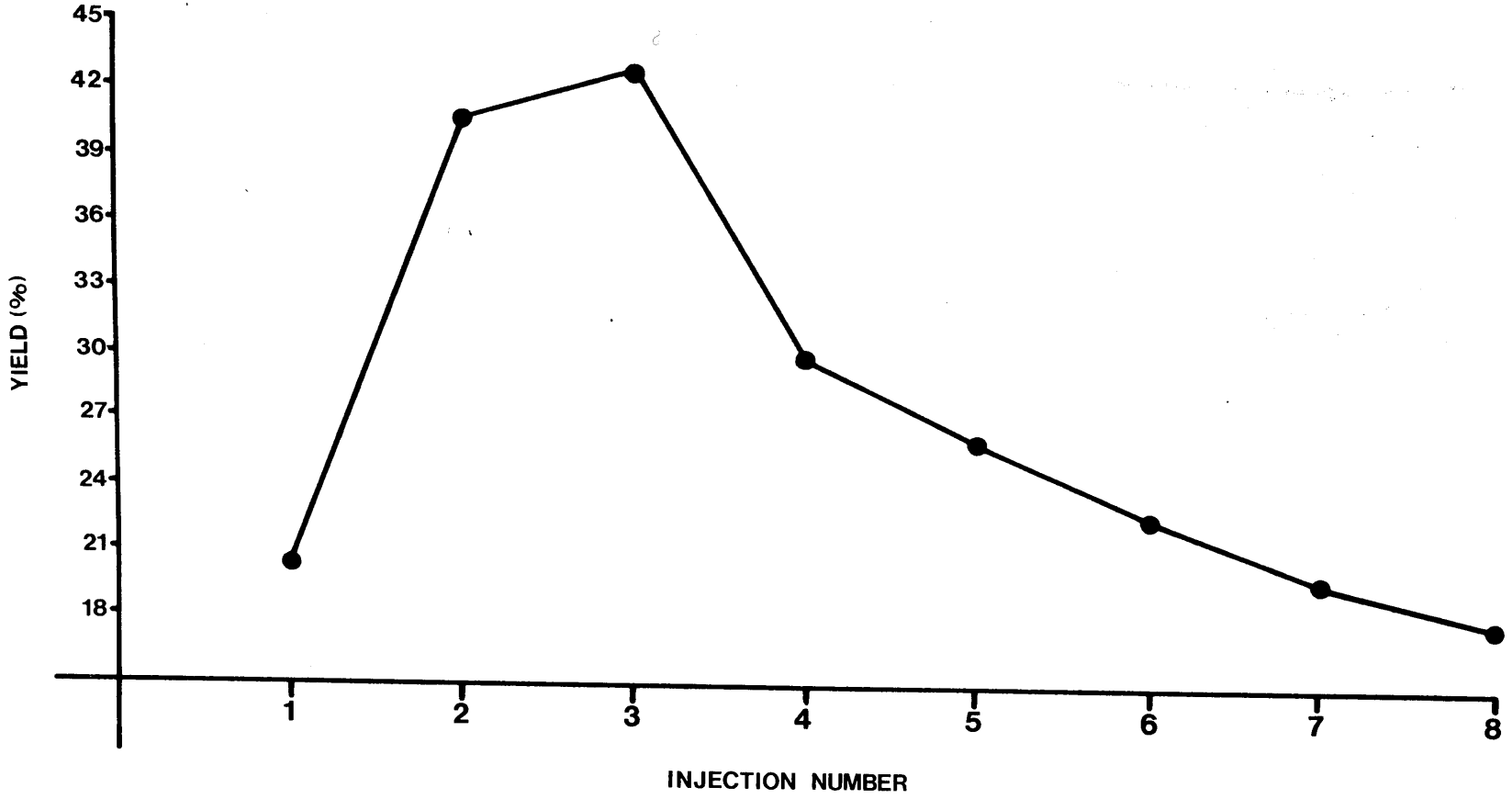

Figure 6·27 – Yield of Toluene versus Injection Number

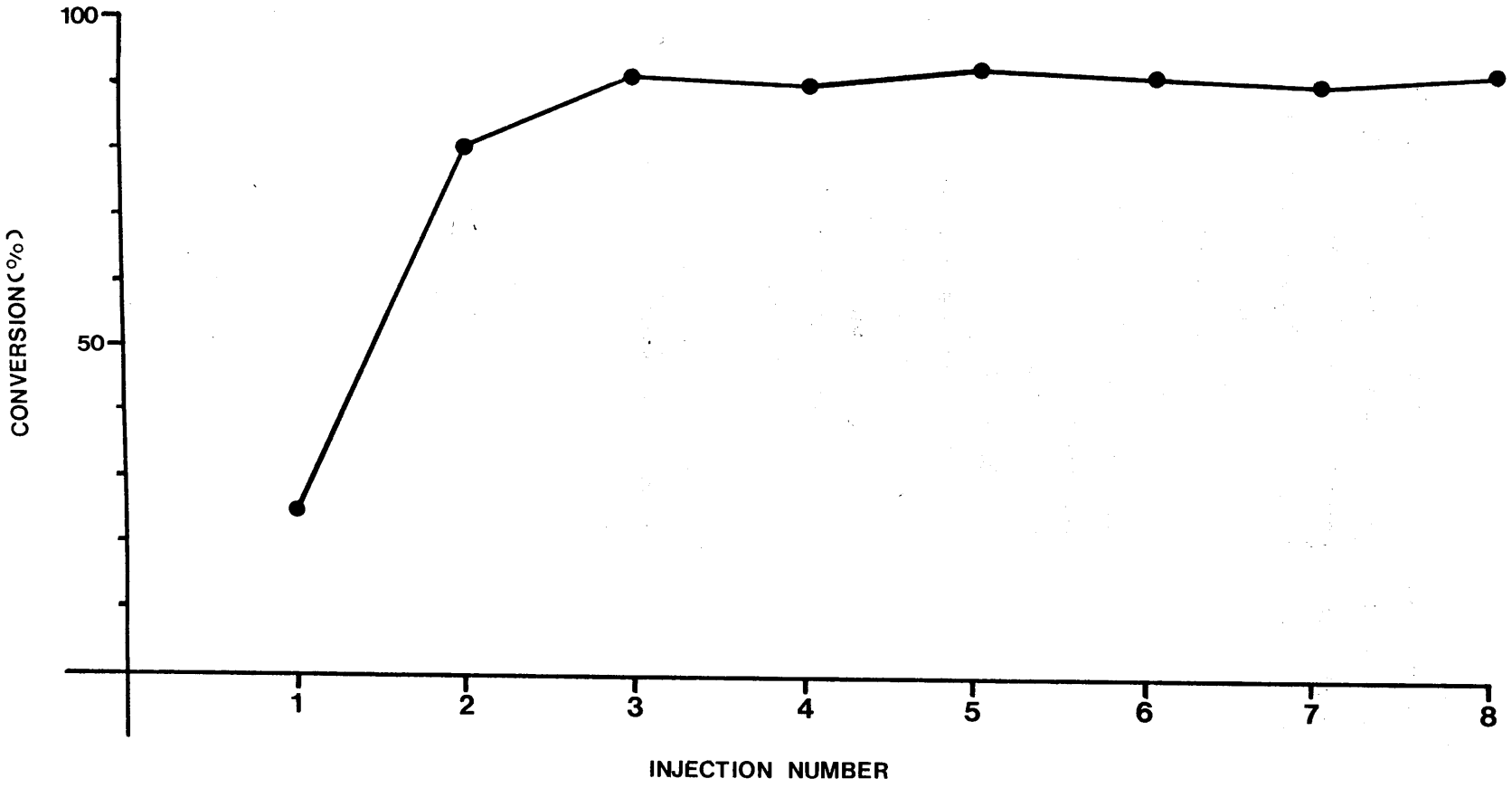

Figure 6.28 - Total Conversion versus Injection Number

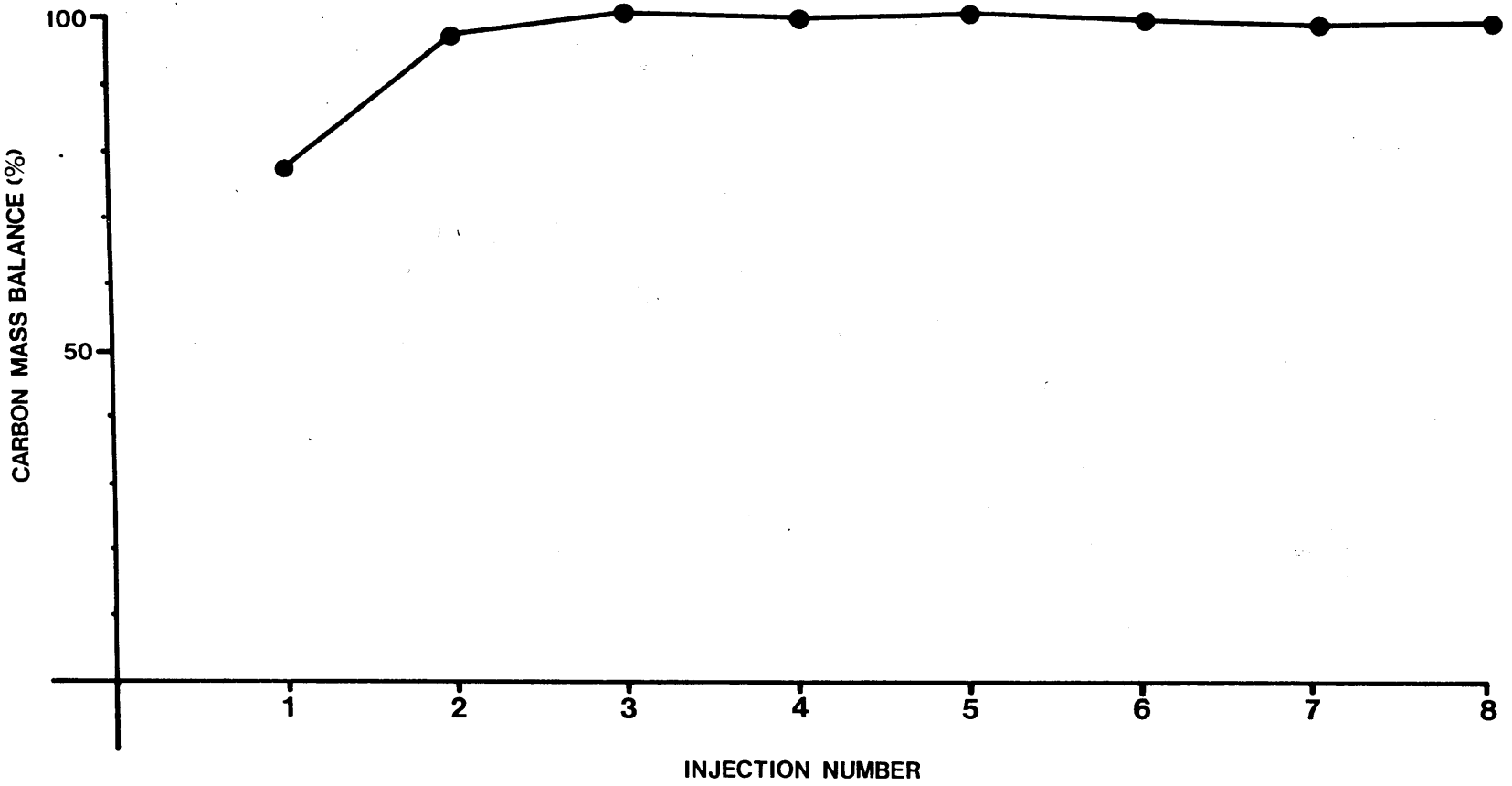

Figure 6.29-Carbon Mass Balance versus Injection Number

considered. These values are tabulated in table 6.13 and are plotted against the appropriate injection numbers in figures 6.30 - 6.35. In the product distribution obtained from the initial injection methane and toluene were the major products, ethane being the only other product formed in any significant quantity. The selectivity for methane was drastically reduced in the second and third injections whereas that for ethane, propane and toluene was greatly enhanced, with appreciable quantities of n-butane also being formed. For subsequent injections the selectivities of the catalyst with respect to methane and propane formation approached stable values with the ethane selectivity showing a slight decrease. This coincided with a more acute reduction in the toluene selectivity and a progressive increase in the tendancy of the catalyst to form n-butane and n-pentane together with the olefinic species, n-butene, n-pentene and n-heptene. Neither n-hexane, n-hexene nor any iso-paraffinic compounds were detected as products following the injections.

The absence of any sharp negative peak at the beginning of each of the chromatograms obtained during the pulse-flow experiment, indicated that molecular hydrogen was not present amongst the product mixtures.

6.2.2 Static Experiment Involving the Interaction of [C-14] N-Heptane and Unlabelled N-Heptane with Catalyst RC1

A total of eleven 5µl injections of liquid n-heptane were made into a static helium filled reaction vessel (section 4.2.1.2) which contained a 0.25 g sample of the reduced catalyst RC1 at 500°C. The injections were made at regular 35 minute intervals throughout a 350 minute period. The first five injections were performed using [14-C] labelled n-heptane (section 4.1.2) whereas non-radiolabelled n-heptane was used in the remaining six injections. Each injected sample was allowed to react for 5 minutes before the reaction vessel was

Table 6.13 – Selectivity with respect to Individual Products versus Time-on-Stream

INJECTION NO.	METHANE	ETHANE	PROPANE	ISO-BUTANE	BUTANE	BUTENE	PENTANE	PENTENE	HEPTENE	TOLUENE
1	52.06	15.31	1.02							32.98
2	17.05	27.16	8.54	0.36	0.86					45.62
3	11.88	26.05	11.97	0.36	1.94	0.34	0.44	0.51	1.26	45.15
4	10.52	33.29	14.73	0.19	2.47	0.78	1.09	1.82	3.31	31.71
5	9.39	30.75	15.74	0.21	2.94	1.31	1.99	2.55	7.61	27.41
6	9.07	30.14	16.10	0.18	3.35	1.43	2.45	2.87	10.42	23.39
7	8.74	29.79	16.42	0.09	3.54	1.51	2.34	3.56	12.75	21.15
8	8.49	29.12	16.84	0.10	3.53	1.78	2.81	4.48	13.82	18.91

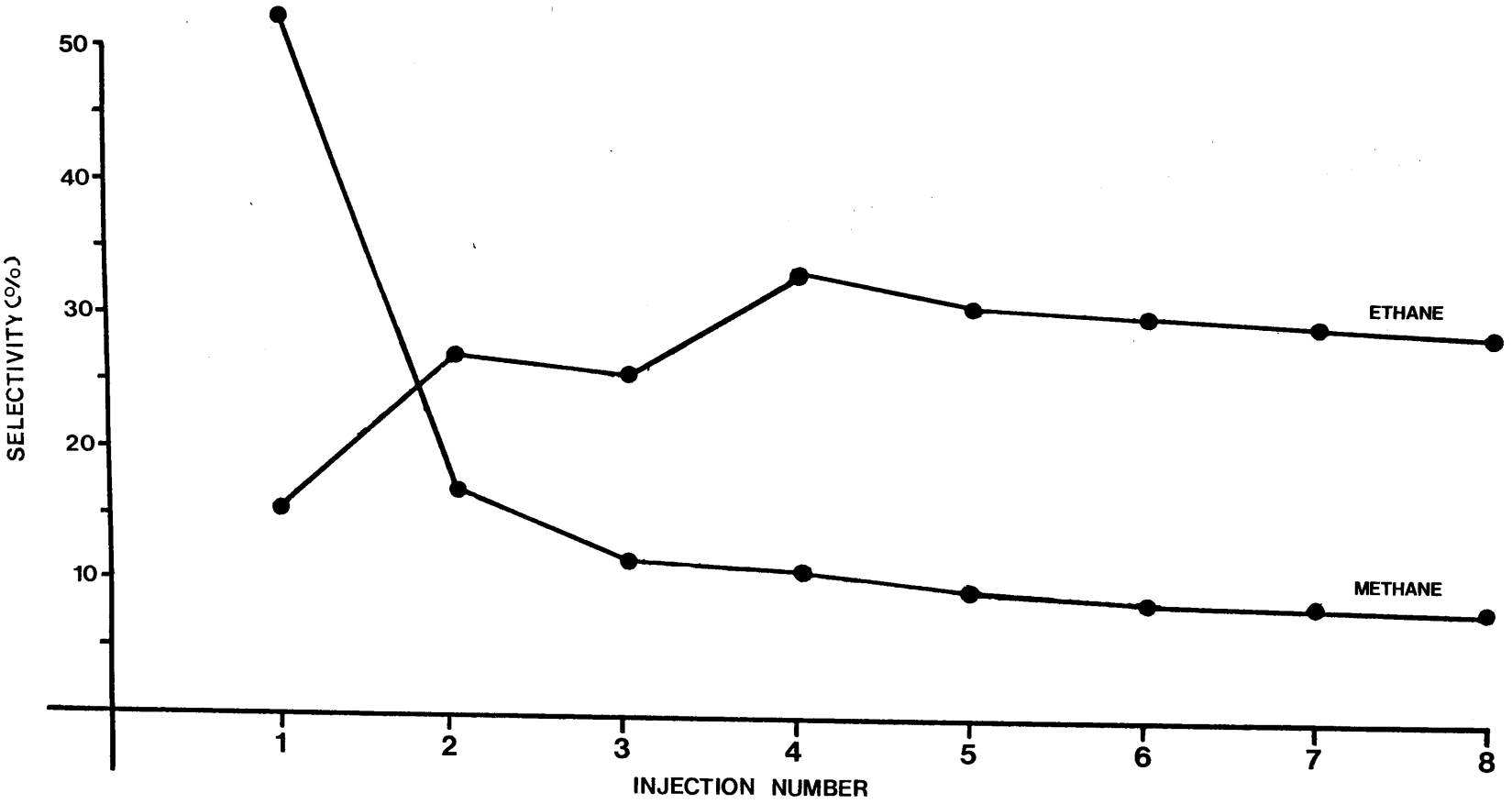

Figure 6.30 – Selectivity with respect to Methane and Ethane versus Injection Number

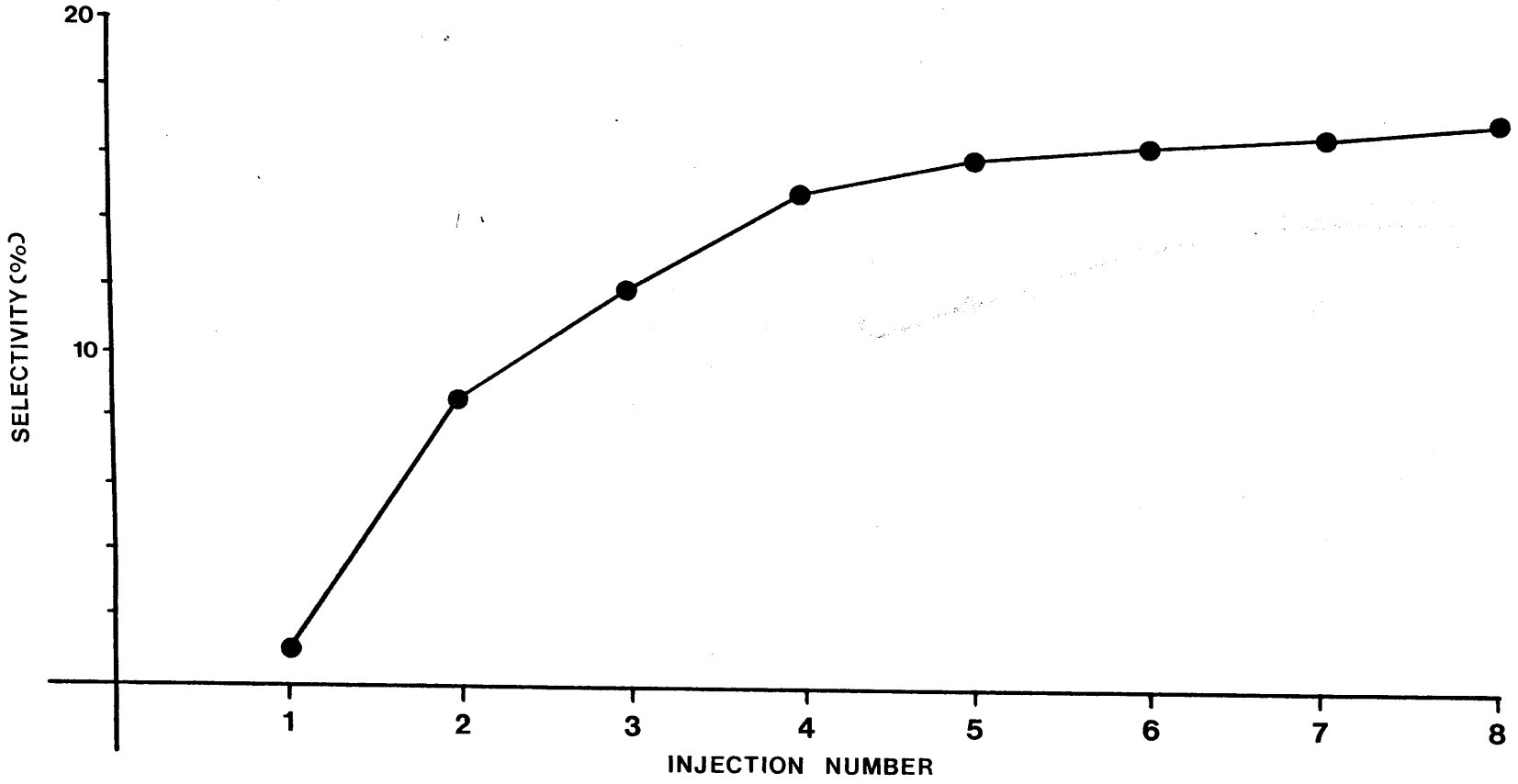

Figure 6.31 – Selectivity with respect to Propane versus Injection Number

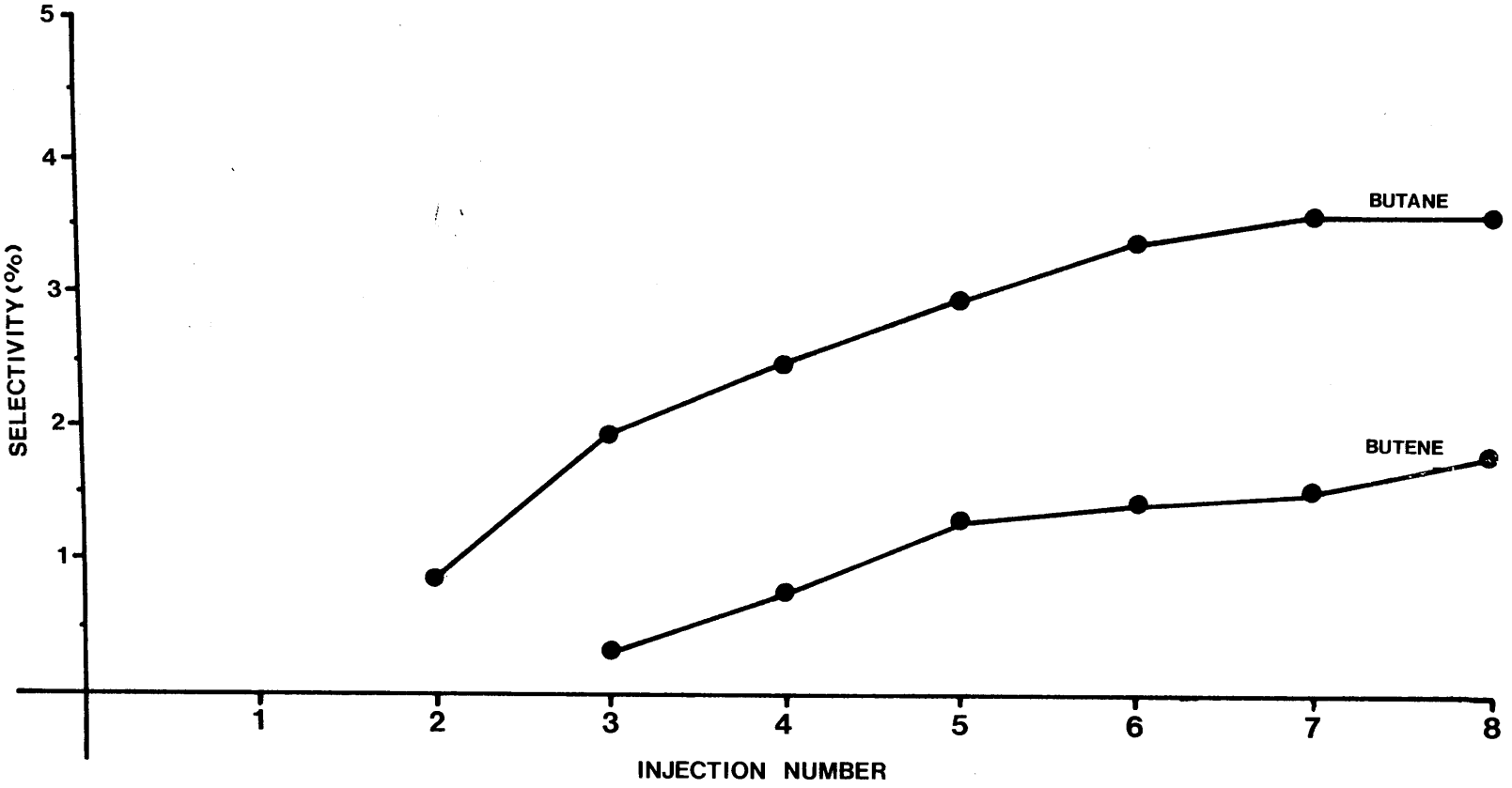

Figure 6·32 – Selectivity with respect to Butane and Butene Formation versus Injection Number.

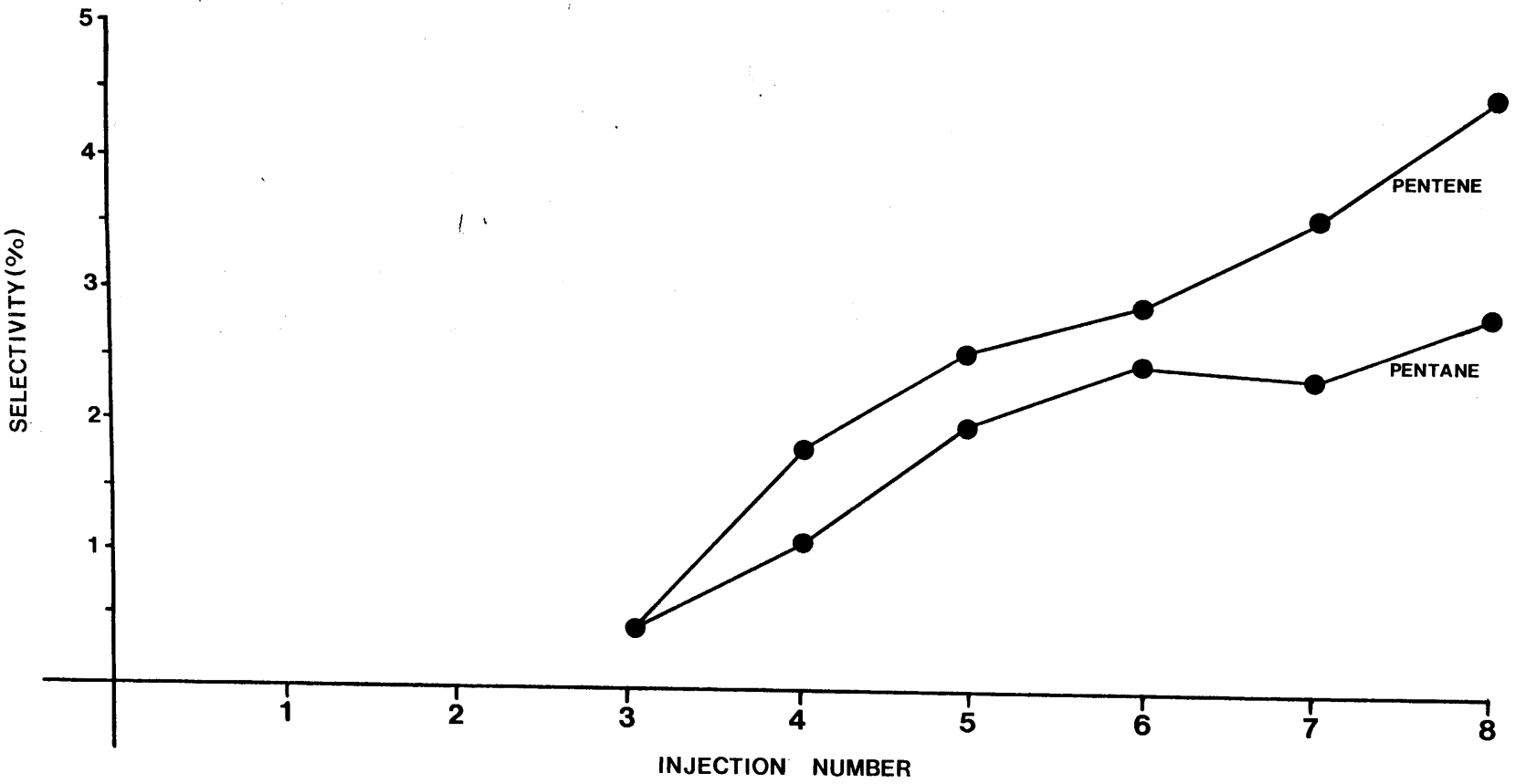

Figure 6.33 – Selectivity with respect to Pentane and Pentene versus Injection Number

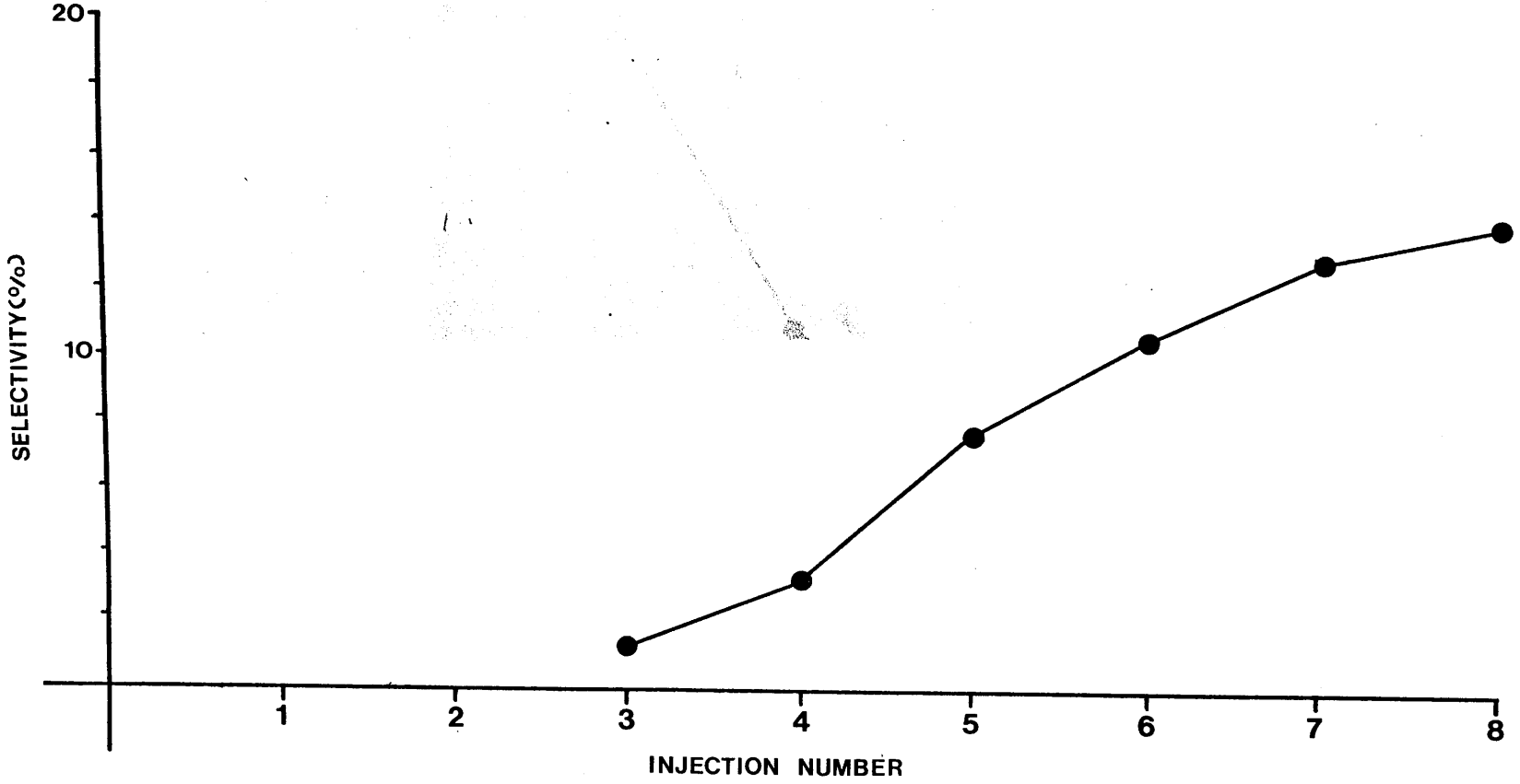

Figure 6.34 – Selectivity with respect to Heptene versus Injection Number

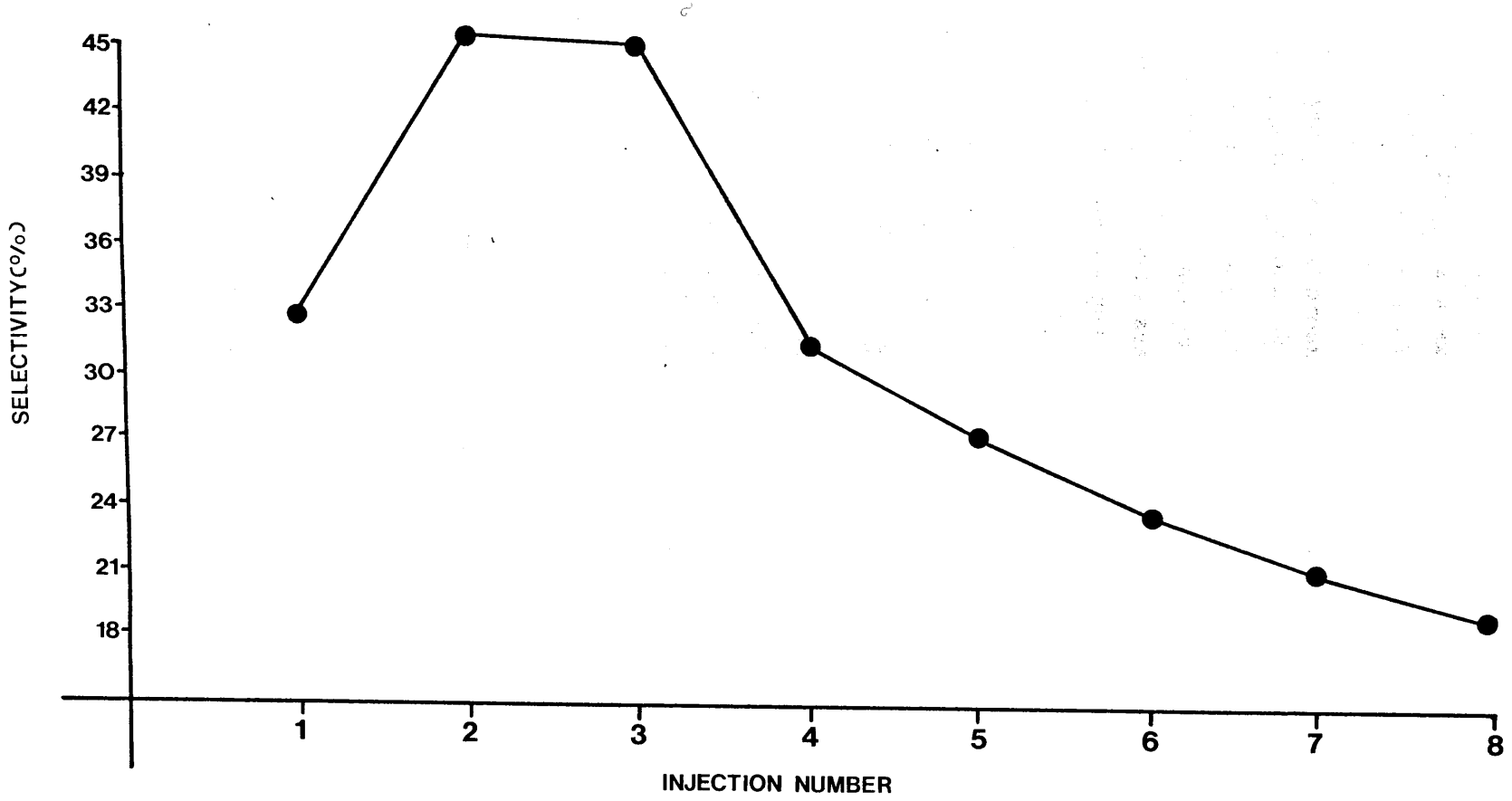

Figure 6.35 – Selectivity with respect to Toluene versus Injection Number

flushed with helium carrier gas and its gaseous contents subjected to radiochromatographic analysis (section 4.2.4). The reaction vessel was left under helium between injections. Negligible quantities of gas phase pyrolysis products were formed during blank experiments (section 4.2.3.3) carried out under the above conditions.

The yields of the product species produced during the static non-continuous flow experiment are presented in table 6.14 against the corresponding injection numbers. In the chromatographic analysis of the eluted compounds the chromatogram peaks associated with the n-heptene, iso-heptane and n-heptane species were not resolved, and therefore, it was not possible to determine the individual molar quantities of these particular compounds present within the product mixtures. Consequently, conversion values were not obtained during this experiment. In performing carbon mass balance calculations, the total area under the unresolved n-heptene, iso-heptane, n-heptane peak was measured manually and this area was considered, for the purpose of the calculations, to be wholly attributable to the elution of unreacted n-heptane reactant. The measured area was then expressed in terms of an equivalent molar quantity of unreacted n-heptane via application of the n-heptane response factor. The resultant molar quantity value was taken as the Y term in equation (3), section 5.1. The calculated carbon mass balance values are tabulated in the second column of table 6.15 and are plotted against the appropriate injection numbers in figure 6.36.

The carbon mass balance values derived for this experiment indicate that, as was the case in the pulse-flow experiment discussed in the previous section (6.2.1), significant quantities of carbon were retained on the surface of catalyst RC1 during its interaction with the injected n-heptane samples. In this instance a weight of residual surface carbon equivalent to approximately 0.94% of the original catalyst weight was predicted by the carbon mass balance values, this being in good agreement

Table 6.14 - Yield of Individual Products versus Injection Number

INJECTION NUMBER	METHANE	ETHANE	PROPANE	ISO-BUTANE	BUTANE	BUTENE	ISO-PENTANE	PENTANE	PENTENE	ISO-HEXANE	HEXANE	HEPTANE / ISO-HEPTANE /HEPTENE	TOLUENE
1	7.96	6.90	6.03	0.33	2.03	0.78	2.08	3.63	3.14	0.19	0.10	18.67	16.63
2	6.52	7.95	8.13	0.31	2.78	0.97	1.73	4.64	4.43	0.25	0.04	20.22	19.94
3	6.44	6.69	7.20	0.13	2.31	1.21	0.74	3.35	4.52	0.17	0.16	35.39	19.21
4	6.78	7.21	6.33	0.05	2.19	1.21	0.30	2.65	4.55	0.17	0.12	43.72	17.00
5	6.05	7.14	6.80	0.05	2.39	1.08	0.41	2.83	4.52	0.14	0.09	48.31	15.03
6	9.93	6.59	5.55	0.04	2.08	1.13	0.38	2.69	4.09	0.12	0.11	54.96	14.88
7	6.18	6.36	5.58	0.04	1.91	0.93	0.31	2.38	4.18		0.10	59.91	13.56
8	6.22	6.72	5.33	0.04	1.93	1.01	0.34	2.23.	4.22			61.77	12.38
9	5.83	7.01	5.61		1.84	0.87	0.25	2.56	3.82		0.04	64.04	12.04
10	6.12	7.61	5.76		2.14	1.04	0.27	2.51	4.34		0.04	64.54	10.45
11	6.02	7.23	5.82		2.03	1.14	0.32	3.00	4.57			64.32	9.64

Table 6.15 – Conversion, Carbon Mass Balance and Total Counts versus Injection Number

INJECTION NUMBER	CONVERSION	CARBON MASS BALANCE	TOTAL COUNTS
1		64.48	30,454
2		77.95	52,266
3		87.55	72,759
4		92.32	90,172
5		94.86	103,247
6		102.57	84,506
7		101.47	48,888
8		102.22	27,650
9		103.28	18,320
10		104.83	12,458
11		104.08	9,190

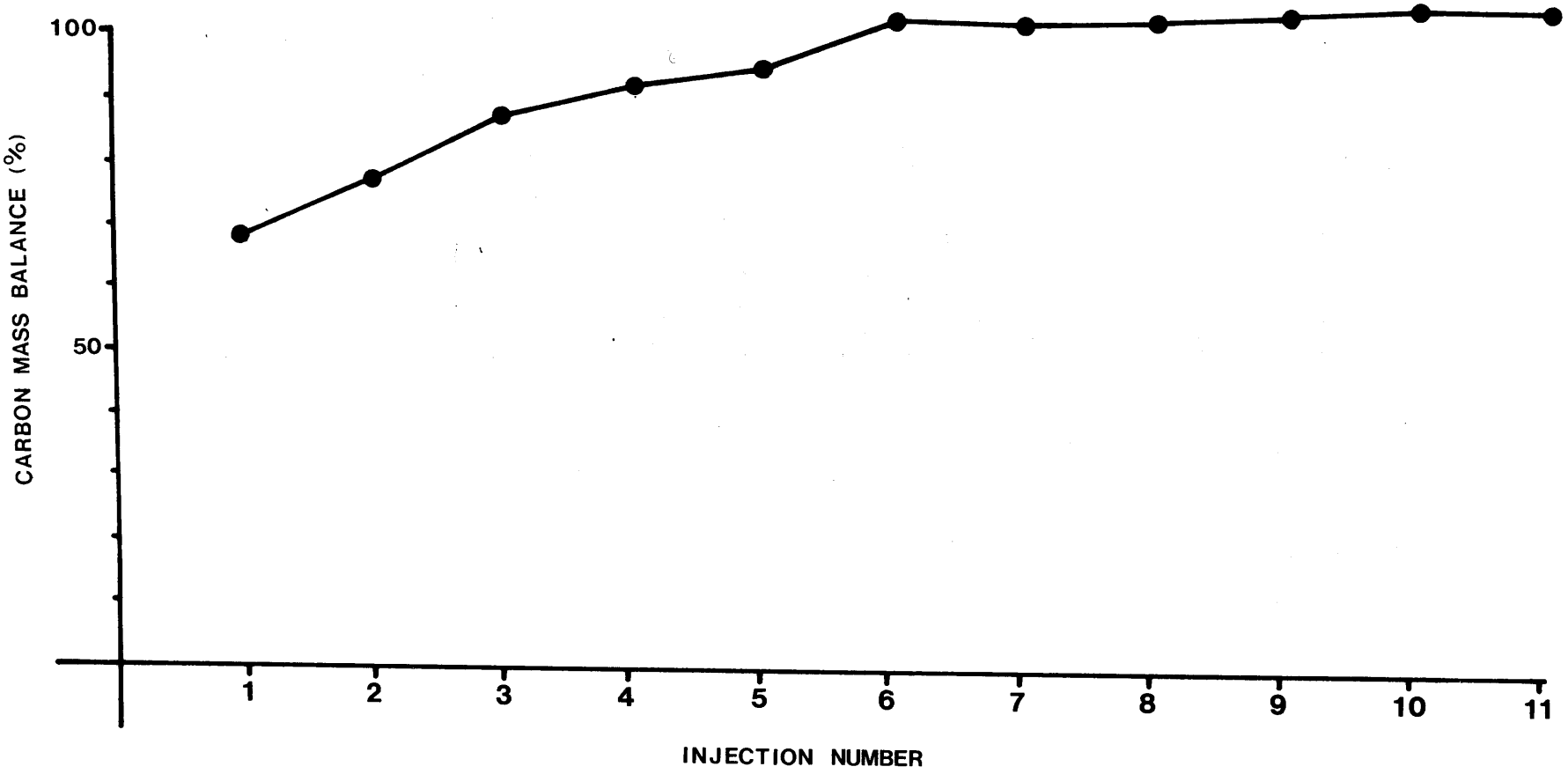

Figure 6.36 – Carbon Mass Balance versus Injection Number

with a corresponding figure of 1.08% which was obtained from the combustion analysis of the spent catalyst (section 3.3.2). Furthermore, figure 6.36 clearly illustrates that, as also observed in the pulse-flow experiment, a maximum amount of surface carbon retention took place during the interaction of the catalyst with the initial n-heptane injection. The amount of carbon retained per injection progressively decreased over the next four injections until a limiting concentration of surface carbon was attained. The latter is implied by the fact that no net retention of carbon occurred during the interaction of the catalyst with the remaining six n-heptane injections.

The third column of table 6.15 shows the total number of counts detected during the radiochromatographic analysis associated with each of the eleven n-heptane injections. The values correspond to a 27 minute counting period which was commenced from the point at which the reaction vessel was flushed with the helium carrier gas. All values have been corrected for background (section 4.2.4.3). The variation in the total count values as a function of injection number is illustrated in figure 6.37. As shown, the total number of counts detected in each of the radiochromatographic analyses increased progressively over the first five injections which, as stated, were performed using [14-C] labelled n-heptane. Thereafter, on switching to injections of non-radiolabelled n-heptane, the total number of counts decreased in an exponential fashion with each subsequent injection. Moreover, for each of the non-radiolabelled n-heptane injections the number of counts detected during each consecutive 30 second retention time interval of the radiochromatographic analyses were recorded as described in section 4.2.4.3. These count values are tabulated against the corresponding retention time intervals in tables 6.16, 6.17 and 6.18 for injections 6-7, 8-9 and 10-11 respectively.

Attempts to correlate the gas proportional counter data contained in tables 6.16 - 6.18 with the corresponding chromatograms, in terms of assigning absolute count values to individual eluted species,

Figure 6.37 – Total Counts versus Injection Number

Table 6.16 – Gas Proportional Counter Data for Injections 6 and 7

INJECTION NO.6

MINS.	ΔC	MINS.	ΔC	MINS.	ΔC
	0		225		455
1	839	10	146	19	357
	839		44		248
2	1385	11	4	20	230
	671		40		260
3	715	12	42	21	209
	203		34		168
4	42	13	141	22	159
	26		4,933		159
5	282	14	12,380	23	89
	459		10,740		261
6	388	15	8,860	24	5,925
	179		6,520		6,630
7	71	16	3,790	25	3,630
	21		2,990		1,322
8	40	17	2,160	26	285
	283		1,370		60
9	587	18	820	27	27

INJECTION NO.7

MINS.	ΔC	MINS.	ΔC	MINS.	ΔC
	6		143		140
1	21	10	54	19	120
	736		24		139
2	607	11	6	20	191
	298		22		188
3	298	12	22	21	232
	91		21		246
4	22	13	1,202	22	163
	50		5,524		155
5	50	14	6,740	23	126
	214		5,540		1,180
6	134	15	4,080	24	4,440
	28		2,780		3,486
7	30	16	1,910	25	1,602
	16		1,290		480
8	13	17	810	26	142
	166		505		85
9	202	18	305	27	32

Table 6.17 – Gas Proportional Counter Data for Injections 8 and 9

INJECTION NO.8

MINS	ΔC	MINS	ΔC	MINS	ΔC
	6		60		97
1	0	10	34	19	96
	433		28		78
2	290	11	1	20	87
	134		18		144
3	109	12	5	21	136
	35		7		150
4	11	13	173	22	135
	17		2,345		165
5	52	14	3,255	23	79
	86		3,156		141
6	48	15	2,184	24	1,800
	40		1,610		2,758
7	65	16	1,090	25	1,557
	15		940		617
8	22	17	578	26	158
	73		382		84
9	69	18	222	27	22

INJECTION NO.9

MINS	ΔC	MINS	ΔC	MINS	ΔC
	0		40		75
1	0	10	42	19	39
	298		30		22
2	291	11	0	20	50
	113		13		65
3	120	12	26	21	63
	29		8		63
4	22	13	217	22	119
	0		1,775		104
5	10	14	1,775	23	144
	93		1,730		162
6	15	15	1,260	24	1,073
	21		940		1,948
7	21	16	750	25	1,107
	3		390		457
8	32	17	390	26	78
	33		200		68
9	69	18	115	27	40

Table 6.18–Gas Proportional Counter Data for Injections 10 and 11

INJECTION NO.10

MINS	ΔC	MINS	ΔC	MINS	ΔC
1	0	10	37	19	68
	2		2		18
2	201	11	30	20	19
	213		19		45
3	94	12	22	21	46
	91		0		35
4	20	13	19	22	32
	16		155		80
5	9	14	1008	23	66
	14		1173		74
6	58	15	894	24	151
	33		894		718
7	18	16	497	25	1286
	49		497		438
8	24	17	328	26	134
	1		182		20
9	23	18	159	27	25
	63		44		16

INJECTION NO.11

MINS	ΔC	MINS	ΔC	MINS	ΔC
1	7	10	42	19	41
	2		3		51
2	187	11	6	20	15
	164		15		9
3	52	12	0	21	8
	69		17		20
4	13	13	5	22	32
	0		46		28
5	8	14	644	23	45
	8		836		50
6	48	15	635	24	170
	19		630		298
7	14	16	460	25	787
	0		275		580
8	5	17	231	26	252
	18		147		71
9	53	18	91	27	37
	38		91		24

were made difficult by the insufficient resolution of chromatographic peaks. However, what can be seen from, for example, table 6.16 is that large numbers of counts were detected during the 1-4 minute, 5-7 minute and 8-11 minute retention time intervals which, by reference to table 4.1, clearly correspond to the elution of product species having carbon numbers of C1-C3, C4 and C5 respectively, with a smaller number of counts being detected during or immediately after the elution of the C6 species. Similarly, large count values were recorded during the retention time interval in which the elution of the iso-heptane, n-heptane and n-heptene species were expected and also during the elution of toluene.

CHAPTER SEVEN

DISCUSSION

- oOo -

7.1 INFLUENCE OF CARBONACEOUS RESIDUES ON THE ACTIVITY AND SELECTIVITY OF CATALYSTS RC1 AND RC2 UNDER CONTINUOUS FLOW CONDITIONS

As described in detail in the previous chapter, the continuous flow of a hydrogen/n-heptane reactant mixture over samples of catalysts RC1 and RC2 in turn, and under industrial type conditions, resulted in each case in an overall decrease in the conversion of n-heptane with increasing time-on-stream. Similarly, the yields of all individual product species were observed to diminish with time with the exception of iso-heptane formation over catalyst RC1 where a progressive increase in product yield was observed. A substantial increase in the isomerisation selectivity of both catalysts occurred whilst on stream along with a corresponding decrease in the aromatisation and hydrocracking selectivities. The selectivity of both catalysts with respect to hydrogenolysis remained essentially constant. The combustion analysis of a sample of the spent RC1 catalyst charge indicated that carbonaceous residues were retained on the surface of the catalysts under the conditions of the continuous flow experiments.

The activity and selectivity changes that occurred during the continuous flow experiments over catalysts RC1 and RC2, can, as demonstrated by the following discussion, be fully interpreted by considering that they were produced solely or predominantly as a direct result of the retention of carbonaceous materials on the surface of the catalysts.

It is commonly acknowledged that during catalytic reforming carbonaceous residues accumulate on both the metallic and acidic functions of the bifunctional catalyst. Indeed, as described in section 1.2.1, this has been convincingly demonstrated by temperature programmed oxidation studies of spent catalyst samples (48)(49)(50). Whilst the results from the continuous flow studies that have been obtained in the present study are not incongruous with this belief, they do however strongly suggest that carbonaceous residues preferentially reside on the metallic

function of the bifunctional reforming catalyst and that the metal function is more selectively poisoned than the acidic function.

In order to understand the reasoning behind the above assertion, it is necessary to examine in greater detail the role of olefinic species in the reforming process. As described earlier, the initial interaction of paraffinic reactant molecules with a bifunctional reforming catalyst results in the formation of olefins via metal-catalysed dehydrogenation, this reaction proceeding rapidly to equilibrium under typical reforming conditions, even when only very low (0.1%) catalyst metal loadings are present (29). The participation of these olefins as intermediates in the bifunctionally catalysed isomerisation, hydrocracking and dehydrocyclisation reactions is firmly established (24)(25). It should be noted, however, that olefins also feature as intermediates in the mechanisms postulated to account for the metal-catalysed hydrogenolysis and direct 1,6 ring closure reactions (section 1.1.4). The participation of a common olefinic intermediate in both the bifunctionally catalysed reactions and the metal-catalysed reactions, would indeed enable the activity and selectivity changes observed in the present continuous flow studies to be rationalised by invoking the concept of competing mechanisms (Fig.7.1)

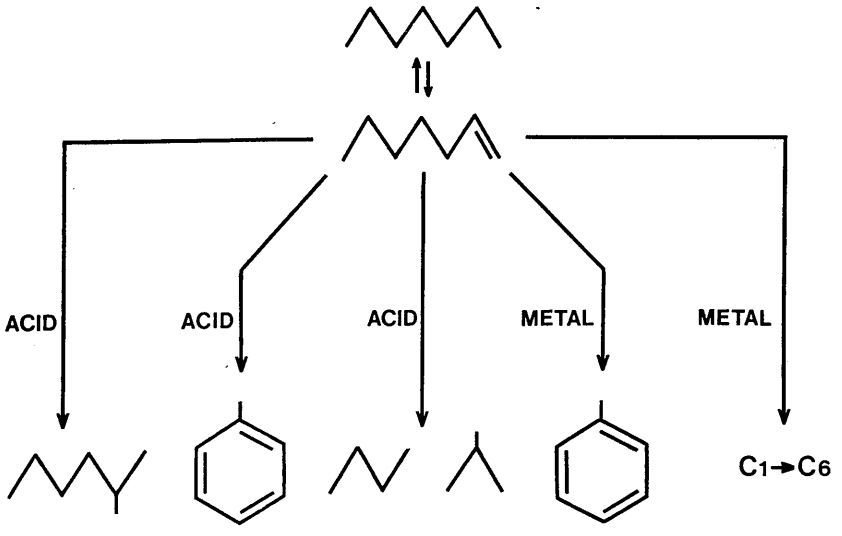

Figure 7.1 - Participation of Olefin Intermediate in the Bifunctional and Metal-Catalysed Reforming Reactions.

In developing this idea, it is convenient to consider first of all the continuous flow experiment involving catalyst RC2 (section 6.1.2). With regard to the aromatisation activity of catalyst RC2 (Fig.6.15), a question immediately arises concerning the relative contributions made by the bifunctional and the metal-catalysed cyclisation routes to the overall toluene yield. Given that the initial dehydrogenation of paraffins to olefins on the metal proceeds rapidly to equilibrium (29), the rate of the bifunctionally catalysed aromatisation mechanism cannot be enhanced by an increase in dehydrogenation activity. Therefore, it is not likely to be affected by an increase in the total metal surface area that is exposed or accessible to the adsorbate. In contrast, several studies, notably those of Dautzenberg and Platteeuw (32), Sinfelt et al (29) and Callender et al (24) have shown that the rate of aromatisation via the metal-catalysed cyclisation route exhibits a strong positive dependence on the metal surface area. Therefore, the higher the metal surface area, the greater the contribution made by the metal-catalysed cyclisation route to the overall aromatic yield. In view of the high platinum surface area of catalyst RC2 ($1.99 m^2.g^{-1}$) it can be concluded that the metal-catalysed cyclisation route is predominantly responsible for the observed overall aromatisation activity of this catalyst. Indeed, working under conditions similar to those used in the present continuous flow studies, Callender et al (24) produced evidence which indicated that, even for a Pt/δ-Al_2O_3-Cl catalyst in which the specific platinum surface area was less than that of RC2, the metal-catalysed cyclisation route accounted for some 70% of toluene formation from n-heptane. Thus, any time-dependent variations that exist in the overall activity and selectivity of catalyst RC2 with respect to toluene formation, are likely to reflect changes in the rate of the metal-catalysed cyclisation reaction and can, therefore, be interpreted in terms of carbonaceous residue laydown on the metal cyclisation sites.

It is evident, therefore, from Figs.6.15 and 6.19 that the laydown of carbonaceous residues on the surface of catalyst RC2 has resulted in a very significant blockage of the metal cyclisation sites. The metal sites responsible for hydrogenolysis have also been poisoned (Figs.6.11-6.13) although to a much lesser extent than the cyclisation sites, the selectivity for hydrogenolysis remaining essentially constant throughout the experiment (Fig.6.21). Consequently, the fall in the total selectivity for the metal-catalysed reactions of around 10%, is wholly attributable to the poisoning of the metal cyclisation sites. It is important to emphasise here that the laydown of carbonaceous materials on the metallic function need not, however, have resulted in a decrease in the concentration of olefinic intermediate present, since, as noted earlier, sufficient dehydrogenation activity generally exists even with very low metal surface areas for equilibrium olefin concentrations to be maintained within a reforming system (29).

It is clear from the nature of the carbonium ion mechanism which is generally considered to apply to the bifunctionally catalysed isomerisation, aromatisation and hydrocracking reactions (section 1.1.4), that the rate at which these reactions occur in a reforming system will generally be limited by either of two parameters; namely, the concentration of intermediate olefin available for reaction, or alternatively, the number of accessible acid sites. If the metal surface area of the reforming catalyst is relatively large, and hence the rate of metal-catalysed cyclisation very rapid, it is readily visualised that the former parameter would be the prevalent rate-limiting factor as, under these circumstances, a lesser proportion of the equilibrium concentration of intermediate olefin would be available for participation in the bifunctionally catalysed reactions. It might therefore have been expected that the proposed blockage of the metal cyclisation sites by carbonaceous residues during the continuous flow study involving catalyst RC2, would have coincided with an increase in the rate of the bifunctionally catalysed reactions. Such arguments would certainly account

for the increase in yield of iso-heptane observed with catalyst RC2 with increasing time-on-stream (Fig.6.15).

In contrast to the iso-heptane yield, however, the yields of all the hydrocracking products decreased continually in the manner shown in figure 6.14. It is, therefore, necessary to postulate that carbonaceous residues are also retained on the acidic function of the catalyst and, further, that those acidic sites responsible for the hydrocracking reactions are particularly susceptible to poisoning by these residues, whilst those sites which are active in the isomerisation reaction are much less vulnerable and remain relatively unaffected by the presence of surface residues. Thus, in the case of the hydrocracking reactions, the proposed increase in the availability of intermediate olefin resulting from the deactivation of the metal cyclisation sites, has no effect on the reaction rates as, in the presence of the surface residues, the deficiency of the acidic hydrocracking sites becomes rate limiting. Consequently, whereas the combined selectivity of the catalyst for the acid-catalysed reactions of isomerisation and hydrocracking undergoes a net increase of approximately 10% during the course of the experiment (table 6.10), the selectivity for the isomerisation reaction itself increases by around 16% whilst the total hydrocracking selectivity falls by approximately 6%.

The apparent absence of any decrease in the yield of toluene during the initial stages of the reaction (Fig.6.15) can be readily accounted for by proposing that, during this period at least, the rate of the bifunctionally catalysed aromatisation reaction is limited by the concentration of intermediate olefin present and increases as the sites responsible for the metal-catalysed cyclisation reaction are poisoned. Thus, although the trends observed in the yield of toluene with respect to time-on-stream are considered to substantially reflect the fate of the metal cyclisation sites, during the initial period of the continuous flow study over catalyst RC2, the expected decrease

in toluene yield, resulting from the deactivation of the metal cyclisation sites, may have been compensated for by an enhancement of the bifunctionally catalysed aromatisation reaction.

A similar argument can be forwarded to rationalise the observation that there is no evident overall decrease in the total conversion during the initial period of the reaction over catalyst RC2 (Fig.6.17). During this period, the potential deactivation of the catalyst which might have resulted from the blockage of the metal cyclisation and hydrogenolysis sites by carbonaceous residues, is nullified by a corresponding overall increase in the conversions associated with the acid sites, the latter occurring in response to the increased availability of the olefin intermediate. With increasing reaction time, however, the contribution made by the bifunctionally catalysed reactions to the total conversion begins to decrease as the progressive accumulation of carbonaceous residues on the acidic support makes the availability of accessible acid sites rate-limiting.

The strong similarities in the performance of RC1 and RC2 as a function of time-on-stream during the continuous flow studies (sections 6.1.1, 6.1.2), indicates that carbonaceous residues interacted with both catalysts in a similar manner. Indeed, the proposals given above, which explain the activity and selectivity changes of catalyst RC2 in terms of the selective interaction of carbonaceous residues with both the metallic and acidic functions of the catalysts, and the effect that this deposition process has on the role of olefinic intermediates in the reforming reactions, are also consistent with the activity and selectivity changes observed with catalyst RC1. The fact that some differences do exist between the two sets of continuous flow data (section 6.2.1) does not invalidate a common interpretation, as these differences can be attributed to the different specific metal surface areas of the two catalysts (section 3.2.1). Thus, the lower initial hydrogenolysis activity (Tables 6.3, 6.7) and selectivity (Tables 6.6, 6.10) of catalyst RC1 relative to catalyst

RC2 is expected in view of the much lower specific metal surface area of the former catalyst. This factor also readily accounts for the difference in the initial isomerisation activities and selectivities of the two catalysts. Assuming that, for both catalysts, sufficient metal dehydrogenation activity was present to maintain the maximum possible concentration of intermediate olefin within the reacting system, the lower activity with respect to the metal-catalysed cyclisation reaction found with RC1 is as expected. Consequently, with catalyst RC1 a greater proportion of the equilibrium concentration of olefin would be available for participation in the bifunctionally catalysed reactions. During the initial stages of the reaction, when the extent of poisoning of the acidic sites by carbonaceous residues would be relatively small, the rates of the bifunctionally catalysed reactions would be limited by the amount of intermediate olefin available for reaction. Consequently, the activity and selectivity of catalyst RC1 for the bifunctionally catalysed reactions were initially greater than those of catalyst RC2. The higher initial isomerisation activity and selectivity of catalyst RC1 relative to that of RC2, could therefore have been predicted. Similarly, for catalyst RC1 a greater contribution to aromatisation from the bifunctionally catalysed reaction accounts for the fact that the initial aromatisation activity and selectivity of this catalyst was very similar to that of catalyst RC2, despite the higher metal surface area, and hence greater metal-catalysed cyclisation activity, of the latter catalyst. It is not clear, however, from these arguments, why there was apparently no significant difference in the initial hydrocracking activity and selectivity of catalyst RC1 and RC2.

Given that in the case of catalyst RC1 a high proportion of the intermediate olefin was available for participation in the bifunctionally catalysed reactions, the steady deactivation of the catalyst with respect to both the hydrocracking and isomerisation reactions which was observed during the continuous flow experiment (Figs.6.4, 6.5), is indicative of the blockage of the hydrocracking and isomerisation sites by carbonaceous residues.

Once again this occurred selectively, with the hydrocracking sites being preferentially poisoned (Fig.6.10). Similar steady deactivation profiles were observed for the aromatisation (Fig.6.5) and hydrogenolysis (Figs.6.1,6.2,6.3) reactions with the net result that the total conversion obtained over RC1 decreased, unlike that over RC2, in a continuous uninterrupted manner (Fig.6.7).

The validity of the above treatment, in which the changes that took place in the activity and selectivity of catalysts RC1 and RC2 during the continuous flow studies have been interpreted in terms of the effects of carbonaceous residue laydown on the catalysts,can be further substantiated.

It has been firmly established (38)(39) that a characteristic feature of the laydown of carbonaceous residues on all hydrocarbon conversion catalysts, when it occurs, is that the rate of residue accumulation, whilst being initially very rapid, gradually decreases with time as the extent of surface residue coverage increases. Moreover, in the case of catalytic reforming processes, a limiting concentration of residues on the surface of the catalysts is eventually approached (40)(41). In the present continuous flow studies, the most severe changes in the activity and selectivity values were experienced during the initial stages of the reactions, with more stable values eventually being attained as the reaction time progressed (Figs.6.7,6.17,6.9,6.10, 6.19-6.21). Hence, in this respect, the nature of the activity and selectivity changes observed during the continuous flow studies can be ascribed to the formation of surface carbonaceous residues.

The removal of chlorine from the surface of the catalysts during the continuous flow reactions must also be recognised as a potential factor which could have contributed to the observed activity and selectivity changes. Bishara and co-workers (67), when studying the reforming of naphtha over bimetallic catalysts under industrial type conditions, observed that the depletion

of the support chlorine level coincided with product yield and selectivity changes similar to those observed in the continuous flow reactions over catalysts RC1 and RC2; the aromatisation and hydrocracking selectivities exhibiting an appreciable decline in response to chlorine loss. In the present study, any assessment of the effect of chlorine loss on catalyst performance is complicated by the fact that it is not clear how much of the detected loss (section 6.1) is actually attributable to chlorine removed during the reforming process itself. Whilst it is probable that during the reforming reactions, chlorine would have been leached from the surface of the catalysts by traces of moisture present in the feedstock gases (78), it is equally likely that a substantial proportion would have been removed during the pre-experimental in-situ reductions of the catalysts (section 3.1)(67)(79). Moreover, analysis of the catalyst samples by neutron activation provides a measure of the overall bulk chlorine content rather than, as required, a value which refers specifically to chlorine adsorbed on the catalyst surface. Furthermore, for the present purposes, a very important point to have emerged from the work of Bishara et al (67) was that the yield and selectivity changes resulting from the loss of chlorine varied linearly with respect to time-on-stream. In the present study the corresponding relationships are distinctly non-linear, and thus it is clear that chlorine loss does not satisfactorily account for the changes in catalyst performance that were detected during the continuous flow studies. Therefore, even accepting that a certain amount of chlorine was leached from the surface of the catalysts during the reforming reactions, the interpretation of the observed activity and selectivity changes in terms of the laydown of carbonaceous residues on the catalysts is still valid.

Further support for the latter interpretation is provided by the work of Beltramini et al (60). These workers, studying the reactions of a wide range of monohydrocarbon feedstocks on a bifunctional Pt/δ-Al_2O_3-Cl catalyst under industrial type conditions,

found that the deposition of carbonaceous residues on the catalyst surface coincided with product yield and selectivity changes which were identical in nature to those observed in the present studies including, in the case of paraffinic reactants, an increase in the yield of the corresponding iso-paraffin. The loss of chlorine from the catalyst was not, however, a feature of this study.

The interpretation of the changes in catalyst performance in terms of the retention of carbonaceous materials on the catalyst surface, is supported by the fact that the lessening in severity of the changes in activity and selectivity with increasing time-on-stream, can be correlated with the trend which is known to apply to the rate of carbon laydown on reforming catalysts. The lack of any discernible pattern in the carbon mass balance values plotted in figure 6.18 indicates, however, that the measurement of carbon mass balance did not provide, in the case of the continuous flow studies, a suitable method of monitoring the laydown of carbon on the catalyst. In support of this, the carbon mass balance values derived during the continuous flow study involving catalyst RC1, (table 6.4), are very clearly incompatible with the value for weight of residual surface carbon that was actually measured at the end of the experiment (section 6.1.1).

In order to rationalise the disparity that exists between the predicted and measured residual surface carbon contents of catalyst RC1 after the continuous flow study, it is proposed that the carbon mass balance values of 82.2% and 90.5%, which correspond respectively to time-on-stream values of 1.8 hours and 8.7 hours (table 6.4), are erroneous and exaggerate the capacity of this catalyst to retain carbon at these particular times. A situation in which the calculated carbon mass balance values were lower than the true values could indeed have arisen if, during the early stages of the experiment, carbon had rapidly accumulated on the surface of the catalyst to such an extent that, at a given level, it had begun to restrict the passage of the

reactant hydrocarbon through the catalyst bed. Consequently, the pressure within the section of the microcatalytic reforming system situated between the hydrocarbon feed restrictor and the reaction vessel (figures 4.3,4.7), would be required to increase in order for the original hydrocarbon flow through the catalyst bed to be re-established. If the pressure increase required to achieve this was relatively small, the feed rate of hydrocarbon across the feed restrictor, as measured from the sightglass (section 4.2.2), would not be significantly affected, as a small increase in pressure would make little difference to the pressure differential across the restrictor (section 4.2.2) which, under normal conditions, was very large (200 p.s.i). Under these circumstances, there would be a period during the continuous flow experiment in which the feed rate of hydrocarbon across the feed restrictor was in excess of the actual hydrocarbon flow rate through the catalyst bed. As a consequence, any carbon mass balance values that were derived during the period in which a significant discrepancy in the flow rates existed would be appreciably lower than the true values, as the **N(X)** value applied in equation (3) of section 5.1 would be too high.

In a catalytic system in which the rate of carbon laydown on the catalyst surface was initially very rapid but gradually tailed off with time, as a stable carbon concentration was approached, any flowrate discrepancy that was created would tend to become less appreciable with time. Moreover, it would cease to exist only when the rate of carbon laydown had become so slow that the pressure increase required to re-establish the original hydrocarbon flow rate through the catalyst bed, could be achieved as rapidly as any increase in restriction was being created. If, during a process in which carbon laydown occurred in this manner, the carbon mass balance values were calculated in accordance with the procedures used in section 5.1 and plotted as a function of time-on-stream, a graph similar to that shown in figure 6.8 would be expected. Therefore, in view of the extent to which the predicted surface carbon content of

catalyst RC1 exceeded that which was actually found, together with the inconsistency that exists between the curve in figure 6.8 and the established coking characteristics of a reforming system, it is believed that the carbon mass balance values derived during the continuous flow study over catalyst RC1 do not accurately reflect the extent of carbon laydown on the surface of this catalyst as a function of time-on-stream.

The occurrence of this flow rate discrepancy would also lead to calculated values for the individual yields and total conversion that were lower than the true values. It would, therefore, readily account for the observation that in a number of the curves displayed in figures 6.1-6.7 the plotted point corresponding to the time-on-stream of 1.8 hours has a value which is well below that predicted by the best-fitting curve. This is particularly apparent in figure 6.7.

7.2 NON-CONTINUOUS FLOW STUDIES

7.2.1 Pulse-Flow of N-Heptane over Catalyst RC1

As noted previously, (section 6.2.1), the retention of carbonaceous materials on the surface of catalyst RC1 which occurred when pulses of n-heptane were passed through the reaction chamber in the absence of reactant hydrogen, coincided, not only with appreciable product yield and selectivity changes, but also with a very significant increase in the total quantity of n-heptane reactant converted into products per injected sample. Thus, despite the loss of catalyst surface area that must inevitably have occurred as a result of the carbon laydown, the overall activity of the catalyst was enhanced in the presence of the surface carbonaceous materials.

The apparent absence of any positive correlation between the catalytic activity and the exposed surface area of the catalyst, strongly suggests that in this particular system, the catalytic

activity was limited by some factor other than the availability of surface sites. Thus, in view of the fact that the reactions were carried out in the absence of reactant hydrogen, it is proposed that the overall activity was constrained by a deficiency in the concentration of surface hydrogen available for participation in the catalytic reactions.

The existence of a correlation between the overall catalytic activity and the availability of surface hydrogen is, in fact, strongly substantiated by the remainder of the experimental data, in that the latter reveals that the increase in catalytic activity which occurred over the first three injections coincided with the growth of a 'pool' of hydrogen on the catalyst surface, as demonstrated by the following experimental observations.

i) The hydrogen mass balance values (table 6.12) show that an appreciable net uptake of hydrogen by the catalyst surface occurred during each of the first three injections. Thus, the concentration of hydrogen present on the catalyst surface was augmented during its interaction with each of these injections.

ii) Whilst the trends noted in the individual product yield and selectivity values (section 6.2.1) may have been influenced, to some extent, by the selective blockage of surface sites resulting from the carbonaceous residue deposition, they can be interpreted much more conveniently in terms of a progressive increase, with each subsequent injection, in the concentration and availability of hydrogen on the catalyst surface.

This latter submission is perhaps best substantiated by considering the variation in the yield of toluene as a function of injection number (Fig.6.27). As described earlier, convincing evidence has been presented by Paál and Tétényi (30) to show that the metal-catalysed dehydrocyclisation of paraffins involves the cyclisation of a tri-olefinic intermediate in its cis- geometric form. Further work (30) has indicated that the rate of this

reaction may, under certain circumstances, be limited by the rate of the geometrical isomerisation of the trans- and cis- tri-olefinic species. As this isomerisation proceeds via half-hydrogenated intermediates (80), its rate, and hence that of the dehydrocyclisation reaction, is promoted by the presence of hydrogen. On the other hand, when sufficient hydrogen is present to ensure that the geometrical isomerisation of the trans- and cis- tri-olefinic species is no longer rate-limiting, the rate of dehydrocyclisation will decrease with increasing hydrogen concentration, as the hydrogen will decrease the concentration of tri-olefinic intermediate attainable at equilibrium. Thus, the trend observed in the activity of catalyst RC1 with respect to toluene formation as a function of injection number is clearly consistent with an increase in the availability of surface hydrogen. Moreover, a curve very similar in shape to that shown in figure 6.27 has been reported previously by Paál et al (30). These workers pulsed n-hexane over a Pt black catalyst at 360°C using a helium/hydrogen carrier gas mixture and examined the variation in the yield of benzene as the hydrogen content of the carrier gas was varied between 0 and 100%. The benzene yield was observed to increase with increasing hydrogen partial pressure over the range 0 to 25% hydrogen. At higher hydrogen contents, however, the benzene yield exhibited an inverse dependence on hydrogen partial pressure.

The validity of the above proposal, in which the aromatisation behavior of the bifunctional catalyst RC1, possessing both metallic and acidic characteristics, has been rationalised solely in terms of a metal-catalysed dehydrocyclisation reaction, can be demonstrated by considering the work of Sinfelt and Rohrer (27). These workers, when studying the dehydroisomerisation of methylcyclopentane to benzene on a bifunctional Pt/δ-Al_2O_3 catalyst, showed that, in the absence of reactant hydrogen, the only reaction to occur to any appreciable extent was metal-catalysed hydrogenolysis. Similarly, Ciapetta and Hunter (81)

have reported that the high activity exhibited by a bifunctional $Ni/SiO_2/Al_2O_3$ catalyst with respect to the isomerisation of n-hexane, was observed only in the presence of reactant hydrogen. In the absence of hydrogen, metal-catalysed hydrogenolysis was once again the dominant reaction. Evidently therefore, in the absence of reactant hydrogen the acidic function of a bifunctional catalyst, such as $Pt/\delta\text{-}Al_2O_3\text{-}Cl$, is essentially redundant, the catalyst being active only with respect to those reactions that take place solely on the metal. That this was indeed the case in the pulse-flow study over catalyst RCl is confirmed by the observation that no iso-heptane or low molecular weight branched species were detected. Consequently, it is highly unlikely that any significant contribution was made by a bifunctionally catalysed cyclisation reaction to the toluene yield obtained during the pulse-flow study. Toluene formation can, in this instance, by considered solely in terms of a metal-catalysed reaction such as that which must have occurred during the study conducted by Paál et al (30).

In order to demonstrate that the trends observed in the yield and selectivity values for the hydrogenolysis products, as a function of injection number, are also consistent with an increased availability of surface hydrogen, it is convenient to invoke a reaction sequence for the hydrogenolysis of n-heptane which is similar in nature to that shown previously for ethane hydrogenolysis (section 1.1.4). The n-heptane hydrogenolysis mechanism shown in figure 7.2 is therefore envisaged, where 'a' is equal to (16-x)/2, 'n' varies between 1 and 6, and $C_7Hx(ads.)$, $CnHy(ads.)$ and $C_7\text{-}nHz(ads.)$ denote the adsorbed hydrogen deficient intermediate and associated carbon-carbon bond rupture fragments respectively containing 7,n and 7-n carbon atoms.

$$C_7H_{16}\,(g) \rightleftharpoons C_7H_{15}\,(ads) + H(ads) \qquad \ldots\ldots (1)$$

$$C_7H_{15}\,(ads) + H(ads) \rightleftharpoons C_7Hx(ads) + aH_2(g) \qquad \ldots\ldots (2)$$

$$C_7Hx(ads) \xrightarrow{(a)} CnHy(ads) + C_7\text{-}nHz(ads) \xrightarrow[(b)]{H_2}$$

$$C_nH_{2n+2}(g) + C_7\text{-}nH_{16-2n} \qquad \ldots\ldots (3)$$

Figure 7.2 - Metal-Catalysed Hydrogenolysis of n-Heptane

In the presence of excess quantities of hydrogen gas, which is indeed the normal situation in all catalytic hydrocarbon conversion processes, the rate of n-alkane hydrogenolysis on platinum is limited by the step involving the carbon-carbon bond rupture of the hydrogen deficient intermediate (step (3a)) (21). Thus, the rate of hydrogenolysis is inversely dependent on the hydrogen partial pressure, as the hydrogen limits the equilibrium concentration of the hydrogen deficient intermediate (step (2)) available for participation in this reaction (36). In the absence of reactant hydrogen however, as in the pulse-flow study over catalyst RCl, it is highly likely that the overall reaction rate would be determined more by the step involving the desorption of the adsorbed carbon fragments that result from the carbon-carbon bond rupture reaction, as this process requires the presence of reactant hydrogen (step (3b)). This desorption step has indeed been shown to be rate-limiting in the case of n-alkane hydrogenolysis over Fe and Re surfaces (82).

A further important consequence of a hydrogen deficiency is that the product distributions obtained from hydrogenolysis will strongly favour the lower molecular weight products, as the adsorbed hydrocarbon fragments resulting from the initial carbon-carbon bond rupture will undergo further carbon-carbon bond scission on the catalyst surface in preference to desorption as saturated products. This will ultimately result in the formation of adsorbed mono-carbon fragments and thence, eventually, methane. If the concentration of hydrogen on the catalyst surface progressively increases, the residence times of the hydrocarbon fragments will be reduced accordingly and, consequently, the carbon numbers of the desorbing molecules are expected to progressively increase.

From these arguments it is clear that the trends noted in the yield and selectivity values for the saturated hydrogenolysis products, provide strong evidence for an increase in the

concentration of available surface hydrogen during the course of the pulse-flow experiment. Moreover, just as an increase in surface hydrogen will tend to promote the desorption of the adsorbed hydrogen deficient species, it will also simultaneously encourage their partial rehydrogenation on the catalyst surface. The subsequent desorption of partially rehydrogenated species would therefore account for the observed increase in the yield of the linear unsaturated hydrocarbons.

The experimental evidence demonstrates very convincingly that the concentration of hydrogen on the catalyst surface was enhanced during the course of the pulse-flow experiment, and that this factor was very likely responsible for the observed increase in the overall catalytic activity. It is therefore appropriate to examine what can be deduced regarding the nature of the hydrogen source. Whilst it is apparent from the work of Taylor, Thomson and Webb (83) that only some of the hydrogen remaining on the catalyst surface after the reduction process is removed during the subsequent helium treatment (section 6.2.1), it is, in any case, difficult to visualise how the availability of any residual hydrogen would be improved as a result of the n-heptane injections. It is clear that an increase in the availability of surface hydrogen must have occurred via the retention on the catalyst surface of the hydrogen contained within the reactant n-heptane molecules themselves. It is conceivable that such a situation arose from the donation to the catalyst surface of hydrogen released during the formation of the unsaturated aromatic and olefinic products. Indeed, as noted above, no molecular hydrogen was detected during the chromatographic analysis of the pulse-flow product mixtures. However, inspection of the product distributions associated with each of the n-heptane samples (table 6.11), shows that, with one exception, the quantity of hydrogen taken up during the hydrogenolysis reactions was in excess of that liberated during the formation

of any unsaturated products. Consequently, an increase in the availability of surface hydrogen could not have arisen simply as a result of the formation of the unsaturated products. This leads to the conclusion that the enhanced availability of hydrogen occurred as a direct result of the formation of carbonaceous residues on the surface of the catalyst.

The veracity of this conclusion is further substantiated by the fact that the most pronounced changes in the conversion values, and in the individual product yield and selectivity values, occurred between the first and second injections, which can be correlated with the observation that more surface carbonaceous material was retained during the first injection than during any of the subsequent injections (Fig.6.29). It is not possible, however, from the existing data, to ascertain whether the increased availability of hydrogen was attributable to hydrogen actually present within the surface carbonaceous residues themselves, or to that which was generated during the condensation and polymerisation reactions which occur during carbonaceous residue formation (section 1.2.2). Both sources may be important. The importance of the former source has, however, certainly been implied by the work of Thomson and Webb (84) and Somorjai and co-workers (42)(53) which has emphasized the dynamic ability of the carbonaceous residues, associated with various supported metal catalysts and with platinum single crystals, to donate or exchange hydrogen with reacting surface species. Moreover, Davis, Zaera and Somorjai (42) have proposed a working model for hydrocarbon conversion catalysts which accommodates very readily the conclusions of the present pulse-flow study, in that the desorption of strongly bound reaction intermediates is believed by these workers to be facilitated by hydrogen donation from permanently retained surface carbonaceous materials.

7.3 STATIC EXPERIMENT INVOLVING THE INTERACTION OF [14-C] N-HEPTANE AND UNLABELLED N-HEPTANE WITH CATALYST RC1

The carbon mass balance and radiochromatographic data obtained from the static non-continuous flow experiment (section 6.2.2) has demonstrated that, during this experiment, the surface of catalyst RC1 became pre-labelled with [14-C] carbonaceous materials as a result of its interaction with a series of consecutive [14-C] n-heptane injections performed in the absence of reactant hydrogen. Moreover, the retained surface label was readily incorporated into the product mixtures obtained during subsequent injections of non-radiolabelled n-heptane reactant into the reaction vessel, despite the absence of any net retention or removal of carbonaceous material on or from the catalyst surface during these latter injections.

In catalytic hydrocarbon conversion processes, the ability of reactant hydrogen to inhibit the formation of carbonaceous residues on the surface of the catalyst is well established (section 1.2.3). This has been ascribed to the accelerated rehydrogenation of the hydrogen deficient precursors, which ultimately lead to residue formation. Owing to the capacity of hydrogen to act in this manner, it has commonly been assumed that the attainment of a limiting concentration of carbonaceous residues on the surface of, for example, a reforming catalyst, corresponds to the establishment of a "steady-state" situation in which hydrocarbon is exchanged between the gas phase and the surface carbonaceous deposit at an equal and constant rate. This exchange is considered to be facilitated by the continual hydrogenolysis, rehydrogenation and removal of the surface residues by the large quantities of hydrogen gas present.

The present study is able to confirm, at least for the particular catalytic system studied, that the formation of a limiting concentration of surface carbonaceous residues is indeed best interpreted in terms of a fixed rate equilibrium

exchange of hydrocarbon between the gas phase and surface carbonaceous deposit. However, the most interesting point to have emerged from the data is that although reactant hydrogen, when present, probably can and does participate in the removal of surface residues, its presence is not a condition upon which the establishment of the steady-state surface residue concentration depends. Thus, as noted previously (section 6.2.2), in the static non-continuous flow experiment which was performed in the complete absence of reactant hydrogen, a limiting concentration of surface carbonaceous residues, equivalent to approximately 1% by weight of the catalyst, was established after the sixth n-heptane injection had passed through the catalyst bed. No further net carbon uptake occurred during the remaining five injections (Fig.6.36). Any possibility that the absence of surface carbon retention during these latter injections was due to the complete saturation of the catalyst surface by carbonaceous residues, can be dismissed by the fact that, as seen from table 6.14, the catalyst remained active with respect to product formation throughout the course of the experiment. This would indicate, therefore, that even although the concentration of surface residues had reached a limiting value, some portion of the catalyst surface remained uncovered.

The existence of a steady-state exchange of hydrocarbon between the gas phase and the surface carbonaceous deposits during the sixth and subsequent injections, can be affirmed by considering the relationship between the carbon mass balance values (Fig.6.36) and the total number of counts detected in the effluent gas mixtures (Fig.6.37). The progressive increase in the total number of counts detected during each of the first five injections which, as stated, were performed using the [14-C] labelled n-heptane feedstock, can be correlated with a corresponding increase in the carbon mass balance values. However, on switching to the non-radiolabelled n-heptane feedstock, the total number of counts

detected in the effluent gas mixtures decreased with each subsequent injection in the exponential manner noted previously, whereas during this time, as described, there was no net retention or removal of carbonaceous materials from the catalyst surface, the carbon mass balance values remaining essentially constant at around 100%.

The very fact that any incorporation of surface label into the gas phase occurred at all during the non-radiolabelled injections, does in itself provide verification that an exchange of hydrocarbon between the gas phase and the surface carbonaceous materials took place. However, the exponential manner in which the total count rate values decreased during this period is significant, in that it is indicative of a controlled and regular exchange process in which the rate of exchange was the same for each of the injections, and as such is consistent with the concept of a steady-state type process. Thus, if during the first five injections the surface of the catalyst was pre-labelled with a limiting concentration of [14-C] labelled surface residues equivalent to a total of x counts, and during each of the remaining six injections a fixed amount of the surface residue equivalent to, for example, half of the total limiting concentration was exchanged with non-radiolabelled feedstock, then the number of counts incorporated into the effluent gas mixtures of the last six injections would be expected to be given by $x/2$, $x/2^2$, $x/2^3$, $x/2^4$, $x/2^5$ and $x/2^6$ respectively. The exponential type decrease in these values is similar in nature to the trend actually observed in the total count rate values of the last six injections. This would indicate, therefore, that for each of these injections the rate of exchange of hydrocarbon between the gas phase and the surface carbonaceous residues remained constant.

From the data considered above, it is clear that even in the absence of reactant hydrogen, the surface carbonaceous residues associated with reforming catalysts do not comprise

of truly irreversibly adsorbed surface species, but can instead be more accurately described in terms of strongly bound species which, by virtue of their ability to exchange with hydrocarbons contained in the gas phase, possess finite residence times on the catalyst surface. In view of this, a question immediately arises concerning the chemical identity of the species that are recovered from the surface carbonaceous residues during the exchange process. The radiochromatographic data relating to the incorporation of the surface label into specific product species (section 6.2.2) is of great significance here, in that, from this data, it is clear that a range of different chemical species having carbon numbers as low as C_1 and exhibiting a variety of structures, must have participated in the exchange process, with toluene being specifically identified.

The incorporation of toluene from the surface residues into the gas phase is perhaps not surprising in view of the consensus of evidence accumulated from many studies affirming the aromatic nature of the carbonaceous residues associated with many hydrocarbon conversion catalysts (section 1.2.1). However, it is very interesting to note that whilst the surface label was also present in species having a lower molecular weight than that of toluene, at no time during any of the radiochromatographic analyses were any product species with a carbon number greater than that of the n-heptane starting material detected. Thus, under the conditions of the experiment, the species liberated from the surface carbonaceous residues during the exchange with gas phase hydrocarbon, were not those consistent with the breakdown of a highly condensed or polymeric aromatic type surface structure. It is considered therefore, that the incorporation of the surface label into the gas phase corresponded to the removal of strongly adsorbed yet uncondensed surface compounds, which may have retained their structural integrity as small discrete species in the presence of a more highly structured and extensive polymeric surface deposit, or which may, alternatively, have acted as precursors to this deposit.

27) Sinfelt, J.H., Rohrer, J.C., J.Phys.Chem., 65, 978 (1961).

28) Rohrer, J.C., Hurwitz, H., Sinfelt, J.H., J. Phys. Chem., 65, 1458 (1961).

29) Sinfelt, J.H., Hurwitz, H., Rohrer, J.C., J. Catal., 1, 481 (1962).

30) Paál, Z., Advan.Catal., 29, 273 (1980).

31) Paál, Z., Tétényi, P., Catalysis, 5, 80 (1982).

32) Dautzenberg, F.M., Platteeuw, J.C., J. Catal., 19, 41 (1970).

33) Davis, B.H., Venuto, P.B., J. Catal., 15, 363 (1969).

34) Paál, Z., Tétényi, P., Acta.Chim.Acad.Sci.Hung., 55, 27 (1968).

35) Sinfelt, J.H., Advan.Catal., 23, 91 (1973).

36) Cimino, A., Boudart, M. Taylor, H.S. J.Phys.Chem., 58, 796 (1954).

37) Greensfelder, B.S., THE CHEMISTRY OF PETROLEUM HYDROCARBONS, 2, (Brooks, B.T., Boord, C.E., Kurtz, S.S., Schmerling, L., eds.), New York, Reinhold (1955).

38) Froment, G.F., Proc. 6th.Int.Cong.Catal., 10 (1976).

39) Beuther, H., Schmidt, B.K., Proc.6th Petrol.Cong., Sect.III, 297 (1964).

40) Cooper, B.J., Trimm, D.L., CATALYST DEACTIVATION, (Delmon, B., Froment, G.F.eds) Elsevier, Amsterdam, 63 (1980)

REFERENCES

1) Edmonds, T., CATALYSIS AND CHEMICAL PROCESSES, (Pearce, R., Patterson, W.R., eds.), London, Leonard Hill (1981).

2) I.C.I., CRACKER - THE LARGE SCALE MANUFACTURE OF ORGANIC CHEMICALS, Educational Publication.

3) Haensel, V., Donaldson, G.R., Ind.Eng.Chem., 43, 2102 (1951).

4) Pines, H., Haag, W.O., J.Amer.Chem.Soc., 82, 2471 (1960).

5) Peri, J.B., J. Phys.Chem., 69 (1), 220 (1965).

6) Peri, J.B., Hannan, R.B., J.Phys.Chem., 64, 1526 (1960).

7) Goble, A.G., Lawrance, P.A., Proc.3rd.Int.Congr. Catal., 320 (1964).

8) Oblad, A.G., Milliken, T.H., Mills, G.A., Advan. Catal., 3, 199 (1951).

9) Gates, B.C., Katzer, J.R., Schuit, G.C.A., CHEMISTRY OF CATALYTIC PROCESSES, New York, McGraw Hill, pp.259,260 (1979).

10) Thomson, S.J., Webb, G., HETEROGENEOUS CATALYSIS, London, Oliver and Boyd (1969).

11) Peri, J.B., J.Phys.Chem., 69 (1), 231 (1965).

12) Parry, E.P., J. Catal., 2, 371 (1963).

13) Boehm, H.P., Advan.Catal., 16, 179 (1966).

14) Dowden, D.A., Catalysis, 2, Specialist Periodical Reports, 1(1978).

15) Bertolacini, R.J., Pellet, R.J., CATALYST DEACTIVATION (Delmon, B., Froment, G.F.eds.) Elsevier, Amsterdam, 73 (1980).

16) Carter, J.L., McVicker, G.B., Weissman, W., Kmak, W.S., Sinfelt, J.H., Appl.Catal., 3, 327 (1982).

17) Biloen, P., Helle, J.N., Verbeek, H., Dautzenberg, F.M., Sachtler, W.M.H., J.Catal., 63, 112 (1980).

18) Sivasanker, S., Ramaswamy, A.V., J.Catal., 87. 553 (1978).

19) Pfefferle, W.C., Amer.Chem.Soc.Div., Pet.Chem. Preprints 15, A21 (1970).

20) Apesteguia, C.R., Barbier, J., J.Catal., 78, 352 (1982).

21) Sinfelt, J.H., Catalysis: Science and Technology, 1, 257 (1981).

22) Mills, G.A., Heinemann, H., Milliken, T.H., Oblad, A.G., Ind.Eng.Chem., 45. 134 (1953).

23) Weisz, P., Advan.Catal., 13, 137 (1962).

24) Callender, W.L., Brandenberger, S.G., Meerbott, W.K., Proc.5th.Int.Cong.Catal., 1265 (1973).

25) Sinfelt, J.H., Hurwitz, H., Rohrer, J.C., J.Phys. Chem., 64, 892 (1960).

26) Christoffel, E.G., Paál, Z., J.Catal., 73, 30 (1982)

41) Parera, J.M., Figoli, N.S., Traffano, E.M.,Beltramini, J.N., Martirelli, N.S., Appl.Catal., 5, 33 (1983).

42) Davis, S.M., Zaera, F., Somorjai, G.A., J.Catal., 77, 439 (1982).

43) Wolf, E.E., Alfani, F., Catal.Rev.Sci.Eng., 24 (3), 329 (1982).

44) Eberly, P.E. Kimberlin, C.N., Miller, W.H., Drushel, H.V., Ind.Eng.Chem.Process Des.Dev., 5, 193(1966).

45) Appleby, W.G., Gibson, J.W., Good, G.M., Ind.Eng. Chem.Process Des.Dev., 1, 102 (1962).

46) Haldemann, R.G., Botty, M.C., J.Phys.Chem., 63, 489 (1959)..

47) Espinat, D., Dexpert, H., Freund, E., Martino, G., Appl.Catal., 16, 343 (1985).

48) Figoli, N.S., Beltramini, J.N., Martinelli, E.E., Sad, M.R., Parera, J.M., Appl:Catal., 5, 19 (1983).

49) Parera, J.M., Figoli, N.S., Traffano, E.M.,Beltramini, J.N., Martinelli, E.E., Appl.Catal., 5, 33 (1983).

50) Barbier, J., Corro, G., Zhang, Y., Bournonville, J.P., Franck, J.P., Appl.Catal., 16, 169 (1985).

51) Barbier, J., Marecot, P., Martin, N., Elassal, L., Maurel, R., CATALYST DEACTIVATION, (Delmon, B., Froment, G.F., eds.) Elsevier, Amsterdam, 53 (1980).

52) Mieville, R.L., J.Catal., 100, 482 (1986).

53) Somorjai, G.A., Zaera, F., J.Phys.Chem., 86, 3070 (1982).

54) John, T.M., Pachovsky, R.A., Wojeiechowski, B.W., Chem.Reac.Eng., 2, 422 (1974)

55) Tauster, S.J., Koros, R.M., J.Catal., 27, 307 (1972).

56) Levinter, M.E., Bortkevich, M.I., Zabotin, L.I., Berkovie, L.M., Kinet. Katal., 16, 221 (1975).

57) Blue, R.W., Engle, C.J., Ind.Eng.Chem., 43, 494 (1951).

58) Thomas, C.L., J. Amer.Chem.Soc., 66, 1586 (1944).

59) Greensfelder, B.S., Voge, H.H., Ind.Eng.Chem., 37, 1038 (1945).

60) Beltramini, J.N., Martinelli, E.E., Churin, E.J., Figoli, N.S., Parera, J.M., Appl.Catal., 7, 43 (1983).

61) Satterfield, C.N., HETEROGENEOUS CATALYSIS IN PRACTICE, New York, McGraw-Hill (1980).

62) Pines, H., THE CHEMISTRY OF CATALYTIC HYDROCARBON CONVERSIONS, New York, Academic Press, P.101 (1981).

63) Gillespie, W.D., Hertz, R.K., Petersen, E.E., Somorjai, G.A., J. Catal., 70, 147 (1981).

64) Figoli, N.S., Sad, M.R., Beltramini, J.N., Jablonski, E.L., Parera, J.M., Ind.Eng.Chem.Proc.Rev.Dev., 19, 545 (1980).

65) Parera, J.M., Figoli, N.S., Jablonski, E.L., Sad, M.R., Beltramini, J.N., CATALYST DEACTIVATION, (Delmon, B., Froment, G.F., eds.) Elsevier, Amsterdam, 571 (1980).

66) Figoli, N.S., Beltramini, J.N., Querini, C.A., Parera, J.M., Appl.Catal., 15, 41 (1985).

67) Bishara, A., Murad, K.M., Stanislaus, A., Ismail, M., Hussain, S.S., Appl.Catal., 7, 337 (1983).

68) Bartholomew, C.H., "CATALYST DEACTIVATION", Chem.Eng., Nov.(1984).

69) Hayes, J.C., Mitsche, R.T., Pollitzer, E.L., Homeier, E.H., Reprints, Amer.Chem.Soc.Div.Pet.Chem., 19, 334 (1974).

70) Lankhorst, P.P., De Jongste, H.C., Ponec, V., CATALYST DEACTIVATION , (Delmon, B., Froment, G.F., eds.) Elsevier, Amsterdam, 43 (1980).

71) Somorjai, G.A., Blakely, D.W., Nature, 258, 580 (1975).

72) Margitfalvi, J., Gobolos, S., Kwaysser, E., Hegedus, M., Nagy, F., Koltai, L., React.Kinet.Katal.Lett., 24, 315 (1984).

73) Toei, R., Nakanishi, K., Yamada, K., Okazaki, M.J., Chem.Eng.Jpn., 8, 131 (1975).

74) Karpinski, Z., Koscielski, T., J.Catal., 63,313 (1980).

75) Wolfgang, R., Rowland, F.S., Anal.Chem., 30, 903 (1958).

76) Schmidt-Bleek, F., Rowland, F.S., Anal.Chem.,36, 1695 (1964).

77) McLachlan, K., Ph.D Thesis, University of Glasgow, Glasgow (1983).

78) Svajgl, O., Int.Chem.Eng., 12, 55 (1972).

79) Sivasanker, S., Ramaswany, A.V., Ratnasamy, P., PREPARATION OF CATALYSTS II, (Delmon, B., Grange, P., Jacobs, P., Poncelet, G., eds.) Elsevier, 185 (1979).

80) Ciapetta, F.G., Hunter, J.B., Ind.Eng.Chem., 43, 1881 (1951).

81) Sinfelt, J.H., J.Catal., 27, 468 (1972).

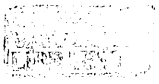

82) Taylor, G.F., Thomson, S.J., Webb, G., J.Catal., 8, 388 (1967).

83) Thomson, S.J., Webb, G., J.Chem.Soc.Chem.Comm., 526 (1976).

APPENDIX 1

Apparatus and Procedure for Making Restrictors

The restrictors were prepared using the apparatus shown overleaf.

The die B was put in a hydraulic press and gently squeezed. The N_2 pressure was gradually increased and the flow rate monitored. If the flow rate was in excess of the desired value the pressure exerted on B was increased until the flow rate was approximately equal to that required. The N_2 was then shut off and allowed to leak out of the system. The hydraulic pressure was then removed and the restrictor annealed to red hot (bunsen). The system was then set up again. The hydraulic pressure was then reapplied (gently) and the N_2 flow re-established. The exact flow at the required pressure differential was them obtained. The N_2 pressure was released and then the hydraulic pressure. The crimped metal was re-annealed avoiding twisting. The tubing was cut off at about point A (crimp being held in the die to avoid distortion). The undrilled connector was disconnected and then reconnected to an 1/8" connector as in finished restrictor (Fig.4.2).

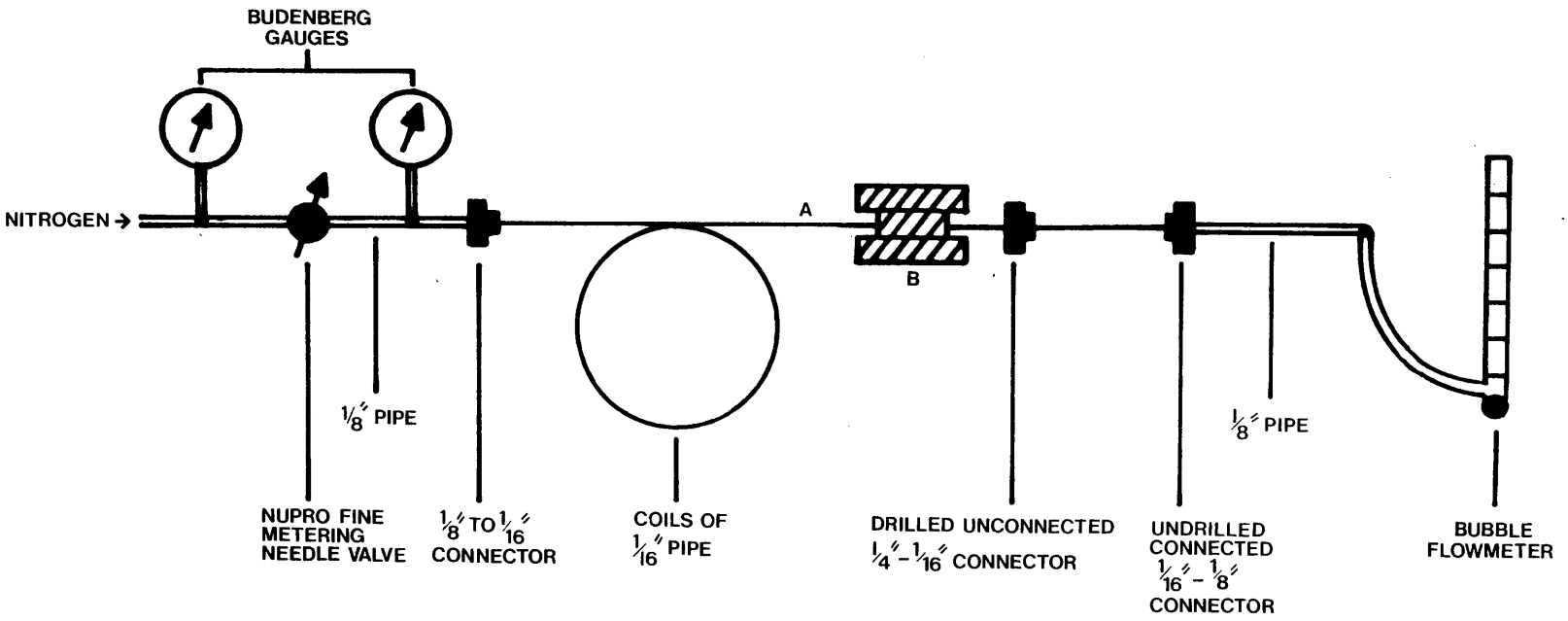

Appendix I – Apparatus for making Restrictors.